[American Journal of Science, Vol. 316, December, 2016, P. 925-980, DOI 10.2475/10.2016.01]

American Journal of Science

DECEMBER 2016

ORDOVICIAN–EARLY SILURIAN INTRUSIVE ROCKS IN THE NORTHWEST PART OF THE UPPER ALLOCHTHON, MID-NORWAY: PLUTONS OF AN IAPETAN VOLCANIC ARC COMPLEX

KURT HOLLOCHER*,†, PETER ROBINSON**, KIRK SEAMAN***, and EMILY WALSH§

ABSTRACT. The Scandinavian Caledonides are a late Silurian–early Devonian orogen that is an amalgam of thrust sheets derived from the Baltican margin, Iapetan arcs, and the Laurentian margin. Here we discuss intrusive rocks in two Iapetan arc complexes of Ordovician–early Silurian age that are now part of the Upper Allochthon in the central-western part of Norway.

Samples from the older of the two arcs were collected near Lensvik and Rissa, on both sides of Trondheimsfjord. These include mafic to felsic, mostly tholeiitic metamorphosed intrusive rocks, with one previously reported age of 482 Ma. These plutons intrude volcanic rocks of the Støren Group, a suite of 495 to 482 Ma oceanic arc rocks that include ophiolites. We assign these plutonic rocks to the Støren Group, based on their similar ages and strong geochemical similarities with Støren Group plutonic and volcanic rocks in the inner Trondheimsfjord region. Part of the Støren Group is unconformably overlain by earliest Middle Ordovician sedimentary sequences that contain warm-water Laurentian faunal assemblages.

Plutonic rocks of the younger arc have previously reported ages of 477 to 440 Ma, are calc-alkaline, span a composition range from ultramafic to granitic, and include a large fraction of adakites. Rocks in the Upper Allochthon with similar ages and lithologic and geochemical characteristics also occur farther north, across the Grong-Olden culmination, and in southwestern Norway, indicating an extensive arc complex. Throughout that extent, the plutonic rocks are spatially associated with older ophiolite-bearing oceanic arc assemblages, thought to be equivalent to the Støren Group.

The Helgeland Nappe of the Uppermost Allochthon contains an extensive suite of igneous rocks that have almost identical characteristics to the younger Upper Allochthon arc we describe. They are also spatially associated with 500 to 480 MA ophiolites, and in addition cut metamorphosed sedimentary rocks that contain evidence for development near or on the Laurentian margin. This evidence suggests that the calc-alkaline rocks of the Upper and Uppermost Allochthons may belong to the same arc complex. The fact that similar-age calc-alkaline arc rocks occur in the Taconian arc system of western New England, the Notré Dame arc of Newfoundland, and in the Midland Valley Terrane and related units in Scotland and Ireland, suggest extensive calc-alkaline Iapetan arc complexes that developed before and during late Ordovician closing of an arm of Iapetus.

Keywords: Caladonide tectonics, Upper Allochthon, igneous geochemistry, Norway, adakites, Iapetan tectonics

* Department of Geology, Union College, Schenectady, New York 12308, USA
** Geological Survey of Norway, N-7491, Trondheim, Norway
*** Haley and Aldrich, Inc., 100 Corporate Place Suite 105, Rocky Hill, Connecticut 06067
§ Department of Geology, Cornell College, Mount Vernon, Iowa 52314, USA
† Corresponding author: hollochk@union.edu

INTRODUCTION

The Scandinavian Caledonides are a late Silurian to early Devonian (Scandian) orogenic belt comprised of a series of composite allochthonous thrust sheets, grouped into the Lower, Middle, Upper, and Uppermost Allochthons (fig. 1). These represent packages of rocks derived, respectively, from regions tentatively believed to have lain progressively farther outboard from Baltica (for example, Andréasson and others, 2003; Gee, 2005; Hacker and Gans, 2005). Our purpose is to present the geochemistry of remnants of an Ordovician calc-alkaline arc in the Upper Allochthon north and west of Trondheim, where it has been little-studied, and discuss its implications for pre-Scandian tectonics.

The Upper and Uppermost Allochthons are composed of five major components that developed in settings far outboard from Baltica, including the Laurentian margin. These are described briefly from southeast to northwest (fig. 1), in approximate order of present position.

Regional Tectonostratigraphy

(1) The Meråker Nappe comprising the eastern part of the Trondheim Nappe Complex of the Upper Allochthon, consists of stratified sedimentary rocks, subsidiary volcanics, and intrusive rocks, possibly as old as Late Cambrian and possibly as young as Middle Silurian. The eastern margin of this unit contains an extensive group of ophiolite fragments, including ultramafic rocks that are geochemically MORB-like (Nilsson and Roberts, 2014). Near Otta, at the southern end of this ophiolite belt, a serpentinite conglomerate contains late Dapingian to early Darriwillian fossils of the cold-water Celtic fauna (for example, Bruton and Harper, 1981; Boe and others, 1993; Harper and others, 2008). These fauna were first identified by Neuman (1964) at the type locality of the Penobscot Unconformity in eastern Maine, U.S.A., an unconformity now recognized as characteristic of the peri-Gondwanan Gander Terrane in the Canadian Maritimes (for example, Kusky and others, 1996). Thus, at least a part of the Meråker Nappe lay at high latitude during early Ordovician time.

(2) The Gula Complex, comprising the central part of the Trondheim Nappe Complex, consists of terrigenous clastic sedimentary rocks of uncertain age, including conglomerates, possibly as old as Mesoproterozoic. It has evidence of low- to medium-grade Silurian regional metamorphism, and is cut by a variety of Silurian intrusions. The nature of the contact between the apparently older Gula Complex and the younger Meråker Nappe remains uncertain, having been variously interpreted as stratigraphic (for example, Bjerkgård and Bjørlykke, 1994; Sturt and others, 1997), an unconformity (Ramsay and Sturt, 1998), and a thrust (Grenne and Lagerblad, 1985).

(3) The Støren Group, in the Støren Nappe of the Trondheim Nappe Complex, is composed mostly of basaltic rocks that include the 500 to 480 Ma ophiolite complexes at Bymarka, Løkken, and elsewhere (for example, Grenne, 1989b; Roberts and others, 2002; Roberts, 2003; Slagstad and others, 2013). These developed apparently in an oceanic arc and back-arc complex (summarized in Hollocher and others, 2012) and have a significant arc component that is lacking in ophiolites of the Meråker Nappe (Nilsson and Roberts, 2014; though present in amphibolites of the Fundsjø Group of the Meråker Nappe, Grenne, 1987). Exposed areas of ultramafic rocks are scarce compared to the Meråker Nappe. Within the Støren ophiolites are rare felsic volcanics and trondhjemitic intrusions. At Løkken, the ophiolite sequence is overlain unconformably by metamorphosed sedimentary and volcanic rocks (hatched unit in fig. 1) that includes the Lower Hovin Group, which contains Dapingian to middle Darriwilian warm-water fossil assemblages of Laurentian affinity (for example, Bruton and Harper, 1988; Pedersen and others, 1992). The fossils indicate that these ophiolites, as distinct from those in the Meråker Nappe to the east, were obducted onto the margin of Laurentia at low latitude in the early Ordovician. The Lower Hovin Group also

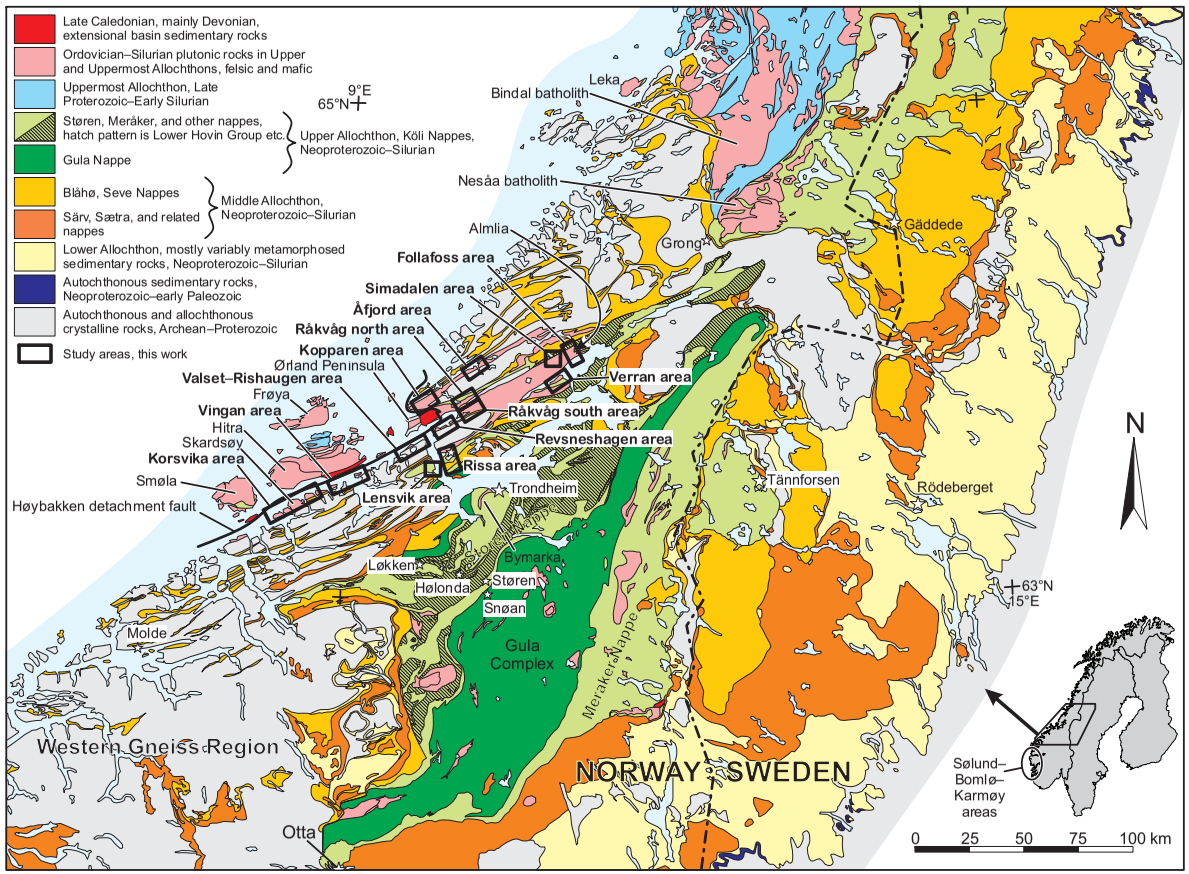

Fig. 1. Simplified tectonic map of the central Scandinavian Caledonides, showing areas from which the 153 samples were collected. Principally adapted from Sigmond and others (1984), Solli and Nordgulen (2008), and Robinson and others (2008).

contains calc-alkaline to alkaline plutons and volcanics having strong arc signatures. These strata have been interpreted to have been deposited in a back-arc basin (Roberts and others, 1984) or as part of a basin–arc sequence (Grenne and Roberts, 1998). The nature of the contact of the Støren Group against the Gula Nappe to the east is uncertain, claimed by some as an obduction surface (for example, Hollocher and others 2012).

(4) In the Støren Nappe, northwest of the exposure area of the Støren Group, the rocks consist predominantly of felsic to mafic intrusions in the age range 477 to 440 Ma (Tucker and others, 2004; fig. 1, pink unit west and north of Trondheim in the Upper Allochthon). These are conveniently divided into an onshore (northwestern) belt where the intrusive rocks (described here) have been deformed into strongly foliated and lineated gneisses during late Scandian sinistral transtension (Osmundsen and others, 2006; Robinson and others, 2014), and a mostly offshore belt on the islands of Smøla and Hitra and on Ørland Peninsula, northwest of the Høybakken brittle–ductile detachment (fig. 1). The offshore belt rocks are from a higher structural level and mostly escaped transtension-related deformation. Clear igneous textures and structures are preserved, including evidence of magma mingling (for example, Gautneb and Roberts, 1989; Tucker and others, 2004). Similar Ordovician intrusions occur in the Upper Allochthon in the Nesåa batholith and related plutons northeast of Grong, and in the Solund, Bomlø, and Karmøy areas of southwest Norway. The island of Smøla in the offshore belt contains an early Ordovician stratified sequence of sediments and volcanics containing the same Laurentian fauna found in the Lower Hovin Group at Hølonda. This sequence was already deformed and metamorphosed when intruded by an undeformed pluton dated at 446 Ma (Tucker and others, 2004). This is key evidence favoring arc magmatic activity tied directly to the Laurentian margin.

(5) Rocks assigned to the Uppermost Allochthon, including the ophiolite at Leka, are exposed north of Grong as well as on the northern part of Hitra and on Frøya. The complex history of this area has been recently described by Barnes and others (2007, 2009, 2011). The main outcome is to suggest that there was early northwest-directed thrusting of high-grade rocks carried over lower grade rocks, including ophiolites, in the period 470 to 460 Ma. This tectonic contact was cut by a series of plutons dated close to 445 Ma. In many ways, the low-grade rocks closely resemble those of the Upper Allochthon further south, and, in Nordland well north of figure 1, they also contain isotopic evidence (Melezhik and others, 2002, 2003), though no fossils, suggesting origin or emplacement near the Laurentian margin.

Sample Collections

This study includes 153 new whole rock chemical analyses of metamorphosed plutonic rocks. One set from the Lensvik and Rissa areas is probably related to the 500 to 480 Ma Støren Group ophiolites (part 3, above), based in part on a radiometric date of 482 Ma from Lensvik (Tucker and others, 2004). The other set is from the younger 477 to 440 Ma calc-alkaline arc (part 4). These have been little-studied compared to ophiolitic Upper Allochthon rocks in central Norway, and are the topic of this paper. Below the Høybakken detachment, where all of our samples were collected, the rocks range from almost undeformed (rare) to completely recrystallized. Three samples come from a polymict conglomerate in a small basin at Almlia, in the Follafoss area (fig. 1), that unconformably overlies calc-alkaline gneiss dated at 460 Ma (Tucker and others, 2004). This conglomerate is deformed, and so pre-dates Devonian extensional basins found elsewhere in Norway that are associated with tectonic collapse of the Caledonian orogen (fig. 1; for example, Andersen, 1998; Osmundsen and others, 2006; Vetti and Fossen, 2012).

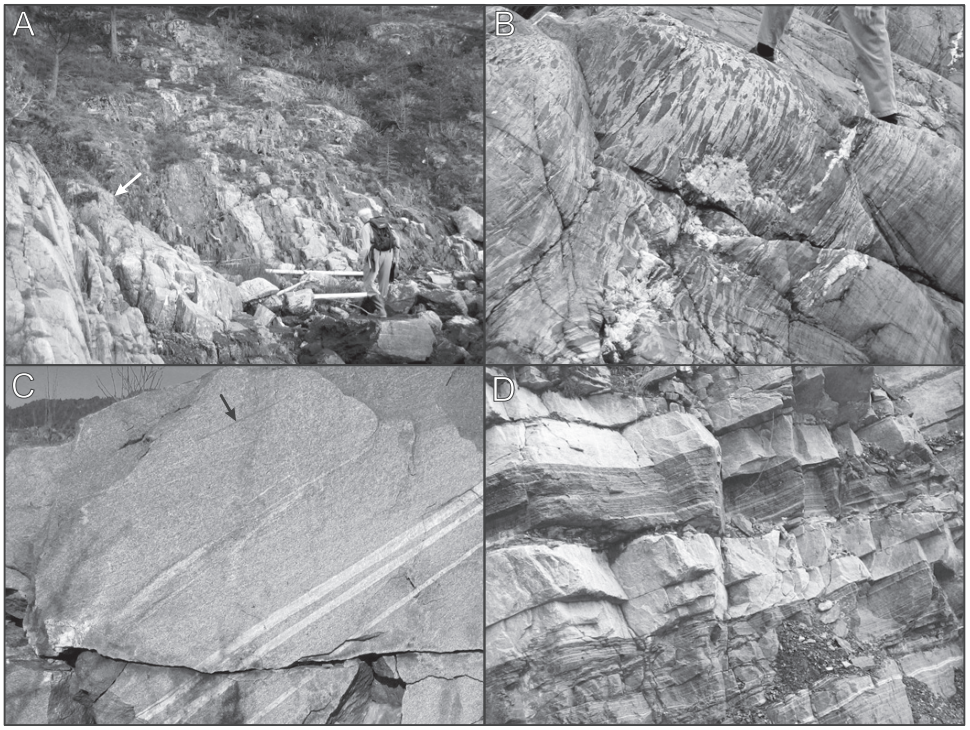

Fig. 2. Field photographs. (A) Rissa area, from the location of samples 459–461 (this work), and 462 and 463 (Hollocher and others, 2012). The image shows a large body of tonalitic rock to the lower left in contact (arrow) with dark-colored Støren Group volcanics to the upper right. Dikes and sills of tonalite intrude the volcanics. This image is from a set of shoreline exposures south of Rissa, along strike across Trondheimsfjord from tonalite, north of Lensvik, dated at 482 Ma (Tucker and others, 2004, sample L). (B) Deformed light-gray tonalitic dike containing numerous mafic inclusions, cutting darker gray tonalitic gneiss. This is the location of sample 420. (C) Relatively homogeneous coarse tonalitic gneiss from Skardsøya, the location of sample 404. The tonalite hosts three sharply-defined, internally layered aplite dikes, some irregular light-colored tonalitic layers and patches, and some dark, highly elongated xenoliths, the largest of which is indicated by the arrow. (D) Strongly deformed plutonic rocks at a quarry south of Råkvågen, the site of samples 503–505. The alternating light and dark layers are both tonalite, but the darker contains numerous thin layers of white tonalite and quartz veins, absent from the white tonalite.

Figure 2 shows examples of the rocks we studied. Figure 2A is from the Rissa area, which is across Trondheimsfjord along strike from the tonalitic gneiss dated at 482 Ma by Tucker and others (2004). The contact between light-colored tonalitic gneiss and dark Støren Group volcanic rocks is visible (arrow), with dikes and sills of tonalite intruding the volcanics. Figure 2B shows a light-gray tonalite dike cutting darker tonalitic gneiss. The dike contains numerous mafic xenoliths, somewhat deformed but with their original angular shapes still apparent. Figure 2C shows a typical outcrop of coarse-grained tonalitic gneiss from the belts northwest of Lensvik and Rissa. The gneiss contains three white, nearly parallel aplitic dikes, irregular light-colored tonalitic layers, and some highly elongated mafic inclusions. Scandian deformation has extended the original features so that they are nearly parallel. In contrast, figure 2D shows alternating layers of dark and light tonalitic gneiss. The dark tonalite contains numerous quartz veins and thin, light tonalite dikelets, whereas the light tonalite is free of them. All have been deformed into parallelism during late Scandian sinistral shear.

Sampling and Methods

Geochemical samples were generally gneisses and amphibolites, and weighed 1 to 10 kg. The object in general was to collect a representative set of exposed rocks, though rare rocks in any given area, such as ultramafic and undeformed rocks, tended to be sampled in higher proportions than their exposed abundance. Standard 30 μm thin sections were prepared for 77 of the 153 samples, which were examined using polarized transmitted light microscopy. Samples for whole rock chemical analyses were prepared and analyzed as described in Hollocher and others (2007). Sample locations are given in table A1, Appendix 1, descriptions in table A2, Appendix 2, and analytical data in table A3, Appendix 3.

DISTRIBUTION OF RADIOMETRIC AGES

Figure 3 shows a compilation of ages from the literature that have been determined for Paleozoic igneous rocks in the Upper Allochthon of the central and southwestern Scandinavian Caledonides, and in the Helgeland Nappe of the Uppermost Allochthon. Figure 3A shows ages of plutonic rocks in oceanic arc-derived units in central Norway, with an age peak at about 483 Ma (part 3, above). Figure 3B shows the 477 to 440 Ma calc-alkaline arc rocks that are the topic of this paper (part 4), including similar rocks on Hitra, Smøla, the Nesåa batholith, the Krutfjellet gabbro (437–436 Ma), both in the Middle Köli Nappe at about 65.7°N, and the Sulitjelma gabbro (437 Ma) at about 67.1°N. These yield an age peak near 441 Ma, but with ages as old as 477 Ma. Figure 3C shows Silurian plutonic rocks that cut the Meråker Nappe, Gula Complex, and Støren Nappe to the south and east of Trondheim (parts 1, 2, 3; fig. 1), having an age peak at about 435 Ma.

Age dates of Upper Allochthon rocks in southwestern Norway (fig. 3D) define two peaks, one for ophiolitic assemblages like those in figure 3A (parts 1 and 3), and one for younger calc-alkaline arc rocks like those in figure 3B (part 4), possibly also the Silurian plutons (fig. 2C). Though precise correlations along strike are uncertain, based on these age dates and igneous rock geochemistry (Hollocher and others, 2012, and references therein) the Upper Allochthon in southwestern Norway contains evidence for both the older (500–480 Ma) and younger arcs (477–440 Ma, and possibly the Silurian plutons).

Figure 3E shows ages for igneous rocks in the Uppermost Allochthon, which is interpreted to consist of rocks originating on or close to the Laurentian margin that were transferred onto Baltica during the Scandian collision (for example, Roberts and others, 1985, 2007; Stephens and Gee, 1985, 1989; Melezhik and others, 2003). The age distribution defines one peak similar to older ophiolites of the Upper Allochthon (figs. 3A and 3D), and a broad peak spanning the age ranges of both the calc-alkaline arc (fig. 3B, part 4) and the Silurian plutons. Figure 2F shows all age dates, clearly showing the bimodal age distribution, one for the older ophiolites, the other for the younger calc-alkaline arc and Silurian plutons.

PETROGRAPHY

Most samples are wholly recrystallized amphibolites and quartz-bearing gneisses having epidote-amphibolite facies mineral assemblages. Based on the examined thin sections, mafic rocks generally have the assemblages: hornblende–plagioclase–epidote–titanite ±quartz, biotite, Fe–Ti oxides, and sulfides. Felsic rocks have the assemblages: quartz–plagioclase–biotite–epidote–titanite ±hornblende, K-feldspar, muscovite, and garnet. Epidote is commonly strongly zoned, and includes clinozoisite in some samples. Cummingtonite is found in felsic gneiss samples 270, 411, and 413. In 270 and 413 the grains are disseminated, occurring with hornblende. In 411, however, cummingtonite forms discontinuous rims around prismatic hornblende, separated by a plagio-

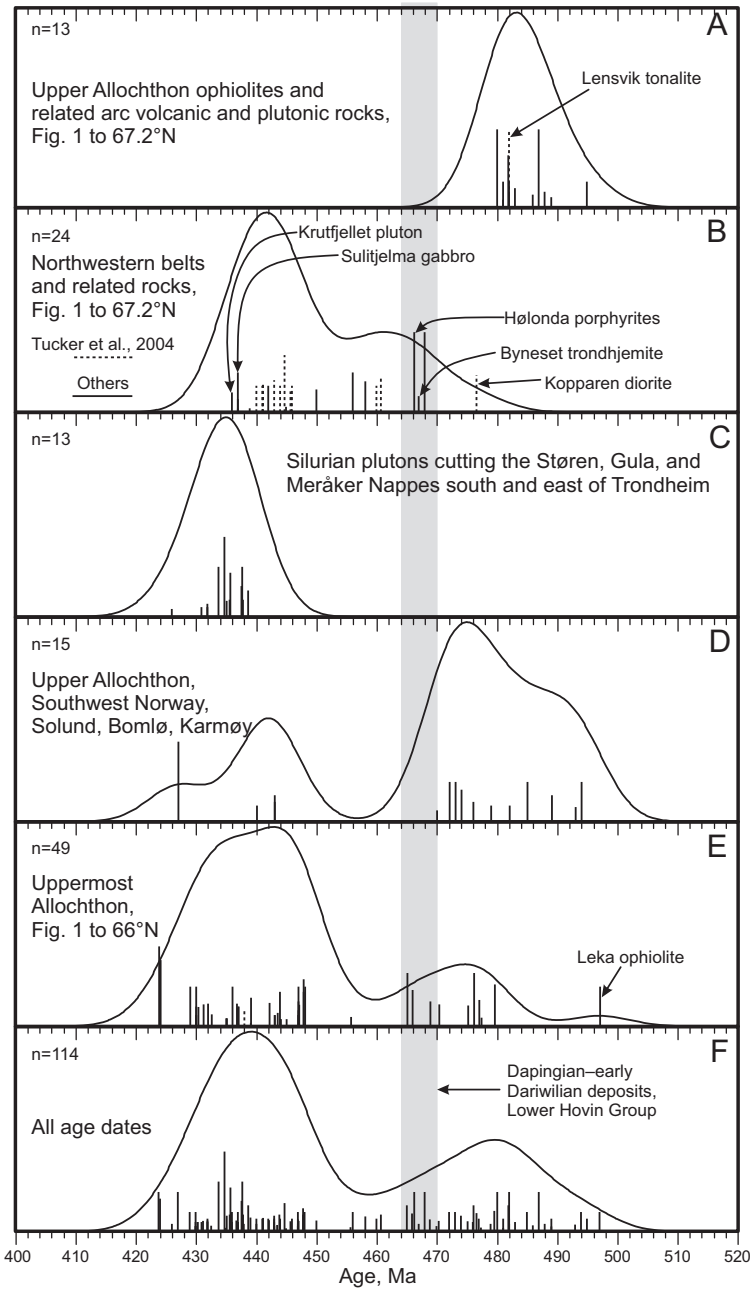

Fig. 3. Kernel probability density estimates of igneous rock radiometric ages in the Upper and Uppermost Allochthons of central and southwestern Norway, and Sweden. These are zircon U–Pb ages, except for two U–Pb titanite, four Nd/Sm isochron, and one stratigraphic age (Hølonda porphyrites, David Roberts, personal communication, 2015). Plotted curves were calculated using the Densityplotter program (Vermeesch, 2012), with a uniform 5 Ma bandwidth. Vertical black lines show analyzed sample ages, longer lines corresponding to more precise ages. (A) 500-480 Ma ophiolites, figure 1 to 67.2°N: Bymarka ophiolite (Roberts and others, 2002), Bymarka and Løkken ophiolites (Slagstad and others, 2013), Ytterøya ophiolite (Roberts and Tucker, 1998), Frosta Peninsula (Gromet and Roberts, 2010), Sulitjelma ophiolitic complex (Pedersen and others, 1991), plutonic rocks in the Köli Nappe east of the Helgeland Nappe Complex (Upper and Middle Köli units, Stephens and others, 1993). (B) Central Norway gneissic and related rocks,

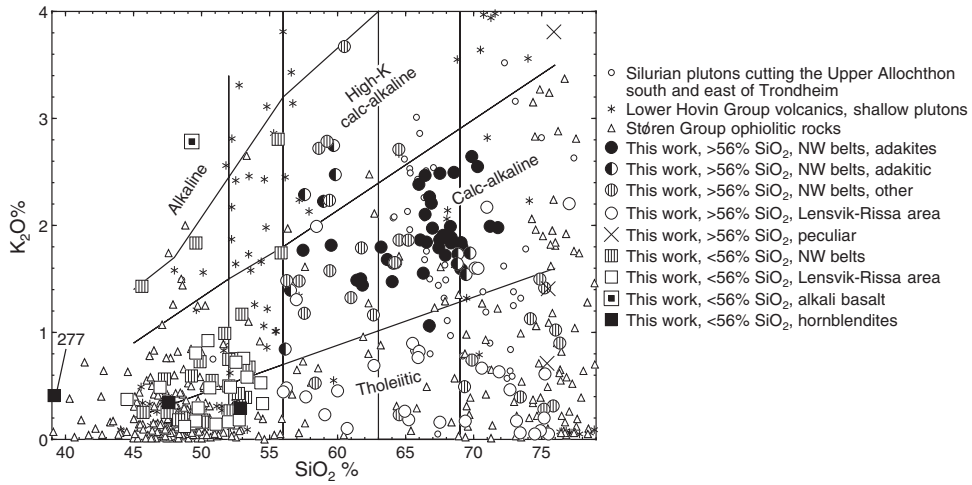

Fig. 4. Igneous series and rock type diagram (after Ewart, 1982), showing igneous rocks in the Upper Allochthon. The Støren Group includes the Bymarka and Løkken ophiolites, and related rocks in the region. "Adakites" satisfy all six criteria of Defant and Drummond (1990), and "adakitic" samples satisfy four or five criteria, including LREE-enrichment and HREE depletion. Data are from Vogt (1945), Gale (1974), Gale and Roberts (1974), Dypvik and Brunfelt (1976), Loeschke (1976a, 1976b), Grenne and Roberts (1980, 1998), Loeschke and Schock (1980), Roberts (1980, 1982a, 1982b, 1982c, 1987), Roberts and others (1984), Grenne and Lagerblad (1985), Heim and others (1987), Grenne (1989a, 1989b), Roberts and Tucker (1998), Dunning and Grenne (2000), Nilsen and others (2003), Pannemans and Roberts (2000), Roberts and Sundvoll (2000), Roberts and others (2002), Slagstad (2003), Lippard and Roberts (2010), Hollocher and others (2012), Slagstad and others (2013), and Vedeler (ms, 2013).

clase moat. Felsic samples 470 and 471 contain small amounts of tourmaline. Limited areas of gabbroic rock from the summit of Kopparen retain igneous textures and mineralogy (for example, enstatite, augite, zoned igneous plagioclase, sample 427). More commonly, igneous texture preservation is limited to millimeter-scale domains of blocky, interlocking, zoned plagioclase crystals between more strongly deformed regions.

GEOCHEMISTRY

Igneous Series

Figure 4 shows the igneous series of rocks in our data set, and compares them to other Upper Allochthon rock sets from central Norway. It shows that our samples span

Fig. 3 (continued). the topic of this work, from figure 1 to 67.2°N: Hitra and gneisses near the coast (Tucker and others, 2004), Nesåa batholith (Roberts and Tucker, 1991; Meyer and others, 2003) and Krutfjellet pluton (Mørk and others, 1997), both in the Middle Köli Nappe, granite in the Upper Köli Nappe near Vilasund, Sweden (Stephens and others, 1993), Middle Ordovician plutons cutting ophiolites (Slagstad and others, 2013). (C) Silurian plutons cutting the Upper Allochthon south and east of Trondheim (Wilson and others, 1983; Dunning and Grenne, 2000; Roberts and Sundvoll, 2000; Nilsen and others, 2003, 2007). (D) Southwestern Norway, Solund to Karmøy: Bomlø ophiolite (Pedersen and Dunning, 1997), Gulfjellet, Karmøy, Solund, and Stord ophiolites (Dunning and Pedersen, 1988), Bremanger granite complex (Hansen and others, 2002), Gåsøy intrusion (in Slagstad and others, 2011), Gufjellet area plutons (Dunning and Pedersen, 1988), Karmøy plutons (Dunning and Pedersen, 1988; Pedersen and Dunning, 1997), dikes cutting the Jotun Nappe (Lundmark and Corfu, 2007). (E) Uppermost Allochthon, figure 1 to 66°N: Leka ophiolite (Dunning and Pedersen, 1988), Bindal batholith and various sub-plutons (Nordgulen and Schouenborg, 1990; Birkeland and others, 1993; Nordgulen and others, 1993; Pedersen and others, 1999; Nordgulen and others, 2002; Yoshinobu and others, 2002; Nissen and others, 2006; Barnes and others, 2007, 2011), Hortavær pluton (Barnes and others, 2003). (F) All age dates, A–E.

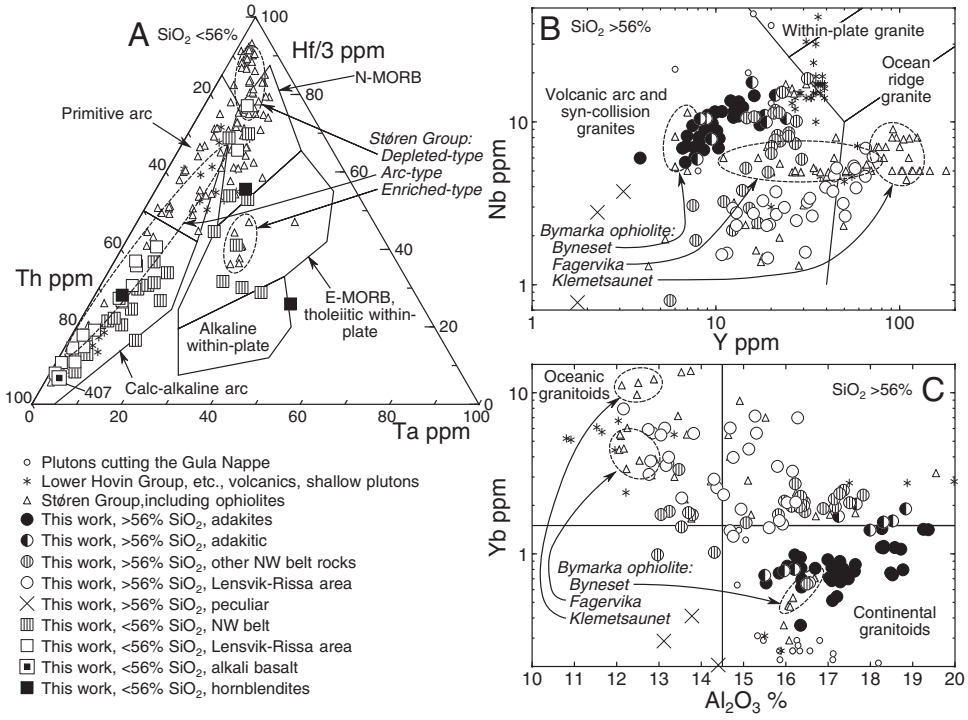

Fig. 5. Tectonic setting discriminant diagrams for our data set and other Upper Allochthon igneous rocks. (A) Mafic rock diagram of Wood (1980). (B) Felsic rock diagram of Pearce and others (1984). (C) Felsic rock diagram of Arth (1979). Data sources are the same as in figure 4.

a range of about 45 to 77 percent SiO_2 except for hornblendite sample 227. There is no obvious silica composition gap, as is commonly found in the 55 to 65 percent SiO_2 range in the Støren Group (for example, Hollocher and others, 2012). Mafic samples from our data set tend to straddle the tholeiitic–calc-alkaline boundary. Felsic samples from the northwestern belts tend to be overwhelmingly calc-alkaline, whereas those from the Lensvik and Rissa areas are tholeiitic.

Mafic rocks from the ophiolitic Støren Group (open triangles, fig. 4) are overwhelmingly tholeiitic, but felsic rocks span both series. Igneous rocks in the Lower Hovin Group and related units (asterisks) include a range of compositions that are dominantly calc-alkaline and high-K calc-alkaline. The Silurian plutons that cut the Upper Allochthon to the south and east of Trondheim (small open circles) are mostly calc-alkaline.

Tectonic Setting Discriminants

Figure 5 shows tectonic setting discriminant diagrams for rocks of this study. Most mafic samples (fig. 5A) plot in the calc-alkaline arc field, including alkaline sample 407. Eleven basaltic samples, however, plot along a line within or very close to the N-MORB and E-MORB fields, two from the Lensvik area (open squares), and the rest from locations scattered along strike in the northwestern belts. There is an apparent gap between the calc-alkaline arc and MORB-type sample trends. It is notable that our mafic samples include essentially none that plot within the primitive arc field. In contrast, mafic rocks from the Støren Group (open triangles)

tend to plot in the primitive arc and N-MORB fields. Mafic rocks from the Lower Hovin Group (asterisks) plot almost entirely in arc fields. Three elliptical fields highlight mafic rock compositional types in the Støren Group, which will be discussed in more detail below.

Figure 5B shows that most felsic samples plot in the field of volcanic arc and syn-collision granites. There appear to be two data groups, one at approximately 6 to 15 ppm Nb containing northwestern belt adakites, and one at approximately 1.5 to 6 ppm Nb containing rocks from Lensvik and Rissa. Both appear to be elongate along lines with positive slopes. The non-adakitic felsic rocks from the northwestern belts plot within and between the two groups. Figure 5C shows that the felsic rocks span a range from oceanic granitoids (mostly samples from Lensvik and Rissa) to continental granitoids (mostly northwestern belt adakites). Other samples from the northwestern belts plot between the extremes, with a possible gap between the adakites and other rocks.

Felsic rocks in the Støren Group (open triangles, figs. 5B and 5C) span a composition range similar to our whole data set, but are dominantly in oceanic fields. Rocks in the Lower Hovin Group and related units (asterisks) have a diverse range of compositions, though lack of sufficient analytical data for most samples makes generalization uncertain. Silurian plutons cutting the Upper Allochthon south and east of Trondheim (small open circles) tend to be Nb-rich, plotting with adakites in figure 5B, and remarkably Yb-poor, plotting below adakites in the continental granitoids field in figure 5C. Figures 5B and 5C have ellipses that encompass three distinctive felsic rock units in the Bymarka ophiolite (fig. 1), which will be discussed in more detail below.

Mafic Rocks, Lanthanides

Figure 6 shows REE diagrams for mafic rocks in the study area. Those in the Lensvik and Rissa areas (figs. 6A and 6B) include all combinations of slightly positive to negative HREE slopes (Gd_n/Yb_n = 0.7–1.2, 1.5 for sample 407), and slightly positive to negative LREE slopes (La_n/Sm_n = 0.6–2.7, 4.0 for sample 407). One amphibolite pattern is quite flat (414), some are smoothly concave-upward (416) or downward (408, 412), and some have flat or positive HREE and MREE slopes, but are distinctively LREE-enriched for the three or four lightest REE (for example, 271, 418, 459). The smoothly concave-upward patterns resemble those of boninites, but these rocks satisfy none of the other boninite criteria (Le Bas, 2000). Sample 407 is strongly LREE-enriched with flat HREEs. Unusual hornblendite sample 422 has 52.87% SiO_2 like a basaltic andesite, but it is also rich in MgO (10.29%), has one of the flattest REE patterns of all our samples, has the largest negative Eu anomaly of our mafic samples, and higher HREE concentrations than most other samples.

Figures 6C and 6D show REE patterns for mafic rocks from the northwestern belts. Most samples (fig. 6C) have negative REE slopes with Gd_n/Yb_n ratios of 1.5 to 3.4, and La_n/Sm_n ratios of 1.6 to 3.7, like sample 407 at Lensvik. Three mafic rocks from the northwestern belts have flatter patterns (fig. 6D) like some from Lensvik (fig. 6A). Figure 6E shows three other mafic rocks from the northwestern belts, a metamorphosed alkali basalt from a dike cutting granitic gneiss at Follafoss, and two hornblendites. One of the hornblendites (430, fig. 6E) was taken from a boudin on Kopparen. It is apparently a cumulate, with compatible trace element concentrations that are among the highest in this study (Sc 79 ppm, V 417, Cr 807, Co 69, Ni 275). The other hornblendite (227), from the Valset–Rishaugen area, has a straight, strongly LREE-enriched pattern and high REE concentrations. It has very low SiO_2 (39%), high TiO_2, FeO, and P_2O_5, perhaps like a ferrobasalt (for example, samples UB–89 or UB–313 from the Skaergaard intrusion, McBirney, 1998), but also high MgO (12.05%) and

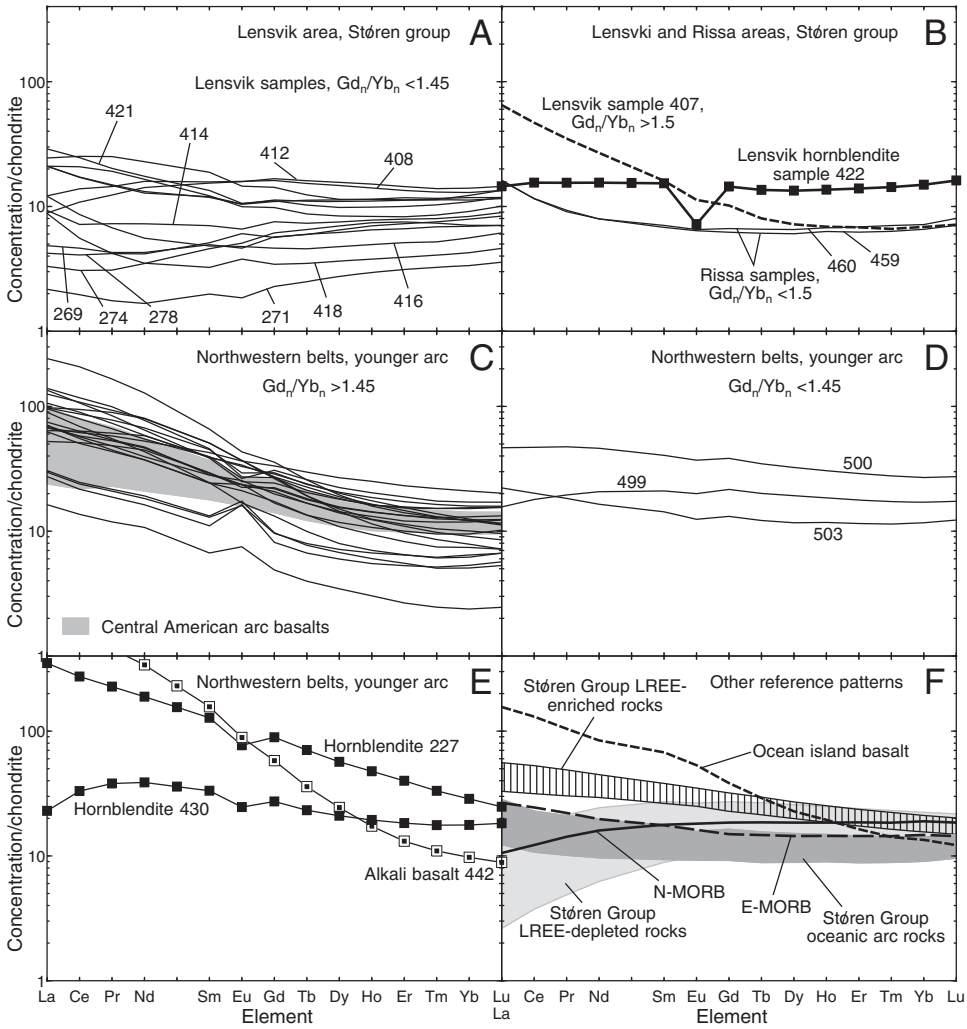

Fig. 6. REE diagrams for mafic rocks of this study (<56% SiO2, A–E), and several reference patterns for comparison (F, also C, E). The reference patterns in F include three geochemically distinctly types from the Støren Nappe (Hollocher and others, 2012). N-MORB, E-MORB, and ocean island basalt reference patterns are from Sun and McDonough (1989). The Central American arc basalt field in C is for 273 samples from that region having 45–56% SiO2, major element totals of 97–102% exclusive of volatiles, and reasonably complete REE data (numerous sources, most from Bolge and others, 2006, 2009; Singer and others, 2011). Reference pattern fields are averages ±1σ. Normalizing factors are from McDonough and Sun (1995).

CaO (13.81%), expected of a more primitive rock, or one rich in cumulus pyroxene and olivine.

Figure 6F shows several reference patterns: N-MORB, E-MORB, and ocean island basalts, and three mafic rock sets from the Støren Group (same as fig. 5A). Several of the REE patterns from Lensvik and Rissa resemble the N-MORB or Støren LREE-depleted patterns (408, 412, 499). Some others are more LREE-enriched and resemble E-MORB and the Støren Group enriched and arc-like patterns (for example, 421, 503). Most REE patterns from the northwestern belts (fig. 6C) most closely resemble the Central American arc basalt range.

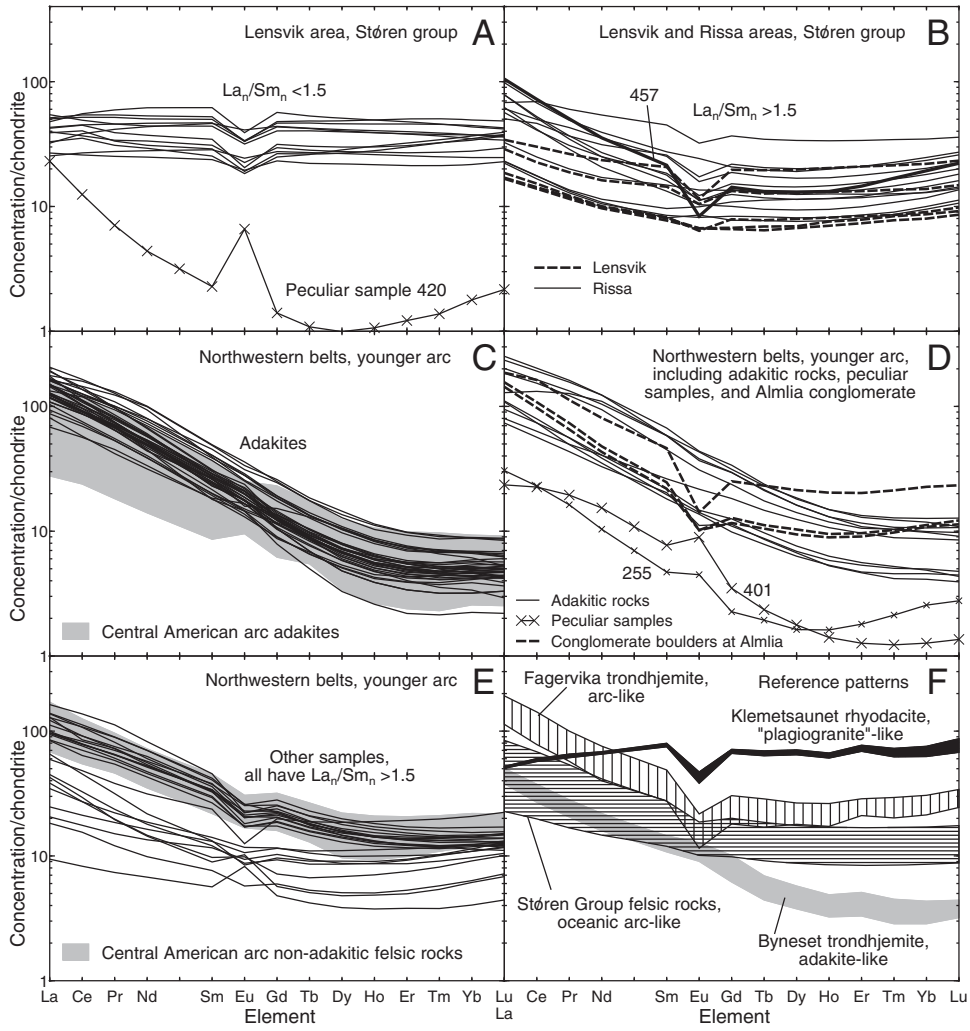

Fig. 7. REE diagrams for felsic rocks of this study (>56% SiO2, A–E) and reference patterns for comparison (F, also C, E). The comparison patterns in F are from Hollocher and others, (2012, all diorite, andesite, dacite, rhyolite compositions), and the Byneset trondhjemite, Fagervika trondhjemite, and Klemetsaunet rhyodacite units from the Bymarka ophiolite (Roberts and others, 2002; Slagstad, 2003, Slagstad and others, 2013). The Central American arc field in C is from 8 samples from that region that satisfy the six criteria of Defant and Drummond (1990) for adakites. The Central American arc field in E is for 86 non-adakitic samples having 56–78% SiO2, major element totals of 97–102% exclusive of volatiles, and reasonably complete REE data. Numerous sources were used for the Central American arc fields, most from Alvarado and others (2006), Bolge and others (2006, 2009), and Singer and others (2011). Fields are averages ±1σ. Normalizing factors are from McDonough and Sun (1995).

Felsic Rocks, Lanthanides

A large fraction of felsic rocks from Lensvik (fig. 7A) have flat REE patterns and negative Eu anomalies. They resemble patterns of the Klemetsaunet rhyodacite from the Bymarka ophiolite (figs. 7F, also 5B and 5C; Slagstad, 2001, 2003), which are typical of "plagiogranites" found in ophiolites and some modern ocean ridge and arc environments (for example, Barbieri and others, 1994; Rao and others, 2004; Whattam and others, 2005; Jiang and others, 2008; Jöns and others, 2009; Kiliç, 2009; Rollinson,

2009; Wanless and others, 2010). Indeed, the Klemetsaunet body was interpreted by Slagstad (2003) to be equivalent to plagiogranite in other ophiolites in Norway and elsewhere. Modeling by Slagstad indicated that the Klemetsaunet Rhyodacite was derived by fractional crystallization of an N-MORB-like parental liquid. Other felsic rocks in the Lensvik and Rissa areas (fig. 7B) are more LREE-enriched, and commonly have concave-upward patterns similar to the Fagervika trondhjemite in the Bymarka ophiolite, and other felsic rocks in the Støren Group (fig. 7F).

In the northwestern belts (fig. 7C), the felsic rocks include a large proportion of adakites, defined as having >56 percent SiO_2, being LREE-enriched and HREE-depleted, and satisfying all six criteria of Defant and Drummond (1990; Sr>400 ppm, Y<18 ppm, Sr/Y>25, Al_2O_3>15%, MgO<3%, and Yb<1.9 ppm). Rocks satisfying four or five of the criteria (fig. 7D) are here termed "adakitic", and they generally plot with the adakites. Both adakites and adakitic rocks have REE patterns like those seen in the Byneset trondhjemite reference pattern (fig. 7F, Slagstad, 2003), and also the Central American arc adakite reference field (fig. 7C).

Non-adakitic felsic rocks in the northwestern belts (fig. 7E) have REE patterns like some in the Rissa and Lensvik areas (fig. 7B), LREE-enriched and concave-upward, though the northwestern belt rocks tend to be more LREE-enriched. They closely resemble reference patterns from the Fagervika trondhjemite and Støren group felsic rocks (fig. 7F), which were interpreted to have been emplaced in an oceanic volcanic arc setting (Slagstad, 2003; Hollocher and others, 2012), and also the non-adakitic felsic rock reference pattern from the Central American arc (fig. 7E).

Three felsic rocks (figs. 7A and 7D) are termed "peculiar" (225, 401, 420). These have overall lower REE concentrations than most other felsic rocks, and the lowest MREE concentrations of all our samples. Other than high SiO_2 contents (approximately 75.5%), and low concentrations of most first-row transition elements, these three samples differ considerably from one another (for example, lithologies tonalite to granite, FeO_t 0.53–2.78%, Sr 169–1047 ppm).

Mafic Rock Multi-Element Anomalies

Figure 8 shows MORB-normalized multi-element diagrams for all mafic rocks on which we report. In general, the mafic rocks from Lensvik with relatively flat REE patterns (Gd_n/Yb_n <1.45, fig. 8A) have negative Nb' anomalies (MORB-normalized Nb, or Ta if Nb was not analyzed), no to moderately negative Zr' anomalies (MORB-normalized Zr, or Hf if Zr was not analyzed), moderately positive Th and U anomalies, and moderate to large positive K, Pb, Sr, and Li anomalies. The two mafic samples from Rissa have similar anomalies. Such anomalies are typical of arc basalts (for example, Sun and McDonough, 1989; Pearce and Stern, 2006). The LREE-enriched sample from Lensvik (407, fig. 8B) has anomalies similar to the other Lensvik mafic rocks, except its negative Nb' anomaly is larger, its K anomaly is negative rather than positive, and it has no Sr anomaly (though Nb, K, and Sr concentrations are within the range of other Lensvik samples).

The northwestern belt mafic rocks in figures 8C–8E, including the Follafoss alkali basalt, have anomalies similar to rocks at Lensvik: almost universal negative Nb' and common negative Zr', anomalies, and positive Th, U, Pb, and Li anomalies. K and Sr anomalies are, however, more variable in the northwestern belts. The northwestern belt anomalies are similar to those found in Central American arc basalts (fig. 8C). Comparison with other reference patterns (fig. 7F) shows that the anomalies of our mafic rock sets closely resemble arc- and possibly back-arc-related basaltic rocks in the Støren Group, but are unlike MORB and ocean island reference patterns. The three hornblendites (one in fig. 8B, two in 8E) have anomaly patterns that are quite different from one another, indicating different origins.

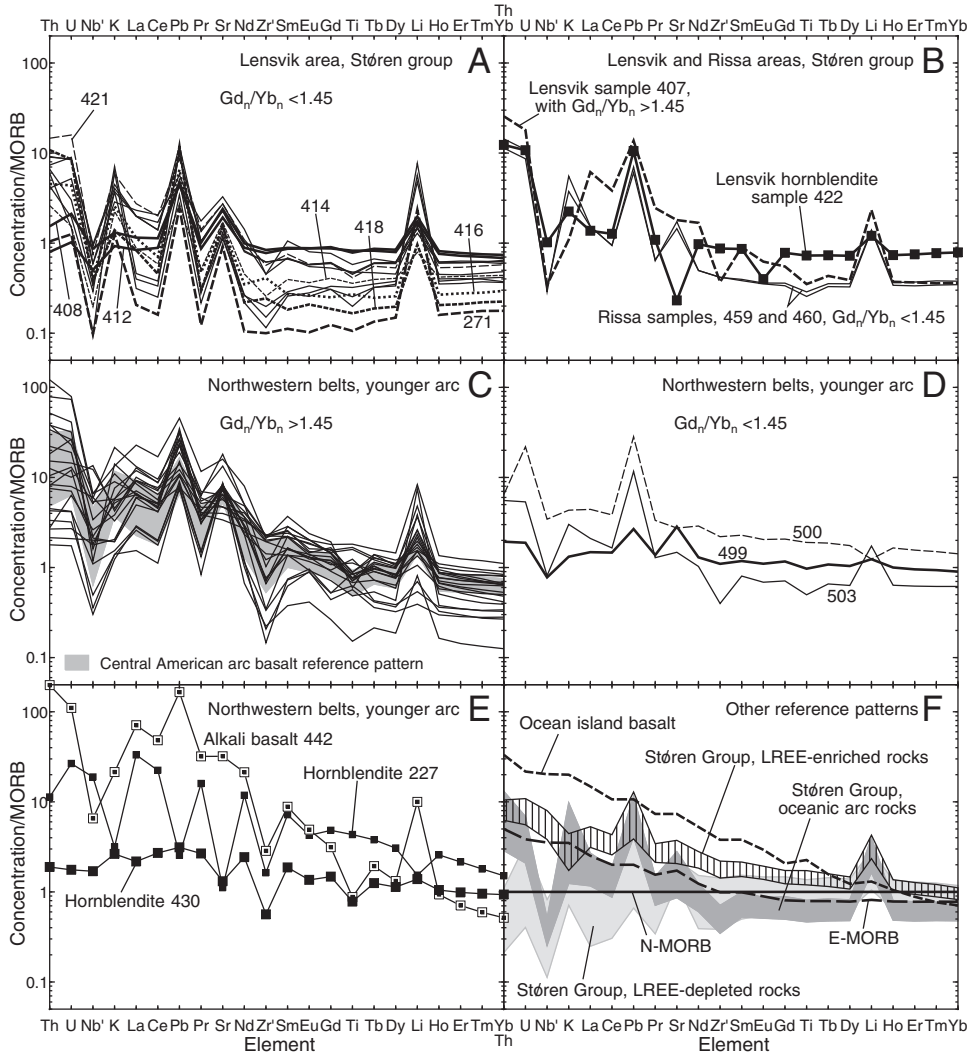

Fig. 8. Multi-element diagrams of all mafic samples (<56% SiO2) in our sample set (A–E), and reference patterns for comparison (F, also C). Zr' represents normalized Zr concentrations, or normalized Hf if Zr was not analyzed. Similarly, Nb' is normalized Nb, or Ta if Nb was unavailable. Sources for the reference patterns and selection criteria are the same as in figure 6. Normalizing factors are from Pearce and Parkinson (1993).

Felsic Rock Multi-Element Anomalies

Figure 9 shows multi-element diagrams for the felsic rocks. All have negative Nb' anomalies, and almost all have negative Ti anomalies which are common in felsic rocks generally. K anomalies range from positive to negative, and Zr' anomalies are small negative or absent. At Lensvik most felsic rocks having La_n/Sm_n <1.5 (fig. 9A) lack Pb anomalies and have large negative Li and Sr anomalies, not seen in the mafic rocks and rare among the other felsic rocks (figs. 9B–9E). Negative Sr anomalies are also seen in the plagiogranite-like Klemetsaunet rhyodacite and arc-like Fagervika trondhjemite reference patterns in figure 9F, though data are lacking for Pb and Li. Most Rissa and

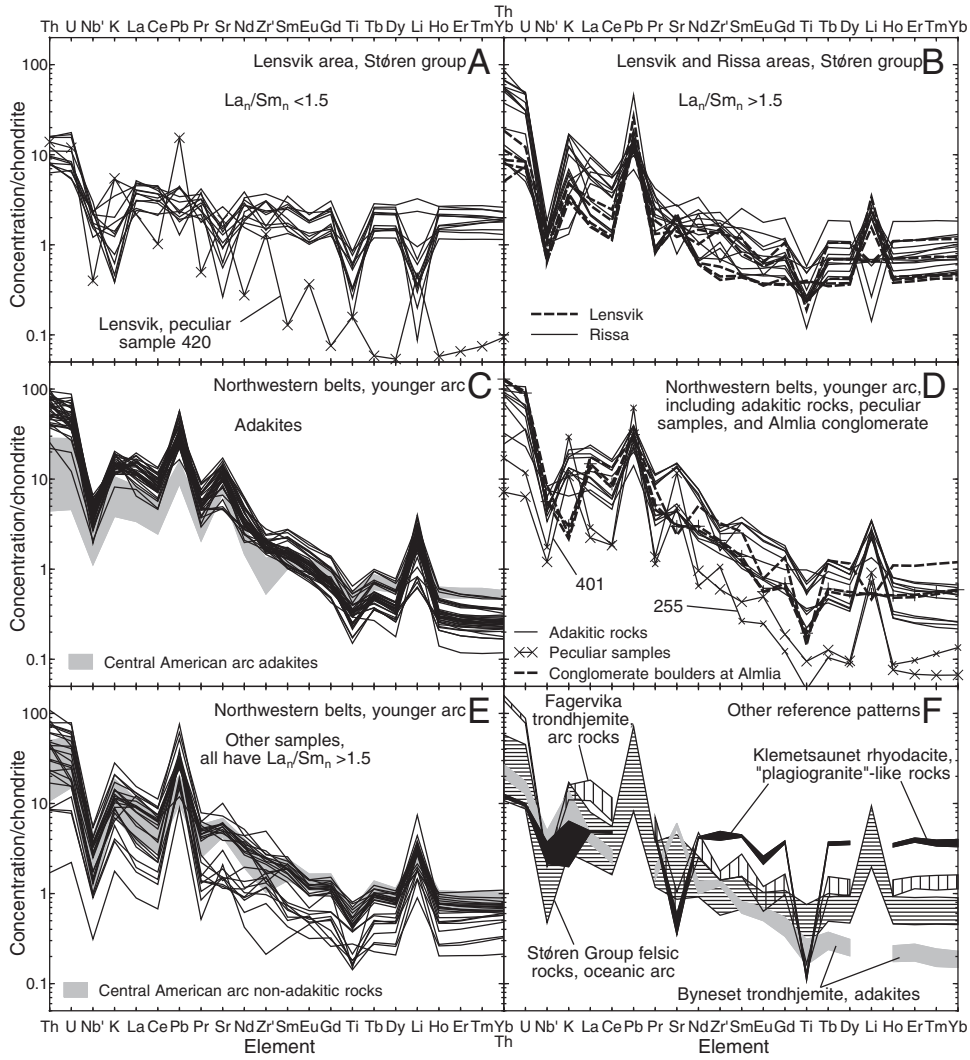

Fig. 9. Multi-element diagrams of all felsic samples (>56% SiO2) in our sample set (A–E), and reference patterns for comparison (F, also C, E). Reference patterns are the same as in figure 7, and Nb' and Zr' are the same as in figure 8. U values for the Klemetsaunet and Byneset reference patterns are interpolated between Th and La. Normalizing factors are from Pearce and Parkinson (1993).

Lensvik samples having La_n/Sm_n >1.5 (fig. 9B) have positive K, Pb, and Li anomalies, and small, variable Sr anomalies.

Positive K, Pb, and Li anomalies are seen in most felsic samples from the northwestern belts (figs. 9C–9E), the main exceptions being the tonalite conglomerate boulders from Almlia (Follafoss area). These have negative K, and, in part, Sr and Li anomalies, and positive Pb anomalies. The boulders more closely resemble many patterns from Lensvik and Rissa (figs. 9A and 9B, respectively), than other felsic samples from the northwestern belts.

Adakites from the northwestern belts (fig. 9C) have anomaly patterns similar to the Central American arc adakite reference pattern, except that the Zr' anomalies in

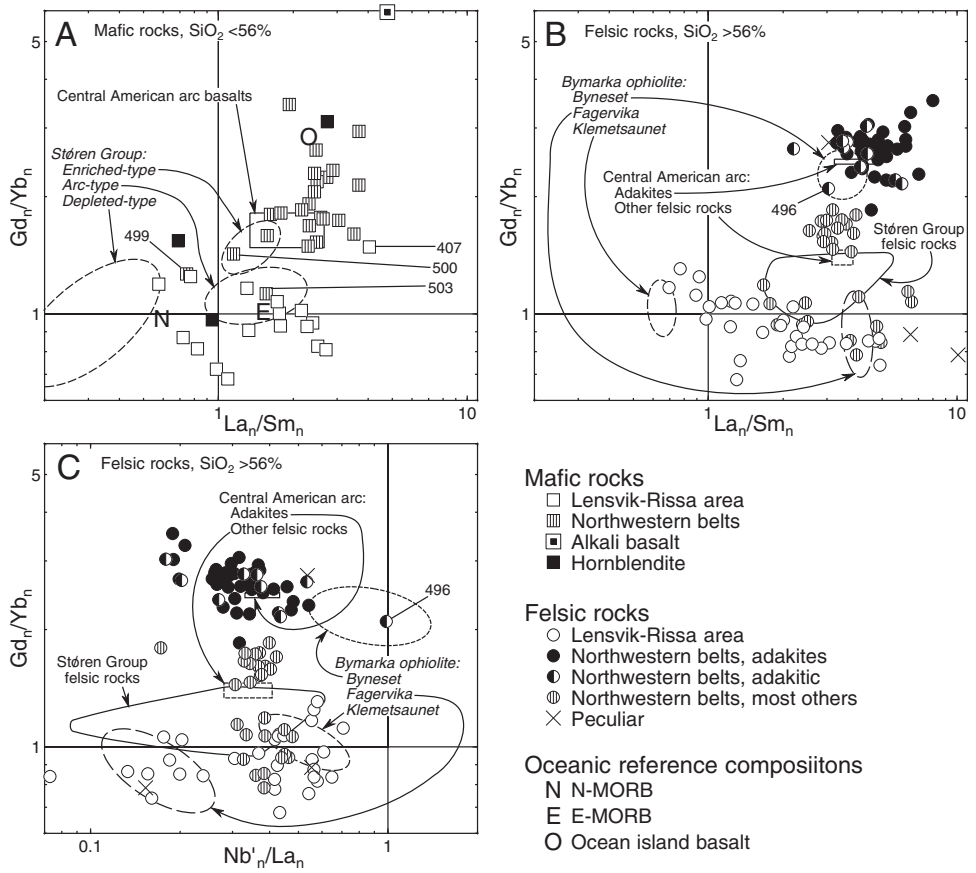

Fig. 10. Summary of REE patterns and Nb' anomalies in all rocks from this study. (A) Mafic rocks. (B, C) felsic rocks. A and B have the same axes, showing LREE enrichment relative to MREE (Lan/Smn values >1) and depletion (<1), and MREE enrichment relative to HREE (Gdn/Ybn values >1) and depletion (<1). Samples having patterns with straight, negative slopes plot in the upper right, and straight positive slopes in the lower left. Concave downward patterns plot to the upper left, and concave upward patterns to the lower right. Perfectly flat patterns plot at the intersection of the 1/1 lines, typical arc rocks having enriched LREE and flat HREE patterns plot to the right of the intersection, and LREE-depleted patterns like N-MORB plot to the left of the intersection. C has Nb'n/Lan for the X-axis, with samples having negative Nb' anomalies plotting approximately to the left of the X=1 line. The reference fields are as in figures 6 and 7, and Nb' is as described in figure 8.

our samples are smaller. Non-adakitic rocks from the northwestern belts (fig. 9E) have patterns like non-adakites in the Central American arc. Anomaly patterns in Støren Group felsic rocks (fig. 9F) are similar to those in the northwestern belts and some in the Lensvik and Rissa areas. Reference patterns from the Bymarka ophiolite are somewhat variable, and lack data for Pb and Li, but all share negative Nb' and Ti anomalies with felsic rocks of this study.

Comparisons with Other Upper and Uppermost Allochthon Rocks

Figure 10, summarizes some aspects of mafic and felsic rock geochemistry illustrated in figures 6 (10A), 7 (10B), and 9 (10C). Mafic rock anomalies in figure 8 are not very diverse and so are not compared here. Figure 10A shows that most mafic rocks from the Lensvik and Rissa areas have relatively flat REE patterns (plot close to

the intersection point of the four quadrants), with a tendency to be somewhat concave downward (lower-right quadrant). Most mafic rocks in the northwestern belts are considerably more LREE-enriched and HREE-depleted (upper right quadrant) than even the Støren group enriched-type reference field. There may be a composition gap between samples from the Lensvik and Rissa areas and samples from the northwestern belts.

In figure 10B, felsic rocks from the Lensvik and Rissa areas span the region between Klemetsaunet plagiogranite and Fagervika arc-type reference fields. Northwestern belt adakites tend to be even more LREE-enriched and more HREE-depleted than the Byneset trondhjemite field. Non-adakitic felsic rocks in the northwestern belts appear to plot in two groups, a compact cluster at slightly lower Gd_n/Yb_n values than the Byneset trondhjemite field, and in a broader field at the LREE-enriched end of the Lensvik and Rissa area samples, with a possible gap between.

Figure 10C shows that all of our felsic samples have negative Nb'_n/La_n anomalies, though sample 496, an otherwise unremarkable tonalitic gneiss from the Revsneshagen area, is barely so. Samples from the northwestern belts have negative Nb' anomalies, with Nb'_n/La_n ratios of 0.17 to 0.5 for both adakites and non-adakitic rocks. The northwestern belt adakites have larger Nb' anomalies than does the adakitic Byneset trondhjemite field (and sample 496), possibly indicating that the Byneset magmas had a deep source more MORB-like than arc-like. Samples from the Lensvik and Rissa areas have a wide range of Nb' anomalies with Nb'_n/La_n ratios of 0.07 to 0.7. Lensvik samples with flat REE patterns ($La_n/Sm_n<1.5$) have a more restricted Nb' anomaly range (0.4–0.7), possibly indicating a more MORB-like source, like the Klemetsaunet plagiogranite reference field.

Figure 11 uses the same format as figure 10 to compare our data set, shown as fields, to intrusive and volcanic rocks of similar ages in the Upper and Uppermost Allochthons in the central and southwestern Scandinavian Caledonides. Mafic rocks in the Støren Group (white triangles, fig. 11A) largely occur in a stripe extending from the Støren depleted- to enriched-type ellipses, an apparent continuum. Several also plot in the Støren arc-type ellipse. Igneous rocks in the Lower Hovin Group and associated units (asterisks) include mildly alkaline varieties that plot in and near the northwestern belt field, and tholeiitic varieties that plot with most of the Støren Group. Mafic plutonic rocks associated with dated Middle to late Ordovician arc rocks (black rectangles and rotated squares) plot within and just below the northwestern belt field. Mafic rocks from the Uppermost Allochthon (black diamonds) are similar, but data extend toward more LREE-enriched compositions within and above the northwestern belts field.

Figure 11B shows that most felsic Støren Group rocks (triangles) have Gd_n/Yb_n ratios of approximately 1, and plot in a stripe from the slightly LREE-depleted Klemetsaunet rhyodacite and Lensvik reference fields to LREE-enriched fields of Fagervika arc-like rocks, and the lower part of the field of northwestern belt non-adakitic rocks. The Byneset trondhjemite field partly overlaps our adakite field, and this intrusive is now known to have an age of 467 Ma (Slagstad and others, 2013), and therefore is probably related to Middle and Late Ordovician northwestern belt arc magmatism, and not the older host ophiolite. Felsic rocks in the Lower Hovin Group and related units (asterisks), like their mafic counterparts, plot in two regions, one having Gd_n/Yb_n ratios <1 near and within the Lensvik field, and another of more alkaline rocks near or in the adakite field. Upper and Uppermost Allochthon calc-alkaline igneous rocks from elsewhere in central and southwestern Norway (black rectangles, rotated squares, diamonds) are largely within and about evenly distributed between our northwestern belt adakite and non-adakite fields.

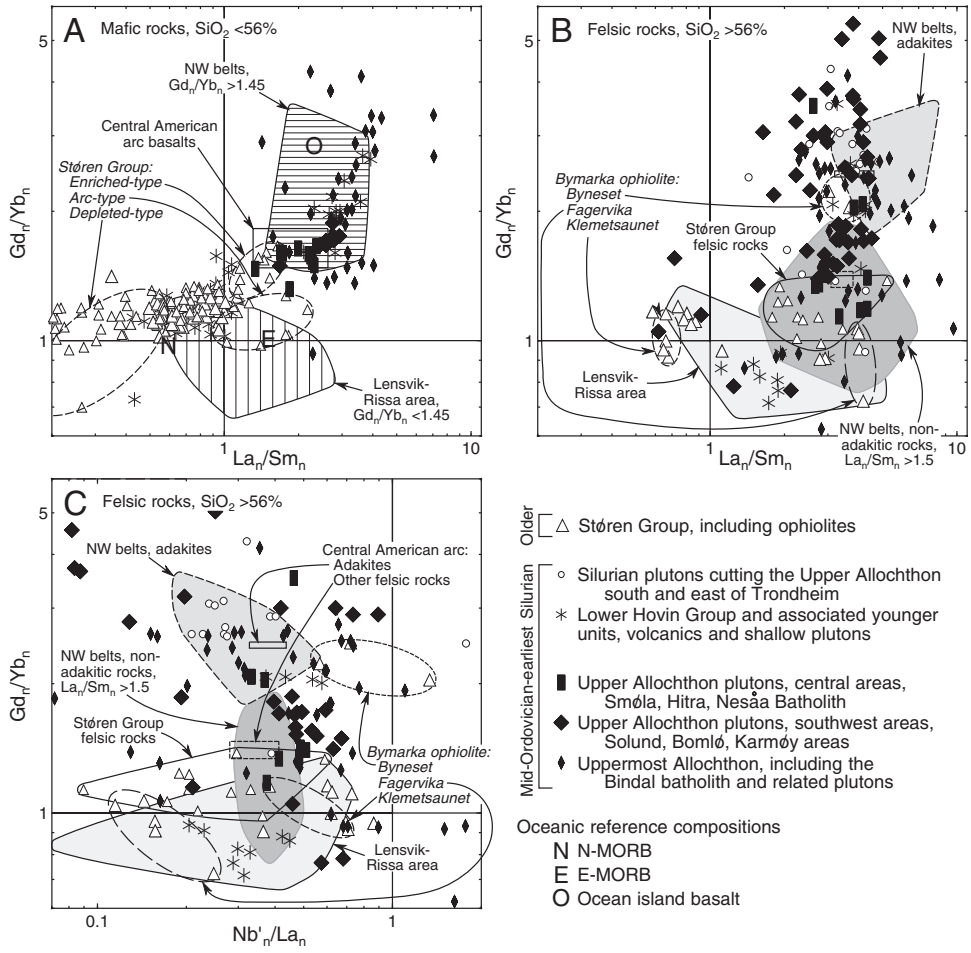

Fig. 11. Comparisons of samples from this study with other plutonic and metamorphosed plutonic rocks from the Upper Allochthon in the area of figure 1, the Upper Allochthon in the Solund–Bomlø–Karmøy area, and the Uppermost Allochthon mostly in the area of figure 1. Shaded fields encompass rock sets of this study from figure 10, and the axes of A–C are the same as in figure 10. The other reference fields are the same as those in figures 6, 7, and 10, and Nb' is the same as in figure 8. Data are from the same sources as in figure 4, but also include data for the Upper Allochthon in southwest Norway and in the Uppermost Allochthon from Furnes and others (1986), Pedersen and Hertogen (1990), Skjerlie (1992), Mørk and others (1997), Hansen and others (2002), and Barnes and others (2003, 2004, 2005).

Figure 11C compares Nb' anomalies in other Upper and Uppermost Allochthon felsic rocks. Although there is considerable scatter, most samples have Nb'_n/La_n ratios <1, characteristic of arcs.

DISCUSSION OF GEOCHEMISTRY

Lensvik and Rissa Areas

One tonalitic gneiss from Lensvik was dated at 482 Ma (Tucker and others, 2004), similar in age to ophiolitic rocks in the nearby Bymarka, Løkken, and other Støren Group ophiolites in central Norway (Stephens and others, 1993; Roberts and Tucker, 1998; Roberts and others, 2002; Gromet and Roberts, 2010; Slagstad and others, 2013).

Mafic rocks in the Lensvik and Rissa areas have REE patterns generally like those in the Støren Group (figs. 6A, 6B and 6F), and also have multi-element anomaly patterns like them (figs. 8A, 8B and 8F). Most felsic rocks in the Rissa area have La_n/Sm_n ratios >1.5, and have REE patterns (figs. 7B and 7F) and anomalies (figs. 9B and 9F) like felsic rocks in the Støren Group, such as the Fagervika Trondhjemite from the Bymarka ophiolite. However, to the extent that data are available, many felsic rocks from Lensvik have flat REE patterns that closely resemble patterns and multi-element anomalies in the Klemetsaunet rhyodacite of the Bymarka ophiolite (figs. 7A, 7F, 9A and 9F), which has been interpreted as an ophiolitic plagiogranite (Slagstad, 2001, 2003; Slagstad and others, 2013). These characteristics lead us to conclude that most of the felsic and mafic plutonic rocks in the Lensvik and Rissa areas are part of the Støren Group.

There are two anomalous geochemical characteristics of these rocks that need further discussion. The first is unusual, sharply negative slopes for the lightest LREE (La–Nd, figs. 6A and 6B), seen in some mafic rocks from Lensvik and Rissa that otherwise have flat or positive slopes (Sm–Lu, samples 269, 271, 274, 418, 459, 460, possibly also 278, 414, 416). The positive LREE slopes may result from mixing of parental basaltic magmas having continuously flat or positive slopes, and a strongly LREE-enriched magma or assimilated wall rock. We calculated model mixtures between apparently anomalous samples and the three most LREE-enriched samples available from the Lensvik and Rissa areas (mafic samples 407 and 421 from Lensvik, figs. 6A and 6B; tonalitic sample 457 from Rissa, figs. 7B and 12).

First, a quadratic expression was fit to normalized Sm to Lu values (excluding Eu) in the mafic samples. The resulting curves are the hypothetical shape of the original, pre-mixing basalt REE patterns (C_{Quad}, thin lines in fig. 12). The LREE-rich contaminant (C_{Con}) was then mixed with the hypothetical parental basalt (C_{Quad}, eq. 1) in different proportions (P_{Con}) to yield the mixtures (C_{Mix}). Variable K offsets the resulting model mixture, which must be richer in all REE compared to the parental magmas, downward onto the actual sample pattern for Sm–Lu. For each sample and for each contaminant, P_{Con} and K were chosen to minimize the sums of the squares of the residuals for all REE (except Pm and Eu) between the actual sample and the model mixture.

$$C_{Mix} = (C_{Con} * P_{Con} - C_{Quad} * (1 - P_{Con})) + K \quad (1)$$

For all nine anomalous mafic samples the lowest sums of the squares of the residuals were found using tonalitic sample 457 as the model contaminant (fig. 12, dashed lines). Hypothetical pre-mixture parental magma compositions were calculated for all analyzed elements (not just REE, not shown) by unmixing the contaminant, in its calculated best-fit proportion, from the original sample composition to check for negative calculated pre-mixture element concentrations. Of 400 element concentrations (50 analyzed elements, nine samples modeled using contaminant sample 457), 5 negative values were found (2 Mo, 1 Ba, 2 Th). Though the mixing models are clearly not perfect, we think mixing uncontaminated basalts with LREE-rich, probably tonalitic material plausibly explains the apparently anomalous, negative LREE slopes for the lightest REE in some mafic samples.

Another aspect of the Lensvik and Rissa area geochemistry that needs additional discussion is the presence, in many felsic rocks, of negative K, Sr, and Li anomalies and lack of positive Pb anomalies (figs. 9 and 9B) that are typical of other samples. Those anomalies are also found in part in the conglomerate boulders from Almlia (fig. 9D), but are rare elsewhere in the northwestern belts (figs. 9C–9E). Globally, felsic rocks with flat REE patterns are quite rare, but are relatively common in ocean ridge and oceanic arc settings, and in many ophiolites. Figure 11 shows multi-element diagrams

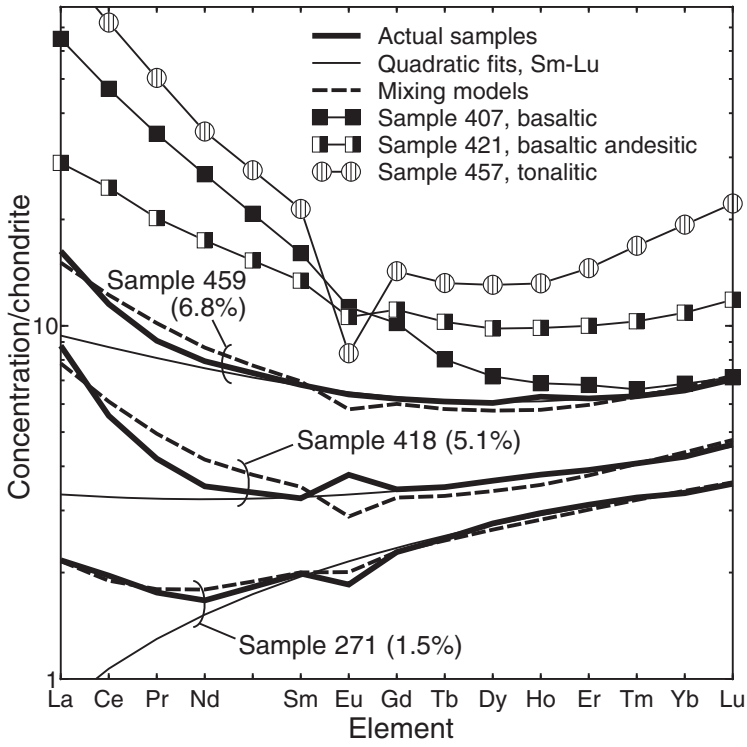

Fig. 12. Models for mafic rocks found at Lensvik and Rissa that have positive or flat slopes in the REE range Sm to Lu, and sharply negative slopes for the lighter REE. Models were calculated as mixtures between several such mafic samples (see text) and three possible contaminants. The model contaminants were samples 407, 421, and 457, which are the most LREE-rich known in the Lensvik–Rissa area. For clarity only models for samples 271, 418, and 459 are shown, for which the contaminant was tonalitic sample 457, which gave the lowest sums of the squares of the residuals for all modeled samples.

plotted for rocks in those environments, including rocks commonly called plagiogranites or quartz keratophyres (modally tonalites, trondhjemites, diorites, or albite granites), or their extrusive equivalents. Though our samples are tonalites, we use the term plagiogranite, after the logic of Coleman and Donato (1979), to distinguish these unusual rocks from other, more typical arc tonalites.

The origin of plagiogranites has been ascribed to a wide variety of processes, including low-pressure, hydrous partial melting of basalt or gabbro, either near axial magma chamber walls or along low-angle detachment faults where the hot lower slab is brought into contact with a cooler, but more hydrous upper slab (Gerlach and others, 1981; Kopke and others, 2004, 2007; France and others, 2010; Brophy and Pu, 2012), low-pressure fractional crystallization of basaltic magma (Coleman and Donato, 1979; Beard, 1998; Floyd and others, 1998; Dilek and Thy, 2006; Bonev and Stampfli, 2008), assimilation of hydrothermally altered crust by evolved mafic magmas (Freund and others, 2013), or more complex processes involving mantle rock (Shervais, 2008).

Volcanics equivalent to plagiogranites from mid-ocean ridges (fig. 13A) tend to have few and small trace element anomalies, with the exception of large negative Sr and Ti anomalies and moderate negative Eu anomalies. Those are probably related to retention of Sr and Eu in plagioclase and Ti in Fe–Ti oxides during low-pressure partial melting or fractional crystallization. In oceanic arcs (fig. 13B)

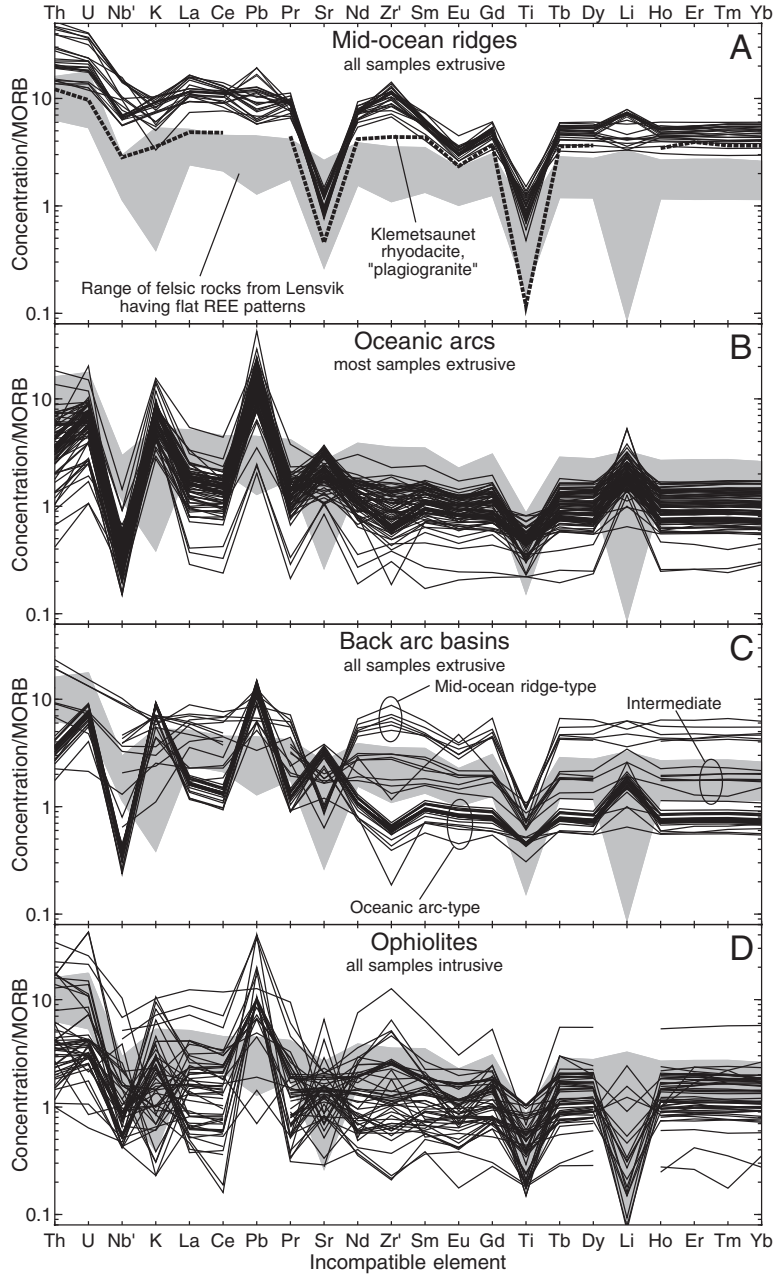

Fig. 13. Comparison of the Lensvik felsic rocks having flat REE patterns (gray field is the full range) with compositionally similar rocks from modern oceanic environments and from ophiolites. Data are from ocean ridges (A; Perfit and Fornari, 1983; Wanless and others, 2010; Freund and others, 2013), oceanic arcs, including forearc parts (B; Reagan and others, 2008, 2010; Straub and others, 2010; Barker and others, 2012; Shaw and others, 2012; Turner and others, 2012), back-arc basins (C; Monjaret and others, 1991; Pearce and others, 1994; Ewart and others, 1994; Nakada and others, 1994; Sinton, and others, 2003; Lytle and others, 2012), and ophiolites (D; Barbieri and others, 1994; Yaliniz and others, 2000; Kaur and Mehta, 2005; Dilek and Thy, 2006; Bonev and Stampfli, 2008; Jiang and others, 2008; Rollinson, 2009; Milovanović and others, 2012; Grimes and others, 2013; Freund and others, 2014). Data were filtered to include only those having 59–75% SiO2 and Lan/Ybn <2, like the Lensvik rocks. MORB normalizing factors are those of Pearce and Parkinson (1993). Nb' and Zr' are the same as in figure 8.

negative Nb' and Ti anomalies and small Zr' anomalies are common, as are positive K, Pb, Sr, and Li anomalies. The positive anomalies are generally interpreted to result from enrichment of the arc basalt mantle source by fluids or melts rising from the subducting slab ("arc component", for example, Pearce and Stern, 2006; Yaliniz, 2008). The arc basalts, derived from mantle melting, carry the subduction component signature into the arc itself, and felsic rocks derived from them inherit the signature. Back-arc basins generally have basalts that range in composition from arc-like to mid-ocean ridge-like, depending on the extent of influence of the subduction zone component (for example, Pearce and Stern, 2006). Figure 13C shows that back-arc basin felsic rocks express the full range between arc and ocean-ridge plagiogranite compositions.

Ophiolite plagiogranites in figure 13D differ from those in 13A–13C in that all are plutonic rather than almost entirely extrusive. The anomalies are generally similar to those of oceanic arcs (fig. 13B), but a substantial fraction have large negative K, Sr, and Li anomalies identical to those seen in many Lensvik felsic rocks (fig. 13, gray fields; figs. 9A and 9B). A smaller fraction of the plagiogranites in figure 13D also have very small or even negative Pb anomalies, like many Lensvik tonalites. Such negative K, Sr, Pb, and Li anomalies in ophiolitic rocks have generally been assumed or modeled to have resulted from element loss by hydrothermal processes involving sea water prior to partial melting of the source basalt (Freund and others, 2013), or after plagiogranite emplacement (Floyd and others, 1998). The concept of extensive water-rock interaction is supported by oxygen and strontium isotope and chlorine content evidence in ophiolitic plagiogranites (for example, Coleman and Donato, 1979; Freund and others, 2013; Grimes and others, 2013). It has also been proposed that the anomalous depletion in K and the other LIL elements was caused by fluid loss during felsic rock crystallization (Beard, 1998). Extrusive plagiogranites generally lack negative K, Sr, Pb, and Li anomalies (figs. 13A–13C), implying that their source rocks and the extrusive plagiogranites themselves never experienced such hydrothermal or fluid loss effects. This implies that, in ophiolites, the negative anomalies developed after emplacement of the intrusive plagiogranite bodies. We infer that the apparent depletion of K, Pb, Sr, and Li relative to REE in most felsic rocks at Lensvik, and some elsewhere, was likely related to post-emplacement hydrothermal processes. If so, then evidence of hydrothermal processes (for example, anastomosing hydrothermal veins) must have either been at a very fine scale, or have been erased by regional amphibolite facies overprinting.

Northwestern Belt Plutonic Rocks and the Implications of Adakites

The northwestern belt plutonic rocks represent magmas produced in a volcanic arc setting, based on calc-alkaline character and subduction zone anomalies in almost all mafic and felsic samples (figs. 4, 5, 8C–8E and 9C–8E). It seems likely that the arc was built on continental crust, based on the abundance of felsic rocks, approximately uniform distribution of lithologies from mafic to felsic (no intermediate SiO_2 composition gap), and comparisons of REE patterns and other chemical characteristics with modern arc analogs. In addition, the relationships between CaO, Na_2O, and MgO and crustal thickness, applied to northwestern belt basaltic rocks, yield estimated crustal thicknesses of 29 km and 38 km, based on CaO and Na_2O, respectively (Plank and Langmuir, 1988). A seemingly unusual characteristic of our northwestern belt data set, and data from calc-alkaline plutonic rocks of similar age elsewhere in the Upper and Uppermost Allochthons (figs. 1 and 11B), is the large proportion of adakites, approximately 50 percent of felsic samples. We have been unable to distinguish adakitic from other felsic rocks in the field or in thin section, so there is unlikely to be any bias toward them in our sample set.

To examine the global abundance and geographic distribution of adakitic rocks, we searched several rock geochemical databases (GEOROC, NAVDAT, PETDB, USGS) for igneous rocks containing non-zero values for Al_2O_3, MgO, K_2O, Na_2O, Sr, Y, La, Sm, Gd, and Yb, and with SiO_2 values in the 56 to 78 percent range. After removing xenoliths, non-igneous, and other irrelevant rocks, we also removed alkaline rocks approximately as defined by Ewart (1982) and Le Bas and others (1986), eliminating analyses having: $K_2O > 0.145*SiO_2 - 5.1$, and $Na_2O + K_2O > 0.176*SiO_2 - 4.2$, respectively. The resulting approximately 15,500 analyses were then compared to the six criteria for adakites defined by Defant and Drummond (1990, listed above). We found that 2200 of the analyses, about 14 percent were adakites according to that definition. Of those, we extracted a subset that also had $La_n/Sm_n > 3$ and $Gd_n/Yb_n > 2$, like adakites in our sample set (figs. 7C and 11B), and 1100, about 7 percent, were adakites with that additional restriction. These percentages assume no important bias toward adakites in the databases.

We plotted the locations of all 15,500 samples on a global map to understand better their distribution and geologic context. Ignoring small numbers of adakites plotting in Precambrian shields, almost all plotted in Phanerozoic arcs or collisional belts. In particular these include the Andes of northern Chile and Argentina (for example, Richards and others 2006) and Ecuador (for example, Hidalgo and others, 2007), the Central American arc (Hildago and others, 2011), the Mesozoic Sierra Nevada (Ratajeski and others, 2001; Paterson and others, 2008) and Idaho (Norman and others, 1992; Gaschnig and others, 2011) batholiths, the northern Cascades (for example, Ickert and others, 2007), the Cretaceous Coast Ranges batholith in southern Alaska and northwestern British Columbia (for example, Drinkwater and others, 1995; Thomas and Sinha, 1999), Mesozoic arc plutons in the eastern Pontides of northern Turkey (for example, Eyuboglu and others, 2011), Neogene volcanics in southern Tibet (for example, Gao and others, 2007), and Miocene volcanic and plutonic rocks in Japan (for example, Shuto and others, 2013).

In general, therefore, adakitic rocks are not particularly rare in Phanerozoic arc environments, and are particularly abundant in arcs on continental margins (for example, the Andes), or otherwise based on continental crust (for example, Japan). Almost no adakites, in our compilation, were found in oceanic arcs. Subduction-related belts rich in adakitic rocks can extend over hundreds of kilometers, much like the extent of the middle Ordovician to earliest Silurian Upper Allochthon arc rocks we discuss, extending from central to southwestern Norway. We interpret these observations to indicate that the northwestern belt rocks we discuss were originally emplaced in a volcanic arc developed on relatively thick continental crust.

Boulders at Almlia Near Follafoss

One granitic gneiss at Follafoss was dated at 460 Ma (Tucker and others, 2004), and we analyzed samples from the same and nearby outcrops (samples 440–443). Just northwest of Follafoss is a small remnant of a sedimentary basin that overlies those gneisses unconformably. The conglomerate clasts include granitoid rocks, rhyolite, and greenschists, and the three boulders we analyzed are tonalites. The sediments are part of the Beitstad Group (Tietzsch-Tyler and Roberts, 1990; see Tucker and others, 2004, and references therein), which is correlated with the Upper Hovin Group, at least in terms of depositional time and setting. The Upper Hovin Group, and the Lower Hovin Group which it immediately overlies, were deposited in the same basin. Multi-element anomalies of the boulders include negative or no Li anomalies, and large negative K anomalies (fig. 9D). These and other characteristics are similar to tonalites from the Lensvik area (fig. 9A) that we have assigned to the Støren Group, and to some felsic rock reference patterns in Støren Group ophiolites (fig. 9F). The trace element evidence indicates that the Almlia tonalite boulders were probably

derived from an ophiolitic source, like the Støren Group, supporting earlier correlations.

NORTHWESTERN BELTS AND AMALGAMATION TIMING

Rocks in the northwestern belts (fig. 3B) are apparently younger than those in the Lensvik and Rissa areas, and the rest of the Støren Group (fig. 3A). The tectonic relationship of the Northwestern Belt rocks to the Støren Group is not entirely clear. Pedersen (1981) and Roberts and others (1984) have suggested that the Lower Hovin Group, which unconformably overlies the Støren Group, and related sedimentary and igneous rocks, were deposited in an arc-related extensional basin. The Dapingian–Darriwilian fauna of warm water, Laurentian affinity in marbles of the Lower Hovin Group are associated with shallow intrusive and volcanic rocks, indicating magmatism around 467 to 465 Ma (David Roberts, written communication, 2015). The adakitic Byneset trondhjemite, which cuts the Bymarka ophiolite of the Støren Group, is dated at 467 Ma (Slagstad and others, 2013), much younger than the host ophiolite but similar in age to the Lower Hovin Group and within the age range of northwestern belt plutons (fig. 3B).

Numerous relatively undeformed 439 to 426 Ma plutons cut the Støren Group and unconformably overlying rocks, the Gula Complex, and the Meråker Nappe (figs. 1 and 3C). These can be thought of as stitching plutons, which, with their negative Nb' anomalies (fig. 11C) and common adakitic REE patterns (fig. 11B), suggest continued subduction after the northwestern belt plutons, Støren Group, Lower Hovin Group and overlying strata, Gula Complex, and Meråker Nappe were all amalgamated, but before Scandian thrusting of allochthons onto Baltica around 425 to 400 Ma (Brueckner and van Roermund, 2004; Gee, 2005; Fossen and Dunlap, 2006).

TECTONIC INTERPRETATION

Figure 14 shows our tectonic interpretation for assemblage of Upper Allochthon segments on Laurentia, with specific reference to calc-alkaline arc rocks in the northwestern belts and related areas in Norway, and to similar composition and age plutonic rocks in the Uppermost Allochthon. Figure 14A shows the starting state of our model, which has a small fragment of continental margin in Iapetus (for example, Harper and others, 1996; Waldron and others, 2014). In this interpretation (figs. 14A–14C, right side), we have put the Tremadoc and older (Gee, 1981; Bjerkgård and Bjørlykke, 1994) Gula Complex, also at a high latitude on the peri-Gondwanan fragment. The oceanic arc to become the Støren Group was active about 500 to 480 Ma, probably close to Laurentia at low southern latitudes (for example, Harper and others, 1996; Torsvik and Cocks, 2013) as indicated by Dapingian–middle Darriwilian fossils in the unconformably overlying Lower Hovin Group (for example, Vogt, 1945; Grenne and Roberts, 1998; figs. 14B and 14C). The Laurentian fauna are found in limestones associated with tholeiitic to alkaline shallow plutons and lavas having strong arc signatures, and which have been interpreted have formed in an arc-related extensional basin (fig. 14C left; Pedersen, 1981; Roberts and others, 1984).

At the same time there was apparently another, possibly shorter-lived volcanic arc and adjacent MORB-type ocean floor that would become incorporated into the Meråker Nappe. This second arc and ocean floor formed at high southern latitudes as indicated by early Darriwilian Celtic cold water fauna found in unconformably overlying serpentinite conglomerate at Otta (fig. 14C right; Bruton and Harper, 1981, 1988; Pedersen and others, 1992; Boe and others, 1993; Harper and others, 2008).

Emplacement of calc-alkaline plutons into the Laurentian margin (fig. 14C) is here related to subduction of Iapetan crust beneath Laurentia. The oldest plutons in this arc may include approximately 479 Ma age rocks in the West Karmøy Igneous Complex in southwestern Norway (Pedersen and Dunning, 1997), and the 477 Ma

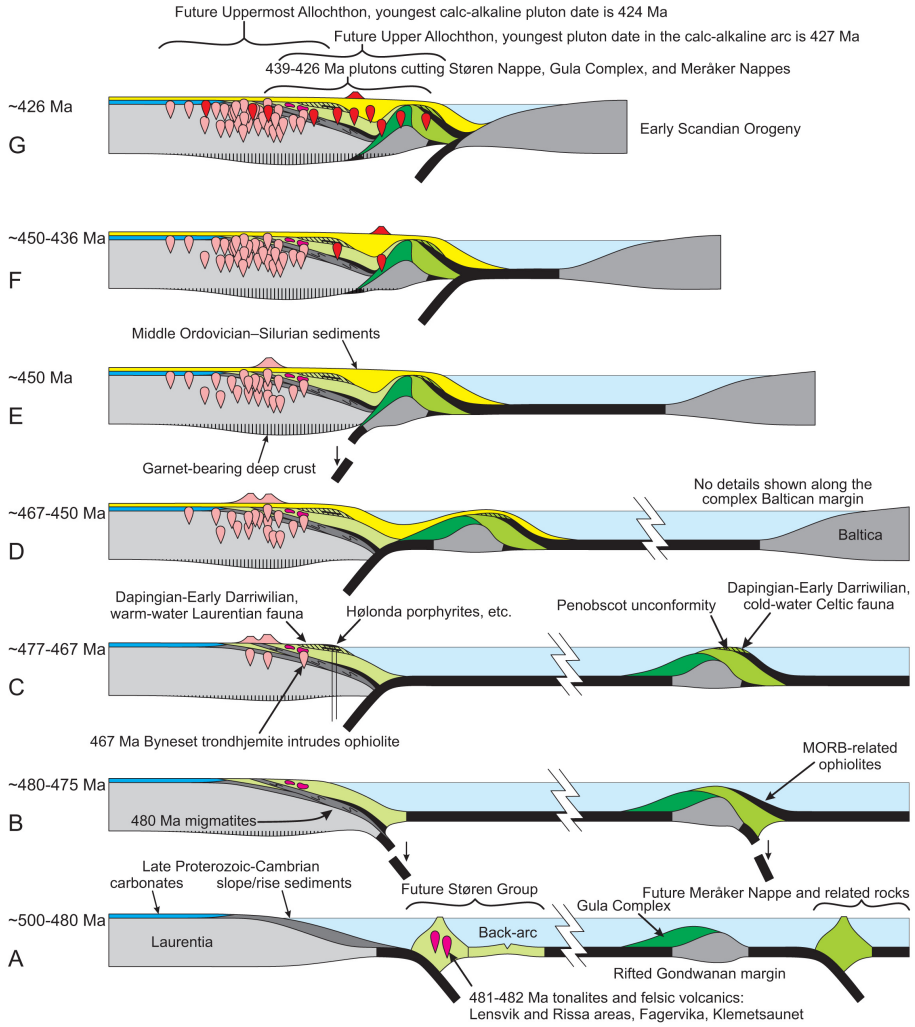

Fig. 14. Tectonic model for the development of different parts of the Upper Allochthon, and their relationships to Laurentia, the Uppermost Allochthon, and Baltica.

Kopparen diorite (Tucker and others, 2004). The presence of middle to early Proterozoic inheritance in zircons from the West Karmøy Igneous Complex, and other isotopic evidence, indicates that arc construction was on continental crust. Because the Upper Allochthon in its eastern part (Gula Complex, Meråker Nappe, figs. 14A–14C) contains little evidence of arc magmatism during middle and late Ordovician time, we interpret the juxtaposition of those rocks with the Støren Group (figs. 12D and 12E) to have occurred after a long episode of subduction beneath the Laurentian margin. Although the exact time of juxtaposition is unclear, it certainly was prior to emplacement of 439 to 426 Ma stitching plutons (figs. 14E and 14F; also fig. 1 south and east of Trondheim). A likely time was during northwest ("Taconian", Roberts and others, 2007) thrusting, recorded in the Uppermost Allochthon (Barnes and others 2007, 2011), ending approximately 450 Ma and before plutons cutting through the thrust sheets dated at 447 Ma. Crustal thickening from accretion of the older arcs, underplat-

ing, and volcanic pile loading permitted the deep crust to reach conditions to stabilize garnet, allowing production of adakitic magmas. Note that in figures 14D–14E, plutons cut Laurentian carbonate rocks, as has been described in the Uppermost Allochthon, in addition to rocks later to become the Støren Group assigned to the Upper Allochthon. Many current workers in Norway now consider it likely that many rocks assigned to the Uppermost and Upper Allochthons do not belong to separate Scandian thrust sheets derived from very different regions, but are parts of the same late Ordovician assemblage on Laurentia.

Figure 14E shows collision of the peri-Gondwanan fragment with Laurentia, though magmatism may have continued for a time during slab detachment and foundering. This collision was followed closely by renewed subduction, ultimately leading to the Silurian–Devonian Scandian collision (fig. 14F). Subduction at that time produced the 439 to 426 Ma plutons, including adakites, that cut the Upper Allochthon south and east of Trondheim, but are absent from the presently underlying Middle and Lower Allochthons. This set of late plutons may also include 437 to 424 Ma plutonic rocks that are present in the Upper and Uppermost Allochthons (see figs. 3B, 3D and 3E) that we have grouped with the older continental arc based on field associations. During the Scandian collision (fig. 14F and afterward), portions of the composite Laurentian margin were transported onto Baltica to form the Upper and Uppermost Allochthons.

comparisons with the northern appalachians

Historically the Bronson Hill magmatic arc of western New England has been described as the arc that collided with the margin of Laurentia to create the Upper Ordovician Taconian orogeny (Stanley and Ratcliffe, 1985). The substrate upon which the arc was built was described as "Medial New England" by Robinson and others (1998). The magmatic rocks are exposed in two belts, an eastern belt of the Bronson Hill Anticlinorium, mostly east of the Connecticut River in western New England, and a western belt west of the river, typified by the rocks in the structural dome at Shelburne Falls, Massachusetts. Geochronology within the Bronson Hill belt in central Massachusetts and southern New Hampshire yielded volcanic ages of 453 and 449 Ma, and ages of intrusive rocks 454 to 442 Ma (Tucker and Robinson 1990). More recent geochronology in the Shelburne Falls and nearby domes yielded ages 479 to 452 Ma (Karabinos and others, 1996, 1998), mostly older than Bronson Hill belt plutons. The apparent age difference between the two belts led these authors to propose that an older Shelburne Falls arc first collided with Laurentia to produce the Taconian orogeny, and that the a separate Bronson Hill arc was produced on the composite Laurentian margin after a flip to a west-dipping subduction zone along a new plate boundary east of the Bronson Hill belt. The arguments for a Middle Ordovician collision and a subduction flip were contested by Ratcliffe and others (1999) and Hollocher and others (2002), who pointed out that an early collision contradicted foreland biostratigraphy, and that the timing of Bronson Hill magmatism in Massachusetts had a close parallel with the final structural stages of Taconian deformation and regional metamorphism ending about 445 Ma, though Hollocher and others did invoke detachment of the east-dipping slab in the interval 449–443 Ma, with magmatism continuing for a time. Dating of volcanic and intrusive rocks in the northern part of the Bronson Hill belt in New Hampshire earlier suggested (Moench 1993, Moench and others 1995, Drake and others, 1989), and now demonstrate (Aleinikoff and others 2015; Valley and others 2015) a Taconian arc age span in that region of 477 to 442 Ma, thus suggesting that both belts belong to the same long-lived arc.

Figure 15 shows a compilation of igneous zircon age dates from the Taconian arc, spanning a 477 to 442 Ma range, which may be compared with the 477 to 440 Ma age range of northwestern belt and similar rocks in the Norwegian Upper Allochthon (fig.

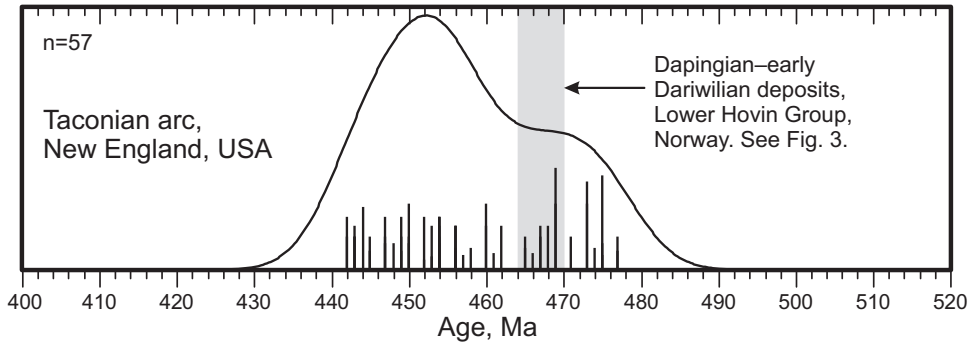

Fig. 15. Kernel probability density estimates of igneous rock U-Pb zircon ages in the Taconian volcanic arc of western New England, U.S.A. See figure 3 for the software reference and plotting details. Data are from Zartman and Leo (1985), Lyons and others (1986), Aleinikoff and Moench (1987, 1992), Tucker and Robinson (1990), Moench and others (1995, and references therein), Karabinos and others (1998), Moench and Aleinikoff (2003), Rankin and others (2012), Aleinikoff and others (2015), and Valley and others (2015). Plotted data includes calc-alkaline gneisses in the Bronson Hill anticlinorium, the Ammonoosuc Volcanics, volcanic rocks in the Partridge Formation, the Highlandcroft plutons, and gneisses in domes of the Shelburn Falls belt. Excluded were Pb/Pb-only dates, and rocks in New Hampshire of uncertain affinity (Moody Ledge, East Inlet plutons) or with zircons of uncertain origin (Tunnel Brook pluton).

3B). The Norwegian rock ages extend to 436 Ma including the Krutfjellet pluton (436 Ma, 65.7°N, Mørk and others, 1997) and Sulitjelma gabbro (437 Ma, 67.1°N, Pedersen and others, 1991). Similarly, the Taconian arc age range may be as young as 435 Ma with inclusion of the Tunnel Brook pluton of New Hampshire, though its zircons apparently require more work (Moench and Aleinikoff, 2003, p. 132).

Detailed studies in New Brunswick and Newfoundland (van Staal and others, 2007; Zagorevski and van Staal, 2011) provided the interpretation that the colliding mass of Medial New England can be interpreted as the western part of a magmatic arc based on the peri-Gondwanan fragment, Ganderia, delineated from Laurentia by the 'Red Indian Line'. These authors drew the 'Red Indian Line' across northern New England to the west of the Bronson Hill belt. A key feature of Ganderia in Canada and eastern Maine is the Penobscot unconformity, overlain by fossiliferous strata containing early Ordovician Celtic cold-water fauna (Neuman, 1964; Neuman and Harper, 1992). The faunal assemblages above the unconformity imply that Ganderia lay at high southern latitude at 477 to 467 Ma, too far away to have collided with low-latitude Laurentia that early. Such a Ganderia interpretation is now supported by detrital zircon studies (MacDonald and others, 2014; Wintsch and others 2015; Coish and others 2015) in units apparently older than the Penobscot unconformity (Boone, 1983) showing that the Moretown Formation in Vermont, and equivalents in New Hampshire, western Maine, western Massachusetts, western Connecticut, and probably extending even into southeastern New York, have a Ganderian signature.

In addition to a Taconian arc age range similar to that of northwestern belt gneisses in Norway, the Taconian arc also contains adakites. These occur in parts of the southern Bronson Hill anticlinorium (Hollocher and others, 2002), some Highlandcroft plutons of northwestern New Hampshire (Dorais and others, 2008), and also in the Notré Dame arc, Newfoundland (Whalen and others, 1997), though in none of those publications were the rocks actually called adakites. The presence of adakites suggests that the Taconian arc, too, was built on thick crust having garnet in its deepest felsic magma source regions.

All present evidence implies that the bulk of the Shelburne Falls–Bronson Hill arc, including the adakites, was built during most of its history on the continental crust of

Ganderia over an east-dipping subduction zone, with scarce need to invoke west-dipping subduction, except perhaps to explain a few late intrusions such as the 445 Ma Middlefield Granite (MacDonald and others 2014) that cuts the trace of the Red Indian Line in Massachusetts (though also possibly explained by magmatism related to Taconian slab detachment, Hollocher and others, 2002). In contrast, the presently understood situation for the equivalent Middle to Late Ordovician magmatic arc in the Scandinavian Caledonides virtually requires subduction beneath Laurentia at times when Ganderia was far away to the south. We suggest that the boundary between the Taconian arc, apparently based on Ganderia at low southern latitudes in Iapetus, and the arc generating the Norwegian northwestern belt plutons, apparently built on the Laurentian margin, was an oceanic transform fault. Such a fault may have been akin to those shown in an Iapetan tectonic model by Waldron and others (2014). An approximate modern analog may be the sinistral transform boundary linking the South Sandwich Islands oceanic arc with the southern Andes continental arc, though direct comparison to our suggested transform fault model requires that the subduction polarities be reversed, with converging rather than diverging arcs.

CONCLUSIONS

It has long been understood that the Paleozoic orogenic belts of the northern Appalachians (for example, Murphy and Dostal, 2007; Fyffe and others, 2011; van Staal and Barr, 2013; Macdonald and others, 2014), the Caledonides of Scandinavia (for example, Pedersen and others, 1992; Roberts, 2003; Gee and others, 2008; Slagstad and others, 2011; Furnes and others, 2012), and the Caledonides of Ireland and Britain (for example, Armstrong and Owen, 2001; Mendum, 2012; Chew and Strachan, 2013) are composite terranes made up of amalgamated parts from within Iapetus, from the Laurentian side, and from the Baltican or Gondwanan sides. In these amalgamations a common element is a long-lived calc-alkaline arc system that was apparently based on thick continental crust, active from the Middle Ordovician into the earliest Silurian. These include but are not limited to the Taconian arc in western New England, the Notré Dame arc of Newfoundland, the Midland Valley terrane of Britain and related rocks in Ireland, the northwestern belts of metamorphosed plutons in the Upper Allochthon of western Scandinavia, and extensive intrusive rocks in the Uppermost Allochthon. The data and interpretations we present help constrain the nature of that arc complex, including the apparent correlation of Ordovician calc-alkaline arc rocks in the Upper Allochthon with a nearly identical set in the Uppermost Allochthon. In our interpretation, plutons in the Upper and Uppermost Allochthons in Scandinavia are from the same arc.

ACKNOWLEDGMENTS

We thank David Roberts for numerous helpful discussions, and particularly for his detailed summary of stratigraphic age relations in the Lower Hovin Group. We thank two reviewers, Michael Dorais and Reinhard Greiling, for their helpful reviews of this manuscript. We thank Union College and the Norwegian Marshall Fund for supporting the field work of Kurt Hollocher, and the Geological Survey of Norway for supporting the field work of Peter Robinson, and Union College again for supporting major element analyses. We thank the National Science Foundation for supporting instrumentation used for trace element analyses (grant DUE–9952410).

APPENDIX 1
TABLE A1
Sample locations

Sample	Quadrangle	Location description	Lat. N	Long. E
225, 226, 227	Ørland	Høgholmen Island, near NGU97.133 Stop 9	63.64031	9.69342
228	Ørland	Høgholmen Island, near NGU97.133 Stop 9	63.64215	9.69352
229	Ørland	Høgholmen Island, near NGU97.133 Stop 9	63.64132	9.69165
230	Ørland	Meholmen Island, near ferry dock., NGU97.133 Stop 9	63.63914	9.68609
231, 232, 233	Ørland	Meholmen Island, near ferry dock., NGU97.133 Stop 9	63.63836	9.68550
234, 235, 236, 238	Ørland	Rishaugen Hill road	63.59597	9.53537
266, 267, 268, 269, 270, 271, 272, 273	Rissa	Almvikneset, NGU97.133 Stop 6	63.53204	9.82939
274, 275, 276, 277, 278, 279, 280	Rissa	Almvikneset, NGU97.133 Stop 6	63.53234	9.82967
290	Hitra	Hagaskjera	63.50042	9.11975
291	Hitra	Hagaskjera	63.49865	9.10695
292	Hitra	Hagaskjera	63.49924	9.11233
293	Hitra	Hagaskjera	63.50027	9.11672
294	Hemne	Hagaskjera	63.49937	9.12558
295	Hemne	Kamvika	63.52731	9.28470
296, 297	Hemne	Kamvika	63.52735	9.28648
298	Hemne	Kamvika	63.52776	9.29057
394	Hemne	Road cut next to the east side of the bridge.	63.41148	8.73084
395	Skardøya	Road cut ~37 m S of the main gate to the gas complex	63.40784	8.69370
396	Skardøya	Road cut at corner ~300 m S of the main gate	63.40467	8.69644
397	Skardøya	Road cut near the intersection with the main road	63.40444	8.70966
398	Skardøya	Myra	63.38956	8.57884
399, 400	Skardøya	Ringskjæret	63.38979	8.59102
401	Skardøya	Skipnesodden	63.39144	8.58552
402	Skardøya	Skogly	63.38597	8.59264
403	Skardøya	Hannholhammaren	63.37134	8.65220
404	Skardøya	Finnset	63.36589	8.51137
405	Skardøya	Blasted outcrop behind the house right next to the abandoned factory building	63.33563	8.45263
406	Hemne	Near Bukta, up the hill E of Kjørsvik	63.41489	8.74433
407	Rissa	Kinebbneset north of hay field	63.54021	9.83108
408, 409, 410, 411, 412	Rissa	Kinebbneset north of hay field	63.53976	9.83115
413	Rissa	Kinebbneset south of hay field	63.53684	9.83116
414, 415	Rissa	Kinebbneset south of hay field	63.53642	8.83111
416	Rissa	North of Almvikneset point	63.52740	9.82601
417	Rissa	North of Almvikneset point, right in front of the boat house	63.52740	9.82601
418	Rissa	North of Almvikneset point	63.52740	9.82601

Table A1
(continued)

Sample	Quadrangle	Location description	Lat. N	Long. E
419	Rissa	On Almvikneset point	63.52740	9.82601
420, 421, 422, 423	Rissa	South of Almvikneset point	63.52569	9.82544
424, 425	Rissa	710 paved pull-off between Almvikneset and Lensvik	63.52426	9.81932
426	Bjugn	Kopparen summit	63.80680	9.73730
427	Bjugn	Kopparen summit	63.80667	9.73689
428	Bjugn	Kopparen summit	63.80597	9.73591
429	Bjugn	Kopparen summit	63.80580	9.73621
430	Bjugn	Kopparen access road above stream	63.80536	9.73688
431	Bjugn	Kopparen access road above stream	63.80520	9.73951
432	Bjugn	Kopparen access road above stream	63.80325	9.74129
433	Bjugn	Kopparen access road above stream	63.80231	9.73745
434	Bjugn	Kopparen access road above stream	63.80111	9.73529
435	Bjugn	Kopparen access road above stream	63.79929	9.73678
436	Bjugn	Kopparen access road above stream	63.79731	9.74093
437	Bjugn	Kopparen access road below stream	63.79378	9.74703
438	Bjugn	Kopparen access road below stream	63.78707	9.74190
439	Tarva	Shoreline outcrop just E of public swimming beach	63.75978	9.66263
440	Verran	Kistovik, shoreline outcrop	63.98723	11.13322
441	Verran	Kistovik, small roadcut across from parking	63.98735	11.13173
442	Verran	Kistovik, large road cut uphill	63.98727	11.12927
443	Verran	Kistovik, large road cut uphill	63.98743	11.13038
444, 445, 446	Holden	Road cut on hill west of Almlia	64.01815	11.09646
447	Holden	Road cut across street from Nerbybokkvatnet	64.00445	10.85443
448, 449	Holden	Road cut across street from Nerbybokkvatnet	64.00309	10.85543
450	Holden	Road cut across street from Nerbybokkvatnet	64.00173	10.85644
451	Holden	Road cut across street from Nerbybokkvatnet	63.99991	10.85826
452	Verran	Quarry just NW of town	63.98888	10.86516
453	Rissa	Ramnfjellet shoreline outcrop	63.54265	9.91991
454	Rissa	Ramnfjellet shoreline outcrop	63.54016	9.91667
455	Rissa	Ramnfjellet shoreline outcrop	63.54001	9.91652
456	Rissa	Ramnfjellet shoreline outcrop	63.53992	9.91661
457	Rissa	Ramnfjellet shoreline outcrop	63.53785	9.91418
458	Rissa	Esvikneset shoreline outcrop	63.53503	9.90991
459	Rissa	Esvikneset shoreline outcrop	63.53482	9.91045
460	Rissa	Esvikneset shoreline outcrop	63.53468	9.91100

Table A1
(continued)

Sample	Quadrangle	Location description	Lat. N	Long. E
461	Rissa	Esvikneset shoreline outcrop	63.53466	9.91133
469	Rissa	Hammarberget shoreline outcrop	63.58398	9.92031
470	Rissa	Hammarberget shoreline outcrop	63.58597	9.92139
471	Rissa	Hammarberget road cut	63.58630	9.92294
481, 482	Rissa	Vikanesset, shoreline outcrop	63.53040	9.91202
484	Rissa	Vikanesset, shoreline outcrop	63.52992	9.91261
488, 489, 490	Rissa	Bukksteinen Quarry, NE side of island on main road	63.68703	9.84722
491	Rissa	Fevåg, N shore, beneath electric cable submergence, shoreline outcrop	63.68982	9.82944
492	Rissa	Westernmost point, shoreline outcrop	63.68457	9.81549
493	Rissa	Westernmost point, shoreline outcrop	63.68382	9.81537
494	Rissa	Nygard, SW point on peninsula, shoreline outcrop	63.67740	9.81861
495	Rissa	Nygard, SW point on peninsula, shoreline outcrop	63.67653	9.82213
496	Rissa	Nygard, SW point on peninsula, shoreline outcrop	63.67655	9.82338
497	Rissa	Nygard, SW point on peninsula, shoreline outcrop	63.67661	9.82374
498	Rissa	Aspstranda, shoreline outcrop	63.69979	9.90252
499	Rissa	Refsneshagen, shoreline outcrop	63.71395	9.97798
500, 501	Rissa	Refsneshagen, shoreline outcrop	63.71516	9.97717
502	Rissa	Refsneshagen, shoreline outcrop	63.71558	9.97723
503, 504	Bjugn	Quarry in cliff on S side of Storosheia	63.75063	10.09983
505	Bjugn	Road cut ~100 m W of the quarry edge	63.73041	10.09763
506, 507	Bjugn	Road cut E of the quarry edge	63.75056	10.10642
508	Bjugn	Road cut E of the quarry edge	63.75030	10.10114
509, 510	Åfjord	300 m N of 718-715 road intersection	63.78148	10.21960
511	Åfjord	1500 m N of 718-715 road intersection	63.79062	10.23357
512	Åfjord	250 m E of 710-715 road intersection	63.80451	10.23290
513, 514, 515	Åfjord	W side of Mosseheia, next to fjord, from N end of road cut	63.95089	10.22660
516	Bjugn	From the W-most point on the road on Finnsetfjellet	63.93311	10.15723
517	Bjugn	100 m S from the W-most point on the road on Finnsetfjellet	63.93218	10.15872
518, 519, 520	Bjugn	Road cut E of the Grandalen road intersection, E end of the roadcut	63.78681	10.02796
521	Bjugn	Road cut W of the Grandalen road intersection, middle of the outcrop	63.78821	10.01897
522	Bjugn	Road cut on N side of road ~600 m W of the road intersection in Stallvika, from just below the Høybakken detachment	63.75623	9.95778
523	Bjugn	SW point of the island at the end of the causeway N of town	63.76361	10.06669
524	Bjugn	SW point of the island at the end of the causeway W of town	63.76101	10.06213

TABLE A1
(continued)

Sample	Quadrangle	Location description	Lat. N	Long. E
525	Bjugn	Road cut ~400 m N of the main road intersection in town	63.76627	10.07735
526	Leksvik	Shoreline outcrops	63.87040	10.85460
527	Leksvik	Low roadcut.	63.89210	10.96160
528	Leksvik	Shoreline outcrops	63.90580	10.95480
531	Ørland	Høgholmen Island	63.6404	9.6922

APPENDIX 2
TABLE A2
Sample descriptions

Sample	Description
225	Felsic gneiss, fine-grained and very light-gray. From the upper part of the lower of the two layers, which connect.
226	Amphibolite, even-grained, fine-grained, medium-gray, little apparent mineral orientation.
227	Hornblendite, dark-gray, medium-grained, from boudins in between more normal amphibolite layers like that of sample 226.
228	Ordovician gneiss, medium-grained, light-gray, foliated rock. Very homogeneous, biotite–plagioclase–quartz gneiss.
229	Ordovician gneiss, from the NW end of the island. Light-gray.
230	Ordovician gneiss, fine-grained, light-gray, fresh.
231	Amphibolite from 3 m below contact with the gneiss, in a relatively unlayered amphibolite section. Medium-gray, medium-grained.
232	Ordovician gneiss, 4 m above contact with amphibolite, out of the thinly layered zone near the contact. Medium-grained, light-gray.
233	Amphibolite 40 m from the contact with Ordovician gneiss and 4 m from the contact with apparent basement gneisses at the E end of the outcrop. Medium-grained, medium-gray.
234	Ordovician gneiss from the blasted interior of a small hut just W of the summit. Light-gray, medium-grained biotite gneiss, possible epidote.
235	Ordovician gneiss from the E side of the roadcut, 5 m from the N end. K-feldspar-bearing, medium-grained, rather mafic compared to the other, more tonalitic samples of this rock.
236	Ordovician gneiss from the W side of the roadcut, near the S end of the outcrop. Light-gray, even-grained biotite gneiss.
238	Ordovician gneiss, fine-grained, light-gray biotite gneiss from 5 m to the left of the contact with Blåhø. Probably strongly sheared.
266	Amphibolite dike 25 cm thick cutting Ordovician gneisses. Plagioclase streaks, dark-gray, fine-grained.
267	Ordovician gneiss, hornblende-bearing from the SW end of the shoreline outcrop. Light-gray, fine-grained, streaky foliation and lineation.
268	Ordovician gneiss, light-gray, fine-grained with sparse small garnets.
269	Amphibolite dike 15 cm thick, somewhat fissile. Fresh rock id dark greenish-gray, fine-grained with biotite smears along the foliation.
270	Amphibolite dike 20 cm thick. Fine-grained, non-fissile, dark-gray, with sparse, small, pale garnets.
271	Amphibolite dike 1 m thick. Dark greenish-gray, fine-grained, layered in places.
272	Ordovician gneiss, medium-gray, medium-grained, biotite gneiss from a homogeneous layer.
273	Amphibolite dike 40 cm thick, somewhat fissile weathering, dark greenish-gray, fine-grained.
274	Amphibolite dike 35 cm thick, fine-grained and dark greenish-gray. Clearly crosscuts veins and other features in gneiss.
275	Ordovician gneiss, hornblende-bearing, medium-gray from a homogeneous 30 cm above the dike of sample 274.
276	Amphibolite composite dike 35 cm thick, plagioclase-streaked layer.
277	Amphibolite composite dike 35 cm thick, garnet-bearing layer.
278	Amphibolite composite dike 35 cm thick, fissile-weathering layer.
279	Ordovician gneiss, hornblende-bearing, medium-grained, light-gray.
280	Ordovician gneiss, hornblende-bearing, fine-grained, medium-gray.
290	Ordovician gneiss, fine-grained, medium pinkish-gray with some pike feldspar and considerable epidote.
291	Ordovician gneiss, medium-grained and light pinkish-gray with feldspar augen up to 1 cm long. Not dismembered veins. From the point farthest NW toward Hitra, farthest outboard.

Table A2
(continued)

Sample	Description
292	Ordovician gneiss, medium-grained, light gray with very few augen. Considerable epidote in the plane of the foliation.
293	Ordovician gneiss, fine-grained and light-gray. Contains small numbers of large (4 mm) euhedral titanite and similarly large allanite grains.
294	Ordovician gneiss, fine-grained, medium-gray, very homogeneous where sampled, from a low blasted roadcut on the top of the hill on the point.
295	Ordovician gneiss, dark pinkish-gray, somewhat migmatitic, but much less so and much straighter foliation than basement seen on access road. Coarse grained with biotite, hornblende, quartz, K-feldspar, plagioclase.
296	Ordovician gneiss, medium-grained, hornblende-bearing, medium pinkish-gray.
297	Hornblendite dike cutting gneissic layering. Coarse-grained, dark green, 30 cm thick.
298	Ordovician gneiss, medium-grained, medium-gray hornblende-bearing gneiss. More leucocratic than samples 297 and 296.
394	Felsic gneiss, coarse-grained, dark-gray, with large allanite grains and secondary epidote. Thickness of layer indefinite, but many 10s of meters.
395	Felsic gneiss, medium-grained, medium-gray, well-foliated and lineated. Thickness of layer indefinite, but many meters.
396	Felsic gneiss, medium-grained, medium-gray, somewhat foliated and lineated, with hornblende-rich segregations ~1 cm across; sample is without segregations. Thickness of layer indefinite, but many meters.
397	Felsic gneiss, coarse-grained, medium-gray, associated coarse hornblende-rich pegmatitic segregations not included in sample. Thickness of layer indefinite, but many meters.
398	Felsic gneiss, medium-grained, light medium-gray, some epidote, deformed pegmatite with euhedral hornblendes not included in sample. Thickness of layer indefinite, but many meters.
399	Amphibolite, fine-grained, dark-gray amphibolite, folded layer in sample 400 gneiss, only ~8 cm thick.
400	Felsic gneiss, medium-grained, medium-gray, from 3 m W of sample 399, just 5or 6 m from the point. Thickness of layer indefinite, but many meters.
401	Felsic gneiss, medium–grained, light-gray, not so homogeneous but looks like intrinsic inhomogeneities. Lightest collectable gneiss along the outcrops here. 3 m thick layer.
402	Felsic gneiss, coarse-grained, medium-gray. Sparse mafic enclaves. Thickness of layer indefinite, but many meters.
403	Felsic gneiss, fine-grained, light-gray. Thickness of layer indefinite, but many 10s of meters.
404	Felsic gneiss, coarse-grained, medium-gray. Thickness of layer indefinite, but many meters. From next to bonfire pit so sample not useful for fission track or argon work.
405	Felsic gneiss, medium-grained, medium-gray. Thickness of layer indefinite, but many meters.
406	Felsic gneiss, coarse-grained, medium-gray. Thickness of layer indefinite, but many 10s of meters, same appearance as sample 394 down the hill.
407	Amphibolite, fine-grained, gray-green, hornblende-rich layer ~0.5 m thick that is relatively homogeneous.
408	Amphibolite, plagioclase porphyritic, dark-gray, fine-grained, layer 15 cm thick in layered section, very streaky appearance.
409	Felsic gneiss cutting greenstone (?). Large hornblende crystals in a quartz–feldspar matrix. Light-gray, coarse-grained.
410	Felsic gneiss, dike cutting greenstones. This sample is from the S side of the dike and has garnet and cummingtonite.
411	Felsic gneiss, dike cutting greenstones. This sample is from the N side of same dike as 410. Hornblende–cummingtonite, sparse garnet.
412	Amphibolite, medium-grained, dark gray, very fresh. Possible deformed pillow selvages in photo.
413	Felsic gneiss, medium-light gray, medium-grained, biotite gneiss.
414	Amphibolite dike ~1 m thick, dark greenish-gray, coarse-grained, cutting gneiss.
415	Amphibolite dike, medium-grained, dark-gray, from a homogeneous layer 0.6 m thick. Near contact with volcanics so it may be a xenolith in host gneisses. Several like this, look like dikes.
416	Amphibolite, dark-gray, fine-grained, from a layered section.

Table A2
(continued)

Sample	Description
417	Felsic gneiss, hornblende, light-medium gray, medium-grained, sparse garnets.
418	Amphibolite, dark greenish-gray, coarse grained, plagioclase porphyry. From a layer meters thick.
419	Amphibolite, medium-gray, medium-grained with some biotite. 30 cm thick homogeneous layer in very layered section of mafic and intermediate rocks.
420	Felsic gneiss, light gray, medium-grained, matrix to abundant mafic xenoliths in photos. Garnet-bearing.
421	Amphibolite, coarse-grained, dark gray, relatively homogeneous layer of plagioclase porphyry many meters thick.
422	Hornblendite dike cutting coarse gabbroic rocks of 421. Dark-gray, coarse-grained, essentially no foliation, strongly boudinaged into pods up to 0.6 m thick.
423	Felsic gneiss, light-gray, medium-grained, biotite with sparse garnets, from a layer 5 m thick between gabbroic rocks.
424	Amphibolite, dark greenish-gray, medium grained, relatively homogeneous layer ~1 m thick in layered section.
425	Amphibolite, dark-gray, medium-grained, very mafic. From boudin ~0.5 m thick in intrusion breccia section.
426	Felsic gneiss, coarse-grained, medium-gray, little deformed, from Kopperan summit.
427	Felsic gneiss, coarse-grained, medium-gray, little deformed, from Kopperan summit.
428	Felsic gneiss, medium-grained, medium-gray, little deformed, top of quarry at last road turn to summit.
429	Felsic gneiss, medium-grained, medium-gray, bottom of quarry at last road turn to summit.
430	Hornblendite, very coarse-grained, greenish-black ultramafic rock in boudin.
431	Felsic gneiss, medium-grained, medium-gray, massive with little foliation, from above a prominent shear zone.
432	Felsic gneiss, coarse-grained, medium-gray with prominent black and white streaks. From below the northernmost switchback.
433	Felsic gneiss, medium-grained, medium-gray biotite gneiss, middle of this section of road between the switchbacks.
434	Felsic gneiss, medium to fine-grained, medium-gray biotite gneiss from below lower switchback.
435	Felsic gneiss, medium-grained, medium-gray tonalite gneiss.
436	Felsic gneiss, medium-grained, medium-gray hornblende–biotite gneiss.
437	Felsic gneiss, medium-grained, medium-gray hornblende–biotite gneiss, ~200 m below the stream from the swamp.
438	Felsic gneiss, coarse-grained, medium-gray, hornblende–biotite gneiss, low roadcut at rise in road ~1 km below stream from swamp.
439	Felsic gneiss, mylonitic, fine-grained with coarse plagioclase porphyroblasts.
440	Felsic gneiss, coarse-grained, mylonitic, light-gray biotite granodiorite gneiss, feldspar porphyroclasts up to 5 mm. Large allanite.
441	Felsic gneiss, coarse-grained, medium-gray biotite granodiorite gneiss, feldspar porphyroclasts up to 5 mm. Less muscovite and less mylonitic than 440.
442	Mafic dike, 0.7 m thick, medium-grained, greenish-black, biotite–chlorite–quartz, no hornblende recognized.
443	Felsic gneiss, very coarse-grained, light pinkish-gray biotite granodiorite gneiss, feldspar porphyroclasts up to 12 mm. Pervasive epidote.
444	Felsic gneiss, boulder in Almlia Conglomerate.
445	Felsic gneiss, boulder in Almlia Conglomerate.
446	Felsic gneiss, boulder in Almlia Conglomerate.
447	Felsic gneiss, coarse-grained, medium-gray, hornblende–biotite diorite, sparse mafic xenoliths.
448	Felsic gneiss, coarse-grained, medium-gray, hornblende–biotite diorite, sparse mafic xenoliths.
449	Xenolith, 7 meter block of volcanics (?), dark-greenish-gray, fine-grained (mostly), possible pillows, volcaniclastics, or small blocks.
450	Xenolith, small xenolith 4 cm thick, black, fine-grained.
451	Felsic gneiss, coarse-grained, medium-gray, hornblende–biotite diorite, sparse mafic xenoliths.

Table A2
(continued)

Sample	Description
452	Felsic gneiss, coarse-grained, medium-gray, hornblende–biotite granodiorite.
453	Felsic gneiss, medium-grained, medium-gray, strongly biotite-streaked in plane of foliation.
454	Mafic xenolith in felsic gneiss, 0.5 m thick. Medium-grained, dark-gray.
455	Mafic xenolith in felsic gneiss, 0.5 m thick. Medium-grained, dark-gray, but not as mafic as 454.
452	Felsic gneiss, coarse-grained, medium-gray, hornblende–biotite granodiorite.
456	Felsic gneiss, coarse-grained, medium-gray, , taken from a zone ~7 m thick relatively free of xenoliths, sampled as a partner for the xenoliths.
457	Felsic gneiss, medium-grained, light-gray with pinkish oxidation veins, more leucocratic than 453 and 456.
458	Felsic gneiss, medium-gray, medium-grained, typical gneiss in a relatively inclusion-free zone ~50 m N of contact with volcanics.
459	Amphibolite, medium-grained, medium-gray, biotite-rich, part of a mafic-rich layer ~15 m thick closer to the contact than sample 458.
460	Amphibolite, medium-grained, medium-gray, biotite-rich, part of a mafic-rich layer ~3 m thick still closer to the contact than sample 458 and 459.
461	Felsic gneiss dike cutting layered volcanics, 5 m S of sheared gneiss–volcanic contact. Medium-gray, medium-grained. Looks like the other sampled gneisses.
469	Felsic gneiss, medium-grained, medium-gray, hornblende–biotite-garnet tonalite.
470	Felsic gneiss, medium-grained, medium-gray, hornblende–biotite.
471	Felsic gneiss, medium-grained, medium-gray, hornblende–biotite tonalite.
481	Felsic gneiss, medium-grained, medium-gray, biotite–garnet–hornblende.
482	Felsic gneiss, medium pinkish-gray, coarse-grained, ~60' N of sample 481, from edge of rusty cliff on shore.
484	Felsic gneiss, medium to fine-grained, light pinkish-gray, leucocratic, 30 cm N of contact with Støren greenstone.
488	Felsic gneiss, medium-grained, medium-gray, sizable titanite and large allanite, N side of quarry.
489	Felsic gneiss, medium-grained, medium-gray, sizable titanite and large allanite, distributed epidote, W side of quarry.
490	Felsic gneiss, medium-grained, medium-gray, little titanite with moderate size allanite, distributed epidote, S side of quarry.
491	Felsic gneiss, medium-grained, medium-gray, sparse garnets, common titanite.
492	Felsic gneiss, medium-gray, medium-grained, lots of titanite and some allanite. Sample is from extreme N end of outcrop.
493	Felsic gneiss, medium-gray, medium-grained, lots of titanite and some allanite. Sample is from extreme S end of outcrop.
494	Felsic gneiss, medium to fine-grained, medium-gray, little to see besides quartz, biotite, and feldspar.
495	Felsic gneiss, medium to fine-grained, medium-gray, little to see besides quartz, biotite, and feldspar; tiny allanite.
496	Amphibolite, medium to fine-grained, medium to dark gray, hornblende–biotite dioritic.
497	Amphibolite, medium-grained, medium-gray, hornblende–biotite dioritic.
498	Felsic gneiss, coarse-grained, medium-gray, hornblende, titanite.
499	Amphibolite, coarse-grained, very dark gray, 10 cm thick homogeneous layer in a coarse gabbroic section, 7 m N of contact with Blåhø.
500	Amphibolite, medium-grained, very dark-gray, N of decaying wharf, S end of outcrop just above beach gravel.
501	Felsic gneiss, medium-grained, medium-gray, hornblende and small titanite, 5 m N of sample 500.
502	Felsic gneiss, light-gray, medium to fine-grained, from layers ~100 m N along the outcrop from sample 500.
503	Amphibolite, dark-gray, medium-grained, 0.6 m thick layer, W end of the quarry.
504	Felsic gneiss, light-gray, medium-grained, 0.6 m thick layer, biotite-bearing, middle of quarry.
505	Felsic gneiss, medium to fine-grained, medium-gray, hornblende–biotite–titanite.

Table A2
(continued)

Sample	Description
452	Felsic gneiss, coarse-grained, medium-gray, hornblende–biotite granodiorite.
506	Amphibolite, dark-gray, medium-grained.
507	Felsic gneiss, medium-grained, medium-gray, from between dikes, hornblende–biotite–allanite.
508	Felsic gneiss, medium to fine-grained, medium-gray.
509	Amphibolite, dark-gray, medium-grained.
510	Felsic gneiss, medium-grained, medium-gray.
511	Felsic gneiss, medium-grained, medium-gray, biotite–hornblende.
512	Felsic gneiss, coarse-grained, medium-gray, hornblende.
513	Felsic gneiss, medium-grained, medium to dark-gray.
514	Felsic gneiss, medium-grained, medium to dark-gray, hornblende–biotite–titanite.
515	Amphibolite, fine-grained, dark-gray, hornblende–biotite–titanite xenolith in sample 514 gneiss.
516	Amphibolite, dark-gray, medium-grained, hornblende–plagioclase rock.
517	Amphibolite, medium to dark-gray, medium-grained, hornblende–plagioclase rock.
518	Felsic gneiss, medium-grained, medium-gray, biotite.
519	Amphibolite, coarse-grained, dark greenish-gray gabbro.
520	Felsic gneiss, medium to fine-grained, medium-gray.
521	Felsic gneiss, medium to fine-grained, medium-gray.
522	Felsic gneiss, medium-gray, fine-grained and mylonitic, real mylonites here too.
523	Felsic gneiss, light-gray, medium-grained, biotite–titanite–allanite.
524	Felsic gneiss, medium-gray, medium-grained, biotite–titanite–allanite.
525	Felsic gneiss, medium-gray, medium-grained, biotite–titanite–allanite.
526	Felsic gneiss, light-greenish-gray, coarse to medium grained, muscovite–epidote gneiss probably with no biotite.
527	Felsic gneiss, medium-grained, medium greenish pink, perhaps with biotite.
528	Felsic gneiss, coarse-grained, medium pinkish green-gray, more biotite than 526 or 527.
531	Mafic layer in felsic gneiss, 14" thick, 100' N of gneiss contact.

APPENDIX 3
TABLE A3
Sample chemical analyses

Sample	267	268	270	272	275	279	280	409	410	411	413	415	276	277	417	419
Region	L-R	L-R	L-R	L-R	L-R	L-R	L-R	L-R	L-R	L-R	L-R	L-R	L-R	L-R	L-R	L-R
Location	Lens	Lens	Lens	Lens	Lens	Lens	Lens	Lens	Lens	Lens	Lens	Lens	Lens	Lens	Lens	Lens
Type	PG	PG	PG	PG	PG	PG	PG	PG	PG	PG	PG	PG	FE	FE	FE	FE
SiO2	65.23	75.51	60.71	62.68	64.93	74.91	60.00	73.15	73.42	74.49	67.52	59.06	57.66	56.24	71.87	56.01
TiO2	0.72	0.19	1.09	0.97	0.77	0.32	1.07	0.39	0.42	0.41	0.67	0.80	0.49	0.51	0.30	0.31
Al2O3	14.69	12.16	14.76	15.31	15.27	13.14	16.28	12.85	13.05	12.75	15.12	15.80	14.68	14.76	13.54	15.61
FeO	8.31	3.37	8.59	7.09	5.75	2.15	7.87	4.02	4.12	3.23	5.07	9.23	11.33	11.85	4.08	7.89
MnO	0.14	0.06	0.15	0.20	0.14	0.03	0.18	0.07	0.06	0.05	0.07	0.13	0.17	0.16	0.07	0.13
MgO	0.91	0.36	3.04	1.83	1.39	0.60	1.71	0.80	0.91	0.96	1.42	3.22	3.43	3.62	1.15	6.70
CaO	3.05	1.16	4.14	4.61	3.99	1.60	5.13	2.25	0.98	1.88	2.79	6.55	7.40	9.19	4.44	10.78
Na2O	5.95	6.17	6.57	5.33	6.36	6.33	5.83	6.09	6.67	5.91	6.88	4.68	3.47	2.35	3.72	1.96
K2O	0.18	0.05	0.10	0.69	0.26	0.08	0.45	0.17	0.06	0.05	0.16	0.23	0.40	0.48	0.63	0.44
P2O5	0.28	0.02	0.24	0.46	0.33	0.07	0.45	0.09	0.09	0.08	0.17	0.13	0.07	0.06	0.07	0.02
CO2	0.11	0.33	0.22	0.37	0.30	0.22	0.52	0.04	0.11	0.04	0.04	0.04	0.37	0.41	0.04	0.04
S	0.01	0.06	0.01	0.01	0.01	0.01	0.01	0.01	0.02	0.07	0.01	0.03	0.18	0.04	0.01	0.01
SUM	99.58	99.44	99.62	99.55	99.50	99.46	99.50	99.93	99.91	99.92	99.92	99.90	99.65	99.67	99.92	99.90
LOI	1.1	0.2	0.7	1.0	0.6	0.6	0.2	0.9	0.3	0.2	0.1	0.2	0.9	1.3	0.2	0.8
Trace elements, ppm																
Li	1.5	0.4	4.1	10.1	2.9	1.3	13.9	1.4	1.8	2.6	0.9	1.6	14.6	11.0	2.8	6.7
Be	0.85	1.18	1.62	0.76	1.06	0.58	0.99	0.53	0.34	0.28	0.83	1.11	0.87	0.52	0.63	0.31
Sc	14	4	25	15	12	5	20	6	6	7	9	21	42	44	13	37
V	2.2	0.2	156.4	44.8	12.2	0.5	15.9	9.5	6.0	11.9	26.4	188.3	446.1	474.0	47.5	190.9
Cr	2.5	0.7	3.9	2.5	1.9	0.5	2.7	1.6	1.3	0.7	1.1	5.9	15.9	17.3	5.4	76.6
Co	2.2	0.9	14.6	6.6	2.5	1.9	4.8	3.1	3.4	3.1	5.5	18.3	30.4	32.4	8.1	31.5
Ni	0.4	0.2	2.7	0.6	0.5	0.4	1.0	0.7	1.1	0.8	0.7	3.3	14.0	15.0	3.1	32.2
Cu	2	2	5	1	1	3	2	0	3	24	0	10	124	76	7	28
Zn	37	23	67	52	34	14	50	27	31	21	20	40	89	88	36	55
Ga	16.6	14.2	20.4	15.0	15.8	16.3	21.9	12.8	11.1	12.3	15.4	16.5	16.1	16.0	11.8	12.3
Rb	1.9	0.7	0.9	11.2	2.6	2.0	7.2	2.5	0.7	0.1	2.1	1.9	6.0	8.1	15.2	10.7
Sr	135	57	84	143	125	81	170	95	24	50	116	238	146	200	127	144
Y	57.9	65.2	39.6	56.4	65.1	57.3	71.7	44.1	45.4	49.3	43.3	33.5	11.5	10.8	19.6	12.9
Zr	166	262	110	98	149	169	115	217	218	215	117	81	33	29	116	40
Nb	3.9	6.9	4.0	5.4	4.6	5.2	6.1	4.7	5.2	3.2	3.7	2.6	1.6	1.5	2.3	2.3
Mo	1.610	0.534	0.434	1.442	0.205	0.131	0.642	0.106	1.671	0.459	0.055	0.051	0.547	0.325	0.112	0.122
Sn	2.06	2.02	0.80	1.37	1.44	1.85	1.90	1.32	0.97	1.25	2.49	0.86	0.26	0.32	0.31	0.43
Cs	0.06	0.04	0.05	0.48	0.08	0.09	0.24	0.06	0.04	0.01	0.03	0.08	0.15	0.14	0.39	0.18
Ba	54	28	20	208	189	46	167	13	5	6	68	62	43	86	229	76
La	7.6	12.1	6.0	10.2	11.9	12.9	11.3	9.2	10.0	7.8	9.4	6.4	4.0	4.0	6.8	4.4
Ce	23.4	33.2	16.5	27.6	31.8	30.1	33.9	24.7	27.5	21.6	22.6	15.9	8.7	8.5	13.8	9.3
Pr	3.9	5.0	2.6	4.2	4.8	4.2	5.5	3.1	3.6	2.9	3.1	2.3	1.1	1.1	1.7	1.1
Nd	19.9	24.3	12.8	21.2	23.0	20.2	28.2	14.1	17.0	13.4	15.3	11.3	4.5	4.4	7.4	4.6
Sm	6.84	7.74	4.21	6.92	7.38	6.51	9.16	4.28	5.11	3.75	4.58	3.51	1.19	1.14	2.13	1.22
Eu	2.31	1.86	1.37	1.88	1.90	1.78	2.20	1.08	1.15	1.03	1.26	1.10	0.38	0.38	0.59	0.36
Gd	8.71	9.52	5.47	8.64	9.25	8.02	11.27	5.27	6.26	4.95	5.88	4.61	1.34	1.31	2.64	1.57
Tb	1.53	1.75	0.98	1.52	1.68	1.46	1.92	0.95	1.10	0.94	1.02	0.80	0.25	0.23	0.46	0.28
Dy	10.14	11.90	6.54	9.89	11.29	9.77	12.56	6.59	7.35	6.97	6.77	5.39	1.71	1.65	3.17	1.95
Ho	2.21	2.70	1.42	2.14	2.50	2.12	2.69	1.52	1.64	1.66	1.49	1.18	0.41	0.38	0.71	0.44
Er	6.39	8.06	4.06	6.09	7.31	6.11	7.61	4.80	4.91	5.17	4.31	3.41	1.25	1.17	2.12	1.34
Tm	0.95	1.24	0.62	0.90	1.12	0.93	1.13	0.80	0.80	0.84	0.67	0.52	0.21	0.19	0.34	0.21
Yb	6.03	7.94	3.97	5.61	7.17	6.02	6.98	5.63	5.46	5.91	4.47	3.49	1.39	1.29	2.22	1.45
Lu	0.91	1.19	0.61	0.84	1.05	0.89	1.03	0.93	0.90	0.97	0.72	0.56	0.23	0.21	0.36	0.24
Hf	4.79	7.78	3.20	3.24	4.70	5.07	3.40	6.50	6.60	6.50	3.55	2.52	0.92	0.86	2.96	1.22
Ta	0.23	0.39	0.18	0.28	0.30	0.30	0.27	0.30	0.32	0.28	0.20	0.17	0.09	0.08	0.08	0.13
Pb	0.61	0.39	0.71	0.89	1.03	0.72	0.67	1.31	0.54	0.57	1.27	1.34	5.08	7.90	4.18	3.90
Th	0.8	1.3	0.9	0.9	1.1	1.5	1.0	1.9	1.9	1.9	1.2	1.0	1.4	1.0	0.6	1.0
U	0.31	0.51	0.26	0.30	0.37	0.37	0.25	0.73	0.79	0.83	0.39	0.36	0.38	0.40	0.35	0.33
Lan/Smn	0.7	1.0	0.9	0.9	1.0	1.2	0.8	1.3	1.2	1.3	1.3	1.1	2.1	2.2	2.0	2.3
Gdn/Ybn	1.2	1.0	1.1	1.2	1.0	1.1	1.3	0.8	0.9	0.7	1.1	1.1	0.8	0.8	1.0	0.9
Lin/Hon	0.2	0.0	0.7	1.1	0.3	0.1	1.2	0.2	0.3	0.4	0.1	0.3	8.3	6.8	0.9	3.5

TABLE A3
(continued)

Sample	423	453	454	455	456	457	458	461	469	470	471	481	482	484	420	266
Region	L-R	L-R	L-R	L-R	L-R	L-R	L-R	L-R	L-R	L-R	L-R	L-R	L-R	L-R	L-R	L-R
Location	Lens	Riss	Riss	Riss	Riss	Riss	Riss	Riss	Riss	Riss	Riss	Riss	Riss	Riss	Lens	Lens
Type	FE	FE	FE	FE	FE	FE	FE	FE	FE	FE	FE	FE	FE	FE	Pec	MF
SiO2	75.24	70.10	56.97	58.45	70.98	77.02	70.32	70.60	65.51	65.99	65.91	72.68	69.39	75.18	75.40	53.34
TiO2	0.24	0.30	0.62	0.69	0.29	0.15	0.34	0.33	0.30	0.29	0.29	0.61	0.73	0.40	0.20	0.59
Al2O3	13.17	14.94	16.16	16.03	14.37	12.77	14.30	14.53	16.23	15.92	15.85	13.23	13.82	12.80	13.12	17.57
FeO	2.64	3.85	10.24	9.37	3.69	1.61	4.29	3.97	6.44	5.90	6.14	4.42	4.86	2.47	2.78	10.45
MnO	0.05	0.07	0.15	0.18	0.07	0.03	0.09	0.06	0.12	0.11	0.11	0.21	0.14	0.06	0.03	0.16
MgO	0.45	1.20	3.70	3.01	1.12	0.26	1.24	1.07	1.74	1.78	1.82	1.06	1.20	0.53	0.66	3.94
CaO	3.61	3.96	6.75	6.79	3.47	1.37	3.97	4.02	5.54	5.81	5.89	2.13	3.78	2.86	3.17	9.35
Na2O	3.81	3.87	3.93	3.25	3.73	4.45	3.74	4.68	3.05	3.30	3.18	4.83	5.57	5.30	3.67	3.36
K2O	0.61	1.60	1.31	1.99	2.17	2.20	1.60	0.67	0.90	0.82	0.76	0.46	0.17	0.20	0.71	0.58
P2O5	0.06	0.07	0.09	0.12	0.08	0.04	0.09	0.08	0.07	0.07	0.07	0.14	0.21	0.07	0.06	0.07
CO2	0.04	0.07	0.11	0.11	0.07	0.11	0.07	0.04	0.11	0.04	0.04	0.11	0.15	0.07	0.04	0.34
S	0.01	0.01	0.02	0.05	0.01	0.05	0.01	0.01	0.01	0.01	0.01	0.17	0.02	0.12	0.07	0.01
SUM	99.93	100.04	100.05	100.04	100.05	100.06	100.06	100.06	100.02	100.04	100.07	100.05	100.04	100.06	99.91	99.76
LOI	0.2	0.7	0.5	0.6	0.9	0.2	0.5	0.7	0.8	0.2	0.6	0.9	0.4	0.1	0.1	1.1
Trace elements, ppm																
Li	2.7	8.9	10.0	13.1	10.2	3.0	9.9	2.8	9.9	8.7	8.5	2.5	1.1	0.6	2.0	7.1
Be	0.73	0.51	0.71	1.13	0.59	0.62	0.61	0.19	0.44	0.48	0.48	0.60	0.47	0.29	0.54	0.51
Sc	15	9	25	30	10	4	12	10	21	18	20	13	14	8	1	37
V	10.6	37.0	235.8	167.9	33.6	4.4	53.4	56.3	65.0	75.5	80.9	11.8	14.3	6.6	15.0	314.7
Cr	1.1	4.2	5.5	3.1	3.8	0.6	5.2	4.1	3.2	3.4	3.4	1.0	1.1	0.1	2.6	39.4
Co	3.6	8.0	24.3	19.0	6.8	2.5	8.2	8.4	13.3	12.6	13.5	3.0	4.6	2.2	5.1	31.9
Ni	0.9	3.1	7.7	1.0	1.8	0.4	2.4	2.3	3.5	3.7	3.6	0.6	0.7	3.0	1.7	21.8
Cu	3	0	15	16	0	21	0	8	1	3	5	1	0	1	28	74
Zn	22	33	60	73	31	12	37	21	58	52	58	56	24	14	20	102
Ga	11.2	13.9	16.6	16.6	13.5	11.5	14.0	13.2	14.2	14.1	14.2	14.3	17.3	11.3	10.1	17.6
Rb	16.9	43.0	33.5	54.3	51.9	43.8	40.6	19.1	19.9	20.2	19.1	4.6	1.3	1.9	23.0	6.8
Sr	110	149	173	173	136	71	150	250	178	183	176	163	241	152	169	203
Y	31.4	16.0	27.4	19.1	21.3	21.2	23.6	18.9	18.0	12.3	12.9	30.6	50.5	32.4	1.8	17.5
Zr	96	97	36	46	110	160	124	101	50	79	68	106	107	126	100	44
Nb	3.2	2.7	2.5	1.5	2.7	3.7	3.0	2.3	3.3	2.9	2.8	1.6	2.6	3.4	0.8	2.5
Mo	0.344	0.066	0.189	0.350	0.045	1.611	0.058	0.398	0.075	0.041	0.207	0.017	0.090	0.087	0.150	1.019
Sn	0.59	0.55	1.24	1.09	0.51	0.34	0.63	0.54	0.37	0.41	0.42	1.01	1.07	2.67	0.13	0.33
Cs	0.42	0.78	0.77	1.24	1.04	0.21	0.65	0.48	0.50	0.68	0.55	0.31	0.26	0.10	0.59	0.17
Ba	179	335	204	180	375	405	341	489	438	197	183	53	20	29	252	159
La	8.1	14.7	14.4	7.7	18.6	24.8	13.4	18.6	5.4	5.5	5.3	23.3	16.1	11.9	5.5	5.0
Ce	18.5	25.4	30.5	15.3	32.2	44.3	25.0	31.3	10.7	10.8	10.2	41.3	42.4	28.4	7.7	10.5
Pr	2.4	2.7	4.0	1.9	3.4	4.7	2.9	3.2	1.3	1.2	1.2	4.5	5.6	3.4	0.7	1.4
Nd	10.7	9.4	16.1	7.8	12.4	16.2	11.4	11.4	5.2	4.9	4.8	17.9	24.7	14.3	2.0	6.0
Sm	3.06	1.96	3.73	2.20	2.64	3.17	2.73	2.38	1.42	1.20	1.26	4.05	6.65	3.82	0.34	1.75
Eu	0.65	0.58	0.89	0.76	0.63	0.47	0.69	0.64	0.56	0.48	0.46	1.36	1.81	0.97	0.37	0.59
Gd	3.91	1.99	3.72	2.68	2.71	2.84	3.03	2.48	2.16	1.54	1.66	4.12	7.32	4.35	0.28	2.18
Tb	0.70	0.34	0.63	0.46	0.47	0.48	0.52	0.42	0.40	0.28	0.30	0.71	1.25	0.74	0.04	0.41
Dy	4.86	2.30	4.14	3.07	3.15	3.21	3.53	2.80	2.81	1.87	1.99	4.69	8.30	4.93	0.24	2.78
Ho	1.11	0.52	0.93	0.69	0.71	0.72	0.80	0.63	0.63	0.42	0.45	1.09	1.83	1.11	0.06	0.62
Er	3.34	1.59	2.85	2.00	2.18	2.33	2.47	1.93	1.88	1.29	1.37	3.34	5.40	3.35	0.19	1.88
Tm	0.53	0.27	0.47	0.31	0.36	0.42	0.41	0.33	0.30	0.21	0.22	0.56	0.85	0.54	0.03	0.29
Yb	3.53	1.89	3.26	2.08	2.58	3.11	2.91	2.32	2.09	1.53	1.61	3.98	5.58	3.76	0.29	1.89
Lu	0.57	0.33	0.55	0.34	0.45	0.55	0.49	0.40	0.35	0.26	0.28	0.67	0.88	0.64	0.05	0.29
Hf	2.81	2.97	1.63	1.55	3.55	4.97	3.72	3.00	1.47	2.18	1.86	3.53	3.51	4.15	2.60	1.31
Ta	0.15	0.20	0.15	0.09	0.22	0.27	0.22	0.18	0.19	0.19	0.18	0.10	0.12	0.16	0.06	0.12
Pb	3.66	3.24	3.59	13.85	4.35	4.29	3.60	5.59	3.62	4.99	4.35	3.16	2.94	2.06	4.62	2.91
Th	2.2	6.7	4.5	2.3	8.1	10.4	6.8	8.0	1.0	1.5	1.0	6.5	6.1	6.8	1.7	1.1
U	0.57	1.79	1.32	0.80	2.32	2.18	2.20	2.28	0.24	0.40	0.27	1.44	1.46	1.45	0.56	0.40
Lan/Smn	1.7	4.7	2.4	2.2	4.4	4.9	3.1	4.9	2.4	2.8	2.6	3.6	1.5	2.0	10.1	1.8
Gdn/Ybn	0.9	0.9	0.9	1.0	0.9	0.7	0.8	0.9	0.8	0.8	0.8	0.8	1.1	0.9	0.8	0.9
Lin/Hon	0.6	4.0	2.5	4.5	3.4	1.0	2.9	1.0	3.7	4.9	4.5	0.5	0.1	0.1	8.2	2.7

TABLE A3
(continued)

Sample	269	271	273	274	278	408	412	414	416	418	421	424	425	459	460	407
Region	L-R	L-R	L-R	L-R	L-R	L-R	L-R	L-R	L-R	L-R	L-R	L-R	L-R	L-R	L-R	L-R
Location	Lens	Lens	Lens	Lens	Lens	Lens	Lens	Lens	Lens	Lens	Lens	Lens	Lens	Riss	Riss	Lens
Type	MF	MF	MF	MF	MF	MF	MF	MF	MF	MF	MF	MF	MF	MF	MF	ME
SiO2	50.47	51.99	54.36	49.57	50.60	49.57	48.75	49.75	54.49	52.77	53.10	46.95	44.53	52.52	52.13	51.06
TiO2	0.25	0.13	0.57	0.41	0.32	1.05	1.00	0.45	0.34	0.21	0.52	0.61	0.74	0.32	0.37	0.44
Al2O3	13.98	14.38	17.03	14.06	16.52	15.92	16.61	14.41	15.63	15.99	16.40	17.76	18.15	17.11	16.45	12.66
FeO	9.18	8.38	10.34	10.88	10.56	10.12	9.44	10.14	9.70	7.63	10.79	12.82	14.24	7.92	7.99	9.85
MnO	0.26	0.20	0.15	0.18	0.15	0.14	0.14	0.22	0.15	0.14	0.17	0.20	0.24	0.13	0.14	0.15
MgO	9.17	10.95	3.74	9.04	7.78	8.80	8.85	10.87	6.67	7.37	6.16	7.53	7.70	7.21	7.91	12.26
CaO	9.25	8.52	9.36	9.33	7.22	10.96	12.22	10.42	10.97	14.27	9.53	11.58	11.92	11.73	12.84	11.23
Na2O	3.83	4.44	3.30	3.84	4.59	3.00	2.65	3.14	1.55	0.56	2.32	1.78	1.84	2.27	1.61	1.94
K2O	0.92	0.16	0.53	0.81	0.48	0.17	0.12	0.29	0.33	0.18	0.76	0.49	0.37	0.72	0.49	0.14
P2O5	0.05	0.03	0.07	0.01	0.02	0.09	0.08	0.03	0.03	0.02	0.10	0.06	0.08	0.05	0.04	0.06
CO2	2.37	0.49	0.26	1.61	1.50	0.04	0.04	0.18	0.04	0.70	0.04	0.11	0.07	0.04	0.07	0.07
S	0.01	0.01	0.01	0.01	0.01	0.05	0.01	0.01	0.02	0.06	0.02	0.02	0.03	0.01	0.01	0.01
SUM	99.74	99.68	99.72	99.75	99.75	99.91	99.91	99.91	99.92	99.90	99.91	99.91	99.91	100.03	100.05	99.87
LOI	3.6	1.8	0.7	2.3	2.7	0.6	0.6	0.9	1.1	1.3	0.8	1.3	0.8	1.4	1.5	1.0
Trace elements, ppm																
Li	24.4	10.1	5.5	20.6	33.2	7.4	8.5	3.4	7.1	4.1	7.5	6.6	6.2	5.9	6.0	10.0
Be	1.15	0.72	0.50	0.30	0.83	0.25	0.20	0.18	0.23	0.18	0.54	0.43	0.50	0.23	0.17	0.34
Sc	35	44	35	43	42	43	33	39	39	44	33	43	54	38	39	38
V	206.7	177.4	300.8	329.0	291.5	285.9	298.9	292.1	295.5	201.7	292.2	491.9	466.1	224.2	274.7	266.7
Cr	403.6	449.6	41.9	400.9	168.8	312.3	333.7	578.5	63.6	344.1	166.4	66.9	57.8	205.9	90.1	857.4
Co	43.2	45.0	31.1	47.7	43.1	34.7	37.3	45.1	31.3	33.7	33.1	34.5	41.1	33.5	34.7	46.7
Ni	113.7	75.9	21.5	75.5	54.2	68.2	85.0	149.9	32.9	56.8	38.5	24.7	20.2	41.6	62.2	207.9
Cu	1	3	91	84	1	63	83	12	24	47	79	20	86	1	52	112
Zn	103	72	99	71	94	59	53	70	55	47	79	58	78	48	52	64
Ga	14.7	10.7	18.0	12.9	15.4	14.4	13.2	12.6	12.2	12.5	16.3	15.6	18.3	12.5	12.0	11.7
Rb	18.0	2.0	6.3	14.3	9.4	1.6	1.0	3.3	7.7	3.9	20.1	9.1	4.4	14.1	10.3	1.0
Sr	118	83	210	108	101	216	174	154	138	141	246	245	295	155	130	162
Y	11.2	4.5	17.1	12.9	10.1	21.9	22.0	12.5	7.6	5.8	15.6	13.5	17.9	9.6	10.5	11.0
Zr	10	7	44	8	14	62	55	17	32	18	37	29	27	30	29	25
Nb	1.2	0.2	2.3	0.3	0.8	2.0	1.1	0.5	0.9	0.7	1.6	1.4	1.5	0.6	0.7	0.9
Mo	0.035	0.278	1.339	0.828	0.036	0.215	0.035	0.036	0.152	0.066	0.396	0.234	0.074	0.123	0.041	0.057
Sn	0.18	0.18	0.31	0.08	0.47	0.66	0.58	0.13	0.21	0.17	0.64	0.58	0.66	0.29	0.51	0.23
Cs	1.09	0.08	0.20	0.36	0.27	0.06	0.04	0.11	0.14	0.10	0.33	0.25	0.17	0.20	0.66	0.04
Ba	259	24	182	89	144	26	23	73	98	19	136	67	35	111	58	43
La	1.1	0.5	5.0	0.8	1.0	2.9	2.1	2.2	2.9	2.1	6.9	5.0	5.8	3.9	3.8	15.4
Ce	2.8	1.2	10.5	1.9	2.5	8.5	6.6	4.4	5.3	3.4	15.1	12.8	15.4	7.1	7.1	28.7
Pr	0.4	0.2	1.4	0.3	0.4	1.3	1.1	0.7	0.6	0.4	1.9	1.8	2.3	0.8	0.9	3.2
Nd	2.0	0.8	5.8	1.6	1.9	7.3	6.5	3.3	2.5	1.6	8.0	7.5	10.4	3.6	3.6	12.3
Sm	0.73	0.29	1.77	0.68	0.76	2.33	2.28	1.04	0.71	0.48	1.99	1.80	2.78	1.01	1.04	2.38
Eu	0.26	0.10	0.59	0.29	0.34	0.89	0.89	0.37	0.27	0.21	0.60	0.56	0.82	0.36	0.37	0.64
Gd	1.13	0.45	2.24	1.22	1.12	3.21	3.32	1.50	0.92	0.69	2.21	1.95	2.83	1.24	1.32	2.03
Tb	0.21	0.09	0.40	0.24	0.22	0.55	0.58	0.26	0.17	0.13	0.37	0.31	0.45	0.22	0.24	0.29
Dy	1.59	0.68	2.70	1.72	1.52	3.62	3.84	1.85	1.17	0.90	2.42	2.06	2.80	1.49	1.61	1.77
Ho	0.38	0.16	0.60	0.40	0.35	0.77	0.82	0.42	0.27	0.21	0.54	0.45	0.62	0.34	0.37	0.38
Er	1.16	0.50	1.79	1.20	1.06	2.15	2.31	1.27	0.82	0.62	1.60	1.32	1.81	1.00	1.10	1.09
Tm	0.19	0.08	0.28	0.18	0.17	0.32	0.34	0.20	0.13	0.10	0.25	0.21	0.28	0.16	0.17	0.16
Yb	1.27	0.54	1.81	1.14	1.12	2.08	2.25	1.34	0.90	0.69	1.75	1.47	1.97	1.06	1.15	1.10
Lu	0.21	0.09	0.28	0.17	0.17	0.33	0.36	0.22	0.15	0.11	0.29	0.25	0.33	0.17	0.20	0.18
Hf	0.35	0.23	1.30	0.26	0.44	1.72	1.67	0.60	0.81	0.50	1.32	1.08	1.15	0.90	0.92	0.82
Ta	0.02	0.01	0.11	0.01	0.04	0.12	0.07	0.03	0.06	0.06	0.10	0.08	0.07	0.04	0.04	0.04
Pb	1.46	0.74	3.60	1.03	3.24	1.33	1.44	0.80	1.96	3.55	2.60	1.73	1.37	2.10	1.82	4.11
Th	0.5	0.1	1.1	0.7	0.8	0.2	0.1	0.3	0.5	1.3	1.8	0.9	0.5	1.7	1.4	3.1
U	0.09	0.06	0.40	0.07	0.14	0.10	0.05	0.07	0.21	0.40	0.75	0.42	0.24	0.51	0.41	0.85
Lan/Smn	1.0	1.1	1.8	0.7	0.8	0.8	0.6	1.3	2.5	2.7	2.2	1.7	1.3	2.4	2.3	4.0
Gdn/Ybn	0.7	0.7	1.0	0.9	0.8	1.2	1.2	0.9	0.8	0.8	1.0	1.1	1.2	0.9	0.9	1.5
Lin/Hon	15.1	14.7	2.2	12.0	22.0	2.3	2.4	1.9	6.2	4.7	3.3	3.4	2.3	4.1	3.8	6.3

TABLE A3
(continued)

Sample	422	228	229	230	236	290	291	292	293	294	396	398	402	403	404	405
Region	L-R	NWB	NWB	NWB	NWB	NWB	NWB	NWB	NWB	NWB	NWB	NWB	NWB	NWB	NWB	NWB
Location	Lens	Vals	Vals	Vals	Vals	Vin	Vin	Vin	Vin	Vin	Kors	Kors	Kors	Kors	Kors	Kors
Type	HBL	Adak	Adak	Adak	Adak	Adak	Adak	Adak	Adak	Adak	Adak	Adak	Adak	Adak	Adak	Adak
SiO2	52.87	67.92	69.05	69.14	66.74	64.09	70.29	66.43	67.96	69.08	57.46	64.27	63.66	71.78	64.01	66.53
TiO2	0.93	0.39	0.37	0.37	0.45	0.43	0.22	0.29	0.29	0.39	0.82	0.46	0.52	0.19	0.50	0.43
Al2O3	8.80	17.22	16.38	16.35	17.21	18.58	16.37	18.48	17.42	16.21	19.37	18.26	18.52	15.84	18.77	17.28
FeO	15.90	2.73	2.49	2.58	3.18	3.15	1.60	2.11	2.07	2.67	5.76	3.14	3.10	1.51	3.43	2.84
MnO	0.27	0.04	0.03	0.03	0.04	0.07	0.04	0.04	0.04	0.04	0.11	0.07	0.06	0.03	0.06	0.06
MgO	10.29	1.22	1.18	1.14	1.48	1.19	0.54	0.80	0.81	1.12	2.47	1.16	1.37	0.42	1.28	1.13
CaO	9.44	3.60	3.48	3.43	4.36	5.00	3.03	4.06	4.00	3.59	7.12	5.19	5.36	2.95	5.48	4.39
Na2O	0.98	4.50	4.62	4.45	4.82	5.15	4.72	5.09	4.88	4.40	4.38	5.21	5.06	4.81	5.26	4.93
K2O	0.29	1.72	1.60	1.80	1.06	1.65	2.55	2.10	1.91	1.84	1.77	1.65	1.68	1.98	1.47	1.84
P2O5	0.04	0.13	0.12	0.13	0.14	0.20	0.08	0.13	0.13	0.13	0.34	0.20	0.21	0.04	0.18	0.14
CO2	0.11	0.11	0.22	0.13	0.11	0.15	0.15	0.11	0.11	0.11	0.04	0.04	0.11	0.04	0.04	0.07
S	0.01	0.01	0.01	0.01	0.01	0.01	0.01	0.01	0.01	0.01	0.01	0.01	0.01	0.01	0.01	0.01
SUM	99.93	99.59	99.55	99.56	99.60	99.67	99.60	99.65	99.63	99.59	99.65	99.66	99.66	99.60	100.49	99.65
LOI	0.6	0.9	0.8	0.5	0.8	1.1	0.5	0.7	0.6	0.7	0.7	0.6	0.7	0.1	0.4	0.6
Trace elements, ppm																
Li	5.2	13.3	9.6	7.3	2.7	4.5	13.0	10.3	10.9	12.3	13.7	3.6	7.3	9.3	7.3	11.0
Be	0.36	1.34	1.18	1.22	1.07	1.38	1.24	1.20	1.19	1.39	1.55	1.55	1.30	1.35	1.41	1.32
Sc	68	3	3	3	3	3	3	3	3	4	7	3	4	2	4	3
V	619.0	27.6	25.3	25.0	34.2	39.0	14.0	20.1	20.9	25.7	107.9	45.4	41.8	12.3	49.1	32.5
Cr	248.0	9.9	11.2	9.0	12.5	3.0	2.2	2.6	3.0	9.0	5.9	3.3	4.3	0.9	3.5	3.2
Co	51.0	6.5	6.2	5.9	7.2	6.3	3.4	4.1	4.4	6.9	10.9	4.5	7.6	2.5	7.5	6.0
Ni	48.7	5.5	6.8	4.8	6.7	2.6	1.4	2.1	2.1	5.5	4.7	2.1	3.7	0.8	3.6	2.9
Cu	15	2	0	0	4	15	1	2	2	1	3	1	1	18	2	3
Zn	116	40	31	30	38	50	24	28	23	40	58	36	55	19	49	45
Ga	11.9	17.4	16.9	17.0	16.1	21.0	18.8	20.0	19.6	19.5	18.1	15.0	22.2	18.6	22.2	20.7
Rb	2.9	71.3	54.2	65.4	27.0	36.0	62.6	48.4	47.3	71.5	37.1	25.0	38.6	42.1	34.7	40.1
Sr	21	417	422	412	534	1434	933	1134	1089	445	1265	1260	1338	973	1221	1021
Y	22.0	9.4	8.2	3.9	6.8	13.3	7.0	9.1	9.1	12.5	17.1	12.6	9.0	7.7	10.3	10.4
Zr	61	158	155	152	168	158	121	127	140	160	145	165	153	150	165	146
Nb	2.3	9.9	7.7	6.0	5.6	13.3	8.2	9.0	8.4	10.6	10.6	11.7	11.0	6.1	6.9	7.9
Mo	0.225	0.146	0.124	0.136	0.072	0.517	0.089	0.087	0.091	0.095	0.684	0.222	0.417	0.057	0.334	0.180
Sn	0.78	1.50	1.16	0.95	0.92	0.83	0.56	0.63	0.59	1.68	1.19	0.88	0.79	0.59	0.83	0.79
Cs	0.05	1.25	0.84	0.90	0.84	1.62	0.97	0.83	1.16	1.90	0.74	0.39	0.83	0.36	0.64	0.62
Ba	31	398	359	382	319	899	882	939	943	409	529	875	781	809	439	617
La	3.4	28.9	29.3	34.1	19.2	39.6	16.2	27.7	25.7	30.0	38.3	48.8	45.1	20.7	28.0	27.8
Ce	9.5	56.9	56.3	62.5	35.4	83.6	34.6	56.2	53.1	55.8	88.7	101.0	87.2	42.5	55.0	56.1
Pr	1.4	6.2	6.0	6.4	3.9	10.1	4.2	6.6	6.4	6.0	11.4	11.8	9.1	4.9	6.4	6.6
Nd	7.1	21.3	20.3	20.6	14.4	36.6	15.3	23.6	22.9	20.0	45.4	42.8	30.3	17.7	24.5	24.6
Sm	2.27	3.58	3.18	2.66	2.72	6.00	2.69	3.83	3.89	3.90	7.21	5.80	4.53	2.86	4.28	4.16
Eu	0.41	0.93	0.82	0.82	0.94	1.58	0.73	1.00	0.99	0.89	1.89	1.44	1.34	0.77	1.26	1.11
Gd	2.87	2.69	2.27	1.57	2.05	3.80	1.77	2.44	2.44	3.03	5.16	3.66	2.56	1.73	2.80	2.66
Tb	0.49	0.38	0.31	0.18	0.28	0.48	0.24	0.32	0.32	0.47	0.67	0.48	0.32	0.24	0.37	0.36
Dy	3.29	1.97	1.64	0.81	1.44	2.53	1.25	1.69	1.69	2.60	3.56	2.59	1.65	1.32	1.92	1.92
Ho	0.74	0.35	0.30	0.14	0.26	0.46	0.23	0.31	0.31	0.46	0.62	0.46	0.29	0.24	0.35	0.34
Er	2.23	0.87	0.78	0.35	0.64	1.20	0.62	0.82	0.83	1.17	1.57	1.17	0.75	0.69	0.88	0.90
Tm	0.35	0.12	0.11	0.05	0.09	0.17	0.09	0.12	0.12	0.16	0.23	0.18	0.11	0.11	0.12	0.13
Yb	2.40	0.74	0.69	0.36	0.54	1.09	0.62	0.76	0.76	0.98	1.41	1.10	0.74	0.76	0.80	0.90
Lu	0.40	0.10	0.10	0.05	0.07	0.15	0.09	0.11	0.10	0.13	0.21	0.16	0.12	0.12	0.12	0.13
Hf	1.90	4.23	4.16	3.98	4.38	3.88	3.33	3.25	3.51	4.32	3.94	4.24	3.83	3.91	4.00	3.76
Ta	0.14	0.78	0.55	0.17	0.23	0.76	0.45	0.56	0.53	0.97	0.66	0.80	0.60	0.35	0.36	0.46
Pb	3.16	10.02	8.09	7.93	7.12	9.68	8.42	9.99	6.65	10.55	8.86	11.38	11.95	6.69	10.84	8.97
Th	1.5	10.8	11.8	10.1	3.1	4.9	4.6	5.5	4.5	10.0	8.0	6.0	7.9	2.6	5.1	6.1
U	0.51	2.28	2.04	2.02	0.57	1.72	1.86	2.05	1.38	3.24	3.56	2.12	2.10	0.93	1.81	1.97
Lan/Smn	0.9	5.0	5.7	8.0	4.4	4.1	3.8	4.5	4.1	4.8	3.3	5.3	6.2	4.5	4.1	4.2
Gdn/Ybn	1.0	2.9	2.6	3.5	3.1	2.8	2.3	2.6	2.6	2.5	3.0	2.7	2.8	1.8	2.9	2.4
Lin/Hon	1.6	8.9	7.4	12.1	2.5	2.3	13.4	7.9	8.4	6.2	5.2	1.8	5.8	8.9	5.0	7.6

TABLE A3
(continued)

Sample	406	440	441	443	488	489	490	491	492	493	498	511	512	518	520	522
Region	NWB	NWB	NWB	NWB	NWB	NWB	NWB	NWB	NWB	NWB	NWB	NWB	NWB	NWB	NWB	NWB
Location	Kors	Foll	Foll	Foll	Revs	Revs	Revs	Revs	Revs	Revs	Revs	RakS	RakS	RakN	RakN	RakN
Type	Adak	Adak	Adak	Adak	Adak	Adak	Adak	Adak	Adak	Adak	Adak	Adak	Adak	Adak	Adak	Adak
SiO2	61.41	67.52	65.98	66.76	66.89	63.20	61.83	68.29	66.97	66.08	59.53	68.34	61.70	67.51	66.30	66.43
TiO2	0.68	0.45	0.50	0.41	0.42	0.62	0.68	0.32	0.37	0.38	0.72	0.51	0.53	0.39	0.42	0.41
Al2O3	18.72	16.26	16.99	16.36	17.09	18.31	18.32	17.03	17.35	17.64	18.27	16.04	19.25	17.10	17.15	17.29
FeO	4.27	3.10	3.23	2.83	2.93	4.00	4.71	2.34	2.70	2.83	5.81	3.04	3.99	3.06	3.35	3.14
MnO	0.08	0.06	0.06	0.06	0.05	0.07	0.08	0.05	0.06	0.06	0.11	0.04	0.09	0.06	0.06	0.06
MgO	1.85	1.05	1.16	0.78	1.03	1.47	1.68	0.77	0.92	0.94	2.22	1.34	1.20	1.12	1.32	1.18
CaO	6.00	4.02	4.17	4.42	4.25	5.34	6.03	3.91	4.20	4.59	6.58	3.70	5.73	3.91	4.49	4.07
Na2O	4.86	4.61	4.60	5.02	4.86	4.97	4.95	5.16	5.23	5.30	4.62	4.78	5.72	4.79	5.08	4.54
K2O	1.49	2.49	2.38	2.27	2.21	1.80	1.44	1.99	1.97	1.86	1.81	1.84	1.50	1.87	1.55	2.47
P2O5	0.24	0.13	0.16	0.15	0.17	0.21	0.25	0.12	0.13	0.16	0.31	0.14	0.23	0.14	0.15	0.15
CO2	0.04	0.30	0.74	0.92	0.11	0.04	0.04	0.04	0.11	0.15	0.04	0.26	0.07	0.07	0.15	0.26
S	0.01	0.04	0.02	0.05	0.01	0.01	0.01	0.01	0.01	0.01	0.01	0.02	0.01	0.01	0.01	0.03
SUM	99.65	100.03	99.99	100.03	100.02	100.04	100.02	100.03	100.02	100.00	100.03	100.05	100.02	100.03	100.03	100.03
LOI	0.5	0.8	1.5	1.5	0.2	0.7	0.6	0.8	0.6	0.6	0.6	0.7	0.4	0.2	0.8	0.8
Trace elements, ppm																
Li	7.1	15.7	15.9	12.2	9.6	8.0	7.2	5.8	8.1	4.4	11.4	12.9	6.5	3.5	2.6	3.1
Be	1.32	1.22	1.22	1.10	1.08	1.16	1.20	1.20	1.30	1.28	1.38	1.11	1.37	1.13	1.00	0.99
Sc	6	4	4	4	3	5	6	3	3	3	7	4	3	3	4	3
V	59.1	31.1	34.7	30.8	38.4	68.2	49.8	14.9	20.2	23.7	77.4	29.7	45.0	23.0	28.0	27.5
Cr	4.9	3.0	3.4	3.0	2.9	3.7	3.1	1.6	2.0	1.6	3.3	10.0	2.0	3.5	5.9	4.1
Co	9.7	5.4	6.1	5.2	5.2	6.7	9.5	4.3	5.4	5.0	13.1	6.7	5.7	6.2	6.2	4.9
Ni	4.1	2.4	2.8	2.3	2.6	3.3	3.9	2.2	2.5	2.2	5.3	8.3	2.0	2.8	3.8	2.8
Cu	5	5	4	2	1	1	3	3	2	1	4	1	1	1	0	4
Zn	65	43	49	37	35	45	63	28	36	34	72	27	46	26	40	22
Ga	23.1	20.0	19.9	18.8	14.6	15.5	22.5	18.3	20.0	18.9	22.2	15.8	19.2	17.6	18.2	17.5
Rb	33.4	64.5	62.4	55.5	42.9	37.4	32.2	45.6	47.4	37.0	41.0	55.6	24.6	45.8	39.3	48.9
Sr	1205	849	913	869	903	961	1251	1086	1147	1232	1291	424	1545	722	735	599
Y	13.3	9.9	10.8	9.2	7.5	12.0	14.0	8.3	9.7	10.1	17.4	9.6	16.2	6.6	8.6	7.6
Zr	223	151	148	137	122	124	156	125	162	132	181	120	187	116	129	124
Nb	10.8	11.5	11.6	10.8	9.5	13.5	12.3	8.0	8.7	8.8	9.6	9.8	14.4	6.9	6.7	7.0
Mo	0.648	0.340	0.344	0.304	0.145	0.510	0.456	0.107	0.129	0.126	0.428	0.193	0.204	0.104	0.139	0.071
Sn	0.94	0.79	0.83	0.71	0.68	0.95	0.99	0.61	0.64	0.66	1.12	1.14	0.99	0.72	0.76	0.66
Cs	0.60	1.23	1.55	0.82	0.58	0.78	0.71	0.60	0.58	0.47	0.96	0.96	0.45	0.73	0.68	0.65
Ba	580	648	773	656	922	770	546	736	653	857	536	368	808	574	460	591
La	38.2	25.7	30.1	41.3	29.2	31.5	38.0	29.6	35.2	33.3	35.3	22.2	41.8	35.6	27.7	39.5
Ce	76.9	53.1	61.7	68.4	58.9	73.0	77.4	56.4	67.7	66.1	74.6	44.5	97.5	62.8	53.7	73.9
Pr	9.0	6.2	7.3	7.0	6.3	8.7	9.3	6.3	7.5	7.8	9.3	4.9	12.1	6.9	6.0	7.9
Nd	33.3	22.4	26.1	23.5	22.0	31.9	34.9	22.7	26.8	28.5	36.3	17.6	45.9	23.8	22.1	27.6
Sm	5.69	3.87	4.45	3.68	3.50	5.45	6.00	3.69	4.30	4.66	6.70	2.97	7.29	3.41	3.59	4.01
Eu	1.57	1.05	1.18	0.99	0.94	1.42	1.63	0.98	1.13	1.24	1.75	0.85	2.02	1.00	0.99	1.05
Gd	3.68	2.52	2.88	2.30	2.13	3.46	3.81	2.26	2.61	2.89	4.87	2.33	4.98	2.09	2.44	2.50
Tb	0.48	0.33	0.37	0.31	0.28	0.46	0.51	0.30	0.35	0.37	0.64	0.34	0.63	0.25	0.32	0.31
Dy	2.55	1.77	1.97	1.66	1.43	2.38	2.68	1.54	1.80	1.95	3.33	1.79	3.16	1.18	1.58	1.48
Ho	0.45	0.32	0.36	0.30	0.26	0.43	0.48	0.28	0.32	0.35	0.61	0.34	0.56	0.21	0.29	0.27
Er	1.13	0.83	0.93	0.79	0.67	1.11	1.22	0.72	0.83	0.90	1.56	0.90	1.49	0.54	0.77	0.70
Tm	0.17	0.13	0.14	0.12	0.10	0.17	0.17	0.11	0.12	0.13	0.22	0.13	0.21	0.08	0.11	0.10
Yb	1.07	0.86	0.92	0.82	0.68	1.09	1.11	0.71	0.81	0.86	1.43	0.84	1.42	0.51	0.74	0.67
Lu	0.15	0.13	0.14	0.13	0.10	0.16	0.17	0.11	0.12	0.13	0.22	0.12	0.21	0.08	0.11	0.10
Hf	5.30	4.38	4.19	3.89	3.49	3.48	3.95	3.35	4.03	3.42	4.73	3.44	4.74	3.44	3.72	3.66
Ta	0.60	0.71	0.74	0.68	0.61	0.97	0.68	0.46	0.49	0.48	0.52	0.73	0.83	0.34	0.43	0.45
Pb	9.67	17.14	14.56	17.09	7.84	9.14	10.25	9.90	10.11	10.01	10.66	7.53	11.67	7.28	9.97	4.97
Th	5.9	9.1	10.0	11.4	7.6	6.3	5.8	6.0	7.5	5.4	7.6	10.8	4.8	8.4	6.8	9.1
U	2.22	3.79	2.95	4.13	2.32	2.25	1.64	2.67	2.46	1.83	3.12	2.87	1.70	1.83	1.81	1.71
Lan/Smn	4.2	4.2	4.2	7.0	5.2	3.6	4.0	5.0	5.1	4.5	3.3	4.7	3.6	6.5	4.8	6.2
Gdn/Ybn	2.8	2.4	2.5	2.3	2.5	2.6	2.8	2.6	2.6	2.7	2.7	2.2	2.8	3.3	2.7	3.0
Lin/Hon	3.7	11.5	10.4	9.6	8.7	4.3	3.6	4.9	5.9	3.0	4.4	8.9	2.7	3.9	2.2	2.7

TABLE A3
(continued)

Sample	523	524	525	526	527	528	232	234	394	395	397	494	495	496	501	505
Region	NWB	NWB	NWB	NWB	NWB	NWB	NWB	NWB	NWB	NWB	NWB	NWB	NWB	NWB	NWB	NWB
Location	RakS	RakS	RakS	Verr	Verr	Verr	Vals	Vals	Kors	Kors	Kors	Revs	Revs	Revs	Revs	RakS
Type	Adak	Adak	Adak	Adak	Adak	Adak	Ad'tic	Ad'tic	Ad'tic	Ad'tic	Ad'tic	Ad'tic	Ad'tic	Ad'tic	Ad'tic	Ad'tic
SiO2	68.36	67.75	67.45	71.21	68.56	69.86	68.84	69.44	58.97	56.54	57.57	68.80	69.73	56.15	59.71	59.84
TiO2	0.31	0.31	0.32	0.22	0.31	0.27	0.43	0.40	0.70	0.93	0.86	0.28	0.46	1.25	0.66	0.73
Al2O3	17.09	17.48	17.62	15.53	16.69	16.35	16.20	15.96	18.53	18.84	18.31	16.56	15.50	17.99	17.67	17.25
FeO	2.28	2.28	2.37	1.70	2.19	2.09	2.77	2.58	5.24	6.02	5.90	2.46	2.90	7.81	5.75	6.11
MnO	0.04	0.04	0.04	0.04	0.05	0.05	0.04	0.04	0.10	0.11	0.11	0.04	0.04	0.10	0.10	0.11
MgO	0.77	0.83	0.85	0.52	0.71	0.54	1.33	1.22	2.43	3.14	2.81	1.43	1.20	3.72	2.06	2.48
CaO	3.91	3.86	4.09	3.15	3.26	3.06	3.47	3.60	6.72	7.68	6.97	3.90	3.25	7.33	5.56	6.11
Na2O	5.25	5.34	5.29	5.24	5.08	4.95	4.55	4.58	4.20	4.51	4.29	4.71	4.97	4.44	5.29	4.27
K2O	1.89	1.91	1.79	1.99	2.49	2.64	1.73	1.54	2.22	1.39	2.29	1.64	1.74	0.84	2.75	2.47
P2O5	0.11	0.12	0.12	0.09	0.12	0.10	0.12	0.13	0.34	0.38	0.40	0.09	0.13	0.23	0.37	0.34
CO2	0.04	0.11	0.07	0.33	0.52	0.11	0.07	0.07	0.19	0.11	0.11	0.11	0.11	0.11	0.07	0.26
S	0.01	0.01	0.01	0.01	0.03	0.01	0.01	0.01	0.01	0.01	0.01	0.01	0.01	0.06	0.01	0.02
SUM	100.06	100.04	100.02	100.03	100.01	100.03	99.56	99.57	99.65	99.66	99.63	100.03	100.04	100.03	100.00	99.99
LOI	0.6	0.2	0.4	1.2	1.3	0.8	0.9	1.0	0.9	0.9	0.8	0.7	0.6	0.5	0.4	1.4
Trace elements, ppm																
Li	9.6	8.3	11.2	8.4	12.7	17.2	10.4	11.7	14.5	11.7	15.0	12.3	10.0	9.2	5.8	14.8
Be	1.14	1.16	1.14	1.16	1.57	1.82	1.22	1.03	1.72	1.25	1.89	1.52	1.21	0.99	1.88	1.65
Sc	2	2	3	2	2	2	3	3	8	10	8	7	4	16	7	10
V	16.4	16.8	18.7	10.0	16.1	12.9	29.2	28.0	103.0	117.4	129.7	18.3	20.6	145.6	102.5	91.8
Cr	1.9	2.1	2.2	1.0	1.2	0.9	11.7	13.5	6.2	10.9	4.4	4.9	8.7	29.9	0.8	4.0
Co	3.8	3.9	4.1	2.4	3.2	2.9	7.0	6.4	12.2	13.8	12.0	7.7	6.9	23.7	13.9	15.5
Ni	1.6	1.8	1.9	1.1	1.4	0.9	8.5	7.8	5.3	6.9	5.0	7.4	8.7	22.0	2.7	6.8
Cu	1	1	1	1	76	2	1	0	20	1	8	1	1	19	28	33
Zn	20	22	24	16	26	27	31	32	65	67	57	35	33	64	45	73
Ga	17.4	17.1	17.7	15.3	17.1	16.9	16.1	16.6	19.4	19.9	16.6	17.3	17.2	19.6	21.7	21.9
Rb	40.2	41.5	40.5	48.7	64.6	69.3	57.2	54.1	49.5	26.4	41.9	62.1	55.7	20.4	43.8	57.9
Sr	1127	1055	1124	776	924	844	399	395	1260	1202	1328	400	391	479	1360	1216
Y	9.6	8.1	8.7	6.9	8.9	10.0	8.9	9.4	18.4	22.8	18.8	7.9	8.2	15.7	24.1	21.1
Zr	121	108	115	102	109	118	145	139	188	121	230	105	134	134	221	197
Nb	8.5	8.1	8.9	7.1	10.3	11.4	10.5	7.8	10.9	15.2	10.0	5.9	10.4	17.4	10.5	14.6
Mo	0.101	0.095	0.101	0.091	0.151	0.136	0.188	0.157	0.891	0.309	1.172	0.036	0.280	0.238	0.330	1.506
Sn	0.62	0.63	0.67	0.52	0.88	0.73	1.02	1.04	1.08	1.29	1.35	1.90	0.95	1.22	1.19	1.30
Cs	0.51	0.56	0.81	0.54	0.93	2.52	1.05	1.35	1.21	0.74	1.02	1.20	1.31	0.58	0.67	1.40
Ba	953	808	780	671	771	695	371	347	768	521	701	304	335	204	784	627
La	45.9	30.5	27.9	24.5	34.6	35.8	26.2	22.5	43.6	30.5	59.7	17.5	25.7	18.9	55.6	47.7
Ce	83.6	59.6	55.8	46.2	69.0	66.1	48.6	45.1	93.9	80.9	123.9	34.7	45.2	38.7	117.5	100.4
Pr	9.0	6.8	6.6	5.1	7.7	7.4	5.2	5.2	11.3	11.8	15.0	4.0	4.6	4.6	14.5	12.3
Nd	31.0	24.0	23.9	18.4	27.1	26.3	17.6	18.6	43.0	50.2	56.3	15.0	16.0	18.6	56.2	47.5
Sm	4.60	3.95	4.09	2.95	4.24	4.06	2.90	3.22	6.65	8.67	8.62	3.01	2.68	3.89	9.92	8.60
Eu	1.23	1.12	1.17	0.81	1.19	1.11	0.79	0.83	1.74	2.43	2.14	0.63	0.77	1.22	2.46	2.07
Gd	2.73	2.41	2.54	1.80	2.59	2.57	2.19	2.50	4.71	6.23	5.90	2.26	1.96	3.64	6.73	5.86
Tb	0.35	0.31	0.32	0.24	0.33	0.34	0.32	0.35	0.63	0.83	0.76	0.31	0.28	0.53	0.86	0.78
Dy	1.81	1.53	1.63	1.26	1.64	1.75	1.70	1.87	3.47	4.55	3.99	1.65	1.55	3.06	4.45	3.97
Ho	0.33	0.28	0.30	0.23	0.30	0.33	0.32	0.34	0.65	0.81	0.71	0.29	0.29	0.58	0.81	0.71
Er	0.87	0.73	0.79	0.63	0.80	0.90	0.85	0.90	1.69	2.07	1.74	0.74	0.75	1.54	2.13	1.86
Tm	0.13	0.10	0.11	0.10	0.12	0.14	0.12	0.13	0.26	0.30	0.25	0.10	0.11	0.22	0.32	0.27
Yb	0.82	0.70	0.78	0.66	0.81	0.95	0.80	0.78	1.60	1.90	1.57	0.66	0.73	1.40	2.04	1.71
Lu	0.12	0.11	0.12	0.11	0.13	0.15	0.12	0.11	0.24	0.27	0.22	0.10	0.11	0.21	0.31	0.26
Hf	3.37	3.17	3.25	3.15	3.31	3.85	4.04	3.74	4.94	3.23	6.06	3.16	3.79	3.47	5.47	5.17
Ta	0.57	0.50	0.55	0.46	0.53	0.66	0.73	0.58	0.57	1.31	0.60	0.55	0.73	1.00	0.55	0.85
Pb	7.94	8.80	8.65	9.87	13.10	15.01	7.84	7.06	11.83	5.97	11.77	10.56	6.58	4.24	8.16	11.10
Th	8.0	7.2	5.0	8.1	9.2	9.4	13.8	8.4	11.0	2.9	14.7	10.3	10.5	3.9	11.6	13.2
U	1.80	1.71	1.26	2.56	2.92	3.30	2.96	1.63	3.13	1.69	4.32	2.31	2.84	1.08	4.21	4.98
Lan/Smn	6.2	4.8	4.3	5.2	5.1	5.5	5.6	4.4	4.1	2.2	4.3	3.6	6.0	3.0	3.5	3.5
Gdn/Ybn	2.7	2.8	2.6	2.2	2.6	2.2	2.2	2.6	2.4	2.7	3.0	2.8	2.2	2.1	2.7	2.8
Lin/Hon	6.8	7.1	8.8	8.5	9.8	12.4	7.7	8.0	5.3	3.4	5.0	10.0	8.0	3.7	1.7	4.9

TABLE A3
(continued)

Sample	238	295	296	298	431	433	434	435	436	437	438	439	444	445	446	447
Region	NWB	NWB	NWB	NWB	NWB	NWB	NWB	NWB	NWB	NWB	NWB	NWB	NWB	NWB	NWB	NWB
Location	Vals	Vin	Vin	Vin	Kopp	Kopp	Kopp	Kopp	Kopp	Kopp	Kopp	Kopp	Foll	Foll	Foll	Sima
Type	FE	FE	FE	FE	FE	FE	FE	FE	FE	FE	FE	FE	FE	FE	FE	FE
SiO2	64.50	60.50	58.62	59.22	57.18	59.43	65.80	61.75	64.53	69.33	69.88	57.56	75.85	75.17	73.44	64.51
TiO2	0.51	0.54	0.63	0.56	0.84	0.77	0.57	0.67	0.35	0.18	0.27	0.98	0.18	0.22	0.25	0.56
Al2O3	15.97	16.34	17.17	16.44	17.83	17.15	16.45	16.35	16.50	14.31	15.06	17.51	13.21	13.79	13.70	16.42
FeO	4.63	6.08	6.70	6.14	7.34	6.60	4.64	5.88	6.01	4.65	4.17	7.14	1.46	1.58	1.72	4.88
MnO	0.07	0.11	0.12	0.12	0.13	0.11	0.08	0.10	0.11	0.08	0.08	0.12	0.03	0.03	0.03	0.08
MgO	2.82	3.25	3.67	4.10	3.79	3.56	1.83	3.54	1.77	2.23	1.03	3.97	0.42	0.48	0.57	2.27
CaO	4.46	5.23	5.84	6.10	7.21	6.82	4.95	6.16	7.40	5.49	5.00	7.49	1.99	1.84	2.26	5.07
Na2O	2.91	3.60	3.76	3.82	3.84	3.67	4.53	3.44	2.86	3.03	3.64	3.58	6.03	6.51	6.11	3.97
K2O	2.71	3.67	2.72	2.78	1.48	1.58	0.83	1.79	0.23	0.49	0.74	1.18	0.31	0.28	0.40	1.86
P2O5	0.13	0.27	0.31	0.27	0.23	0.18	0.17	0.18	0.10	0.06	0.07	0.24	0.04	0.05	0.06	0.14
CO2	0.59	0.11	0.19	0.15	0.04	0.04	0.04	0.04	0.04	0.04	0.04	0.15	0.37	0.07	1.48	0.26
S	0.24	0.01	0.01	0.01	0.01	0.01	0.01	0.01	0.01	0.01	0.02	0.01	0.01	0.01	0.04	0.01
SUM	99.54	99.71	99.74	99.71	99.92	99.92	99.90	99.91	99.91	99.90	100.00	99.93	99.90	100.03	100.06	100.03
LOI	1.3	0.9	1.0	0.5	0.1	0.3	0.4	0.4	0.2	0.5	0.1	0.7	1.0	0.6	0.3	0.8
Trace elements, ppm																
Li	31.9	15.8	16.4	15.4	8.5	13.1	7.7	18.9	6.2	7.9	7.9	12.1	2.0	2.3	2.3	14.9
Be	1.58	2.14	1.54	1.55	0.87	0.90	0.95	0.94	0.62	0.61	0.68	0.84	0.60	0.47	0.51	0.89
Sc	11	15	16	18	25	18	9	16	19	15	13	20	3	2	3	13
V	68.4	106.2	124.3	116.5	131.8	150.9	72.4	145.5	105.0	119.7	67.9	152.1	3.6	6.6	7.1	63.0
Cr	71.8	50.0	49.8	107.7	30.7	39.4	15.5	69.2	4.5	49.8	3.3	50.2	0.5	1.0	1.3	19.1
Co	11.9	18.6	21.4	21.7	20.5	19.1	9.8	16.9	12.5	12.1	7.7	20.5	1.6	2.2	2.8	12.0
Ni	27.7	15.5	16.2	26.3	17.6	22.3	8.9	27.4	2.9	13.1	2.0	24.7	0.6	0.8	1.0	13.4
Cu	29	69	74	109	46	27	2	35	24	7	16	71	5	11	12	18
Zn	62	72	79	73	69	67	64	56	51	39	47	67	14	18	18	49
Ga	15.6	19.5	19.7	18.7	17.9	17.4	16.0	16.6	14.1	12.1	13.3	17.4	11.4	10.8	11.1	16.3
Rb	99.8	127.4	86.0	78.0	39.0	42.9	26.6	54.4	3.1	12.2	19.6	33.8	7.5	7.5	11.7	52.9
Sr	351	654	904	771	551	496	526	419	188	135	137	536	215	280	268	462
Y	21.1	23.0	20.7	22.1	25.0	21.5	19.2	21.6	5.6	7.8	12.3	22.4	31.5	14.7	16.2	21.0
Zr	164	208	217	165	131	176	216	176	15	53	77	119	223	145	151	185
Nb	11.7	15.2	11.3	11.4	8.6	8.1	4.9	8.2	0.8	1.9	2.2	7.6	18.4	10.6	10.7	7.7
Mo	0.825	0.234	0.158	0.166	0.696	0.866	0.031	0.742	0.051	0.022	0.078	1.239	0.134	0.078	0.121	0.424
Sn	1.90	1.91	1.39	1.37	1.01	1.19	1.09	1.29	0.15	0.32	0.46	1.20	1.84	1.19	1.26	0.99
Cs	5.57	3.41	3.58	2.35	1.31	1.61	0.84	2.00	0.11	0.86	0.79	1.68	0.10	0.12	0.20	1.48
Ba	471	900	1123	917	342	351	272	395	50	95	122	279	64	53	67	417
La	32.6	38.6	30.4	33.0	22.8	23.6	30.6	28.9	2.2	4.3	4.9	22.8	44.1	34.0	37.0	22.3
Ce	65.6	84.1	66.2	69.5	48.2	48.4	52.2	56.1	5.1	9.5	10.8	47.9	99.7	59.6	66.2	46.6
Pr	7.5	10.4	8.3	8.5	6.0	6.0	6.8	6.7	0.7	1.1	1.4	6.0	10.4	6.1	6.8	5.6
Nd	27.5	37.7	32.0	32.2	24.1	23.5	25.5	24.6	3.1	4.5	6.2	24.0	36.9	19.7	21.9	21.6
Sm	5.30	6.73	6.01	5.99	4.92	5.01	4.87	4.80	0.83	1.13	1.72	5.01	6.84	3.24	3.64	4.44
Eu	1.15	1.26	1.46	1.49	1.29	1.14	1.02	1.16	0.46	0.32	0.53	1.20	0.80	0.57	0.57	0.96
Gd	4.22	4.74	4.47	4.52	4.53	4.35	4.05	4.06	0.95	1.18	2.05	4.44	4.99	2.31	2.54	3.76
Tb	0.66	0.69	0.64	0.67	0.68	0.64	0.61	0.62	0.15	0.19	0.34	0.65	0.84	0.38	0.40	0.57
Dy	3.84	3.95	3.60	3.83	4.07	3.87	3.61	3.74	0.95	1.25	2.14	3.82	5.26	2.31	2.54	3.49
Ho	0.77	0.79	0.71	0.77	0.84	0.78	0.72	0.77	0.21	0.28	0.47	0.77	1.11	0.49	0.52	0.70
Er	2.16	2.27	1.97	2.14	2.34	2.18	1.95	2.20	0.61	0.85	1.38	2.14	3.24	1.45	1.54	1.99
Tm	0.33	0.35	0.30	0.33	0.35	0.33	0.29	0.34	0.09	0.14	0.22	0.32	0.52	0.24	0.25	0.30
Yb	2.12	2.26	1.96	2.10	2.31	2.19	1.83	2.28	0.65	1.02	1.56	2.08	3.65	1.74	1.80	1.99
Lu	0.31	0.34	0.29	0.31	0.37	0.34	0.27	0.36	0.11	0.18	0.26	0.32	0.57	0.28	0.30	0.31
Hf	4.79	5.25	5.23	4.07	3.45	5.10	6.24	5.22	0.46	1.70	2.69	3.45	7.10	4.25	4.35	5.23
Ta	0.75	0.61	0.45	0.50	0.43	0.46	0.18	0.51	0.04	0.13	0.14	0.42	1.19	0.88	0.86	0.45
Pb	22.78	18.39	15.54	15.04	9.55	11.11	7.87	9.17	2.68	5.32	5.82	9.25	9.00	9.40	9.35	9.36
Th	13.0	10.0	5.0	6.1	5.8	5.3	5.2	8.8	0.2	1.0	1.1	7.3	15.1	15.3	15.5	9.1
U	3.48	2.04	1.39	1.51	1.91	2.03	0.81	2.76	0.10	0.39	0.56	2.58	4.41	4.01	4.24	2.97
Lan/Smn	3.8	3.6	3.2	3.4	2.9	2.9	3.9	3.8	1.7	2.4	1.8	2.8	4.0	6.6	6.3	3.1
Gdn/Ybn	1.6	1.7	1.8	1.7	1.6	1.6	1.8	1.4	1.2	0.9	1.1	1.7	1.1	1.1	1.1	1.5
Lin/Hon	9.7	4.7	5.4	4.7	2.4	3.9	2.5	5.7	7.0	6.7	3.9	3.7	0.4	1.1	1.0	5.0

TABLE A3

(continued)

Sample	448	451	452	497	502	504	507	508	509	510	513	514	225	401	499	500
Region	NWB	NWB	NWB	NWB	NWB	NWB	NWB	NWB	NWB	NWB	NWB	NWB	NWB	NWB	NWB	NWB
Location	Sima	Sima	Sima	Revs	Revs	RakS	RakS	RakS	RakS	RakS	Åfjo	Åfjo	Vals	Kors	Revs	Revs
Type	FE	FE	FE	FE	FE	FE	FE	FE	FE	FE	FE	FE	Pec	Pec	MF	MF
SiO2	65.20	64.21	60.98	62.64	75.22	76.33	74.87	74.17	58.36	76.03	59.40	56.26	75.90	75.48	48.23	47.27
TiO2	0.59	0.53	0.69	0.49	0.20	0.21	0.19	0.23	0.47	0.23	0.90	1.02	0.06	0.12	1.23	2.41
Al2O3	16.32	16.88	17.36	15.83	13.24	13.05	13.47	13.53	16.14	12.97	16.22	17.27	13.78	14.40	15.82	14.11
FeO	4.74	4.92	5.57	7.55	2.55	2.18	2.62	2.97	9.43	2.38	7.27	8.13	0.53	0.90	10.67	14.38
MnO	0.08	0.08	0.08	0.14	0.06	0.06	0.07	0.06	0.16	0.05	0.11	0.13	0.01	0.02	0.17	0.20
MgO	2.28	2.24	2.85	2.56	0.49	0.44	0.48	0.64	4.37	0.50	3.67	4.07	0.07	0.26	8.79	7.68
CaO	5.04	5.32	5.92	6.51	2.82	2.59	2.77	3.18	7.19	2.81	6.19	7.36	1.45	2.73	11.72	9.42
Na2O	3.72	3.96	4.49	3.02	3.84	4.09	3.96	3.70	3.24	3.90	3.51	3.88	3.77	4.26	2.76	3.26
K2O	1.86	1.65	1.32	1.16	1.42	0.90	1.50	1.13	0.53	1.02	2.23	1.48	3.81	1.41	0.17	0.56
P2O5	0.12	0.13	0.16	0.09	0.05	0.04	0.06	0.06	0.07	0.06	0.25	0.35	0.01	0.04	0.09	0.28
CO2	0.07	0.11	0.59	0.04	0.15	0.15	0.04	0.29	0.07	0.11	0.22	0.04	0.07	0.04	0.37	0.18
S	0.01	0.01	0.02	0.02	0.01	0.02	0.01	0.09	0.01	0.01	0.02	0.02	0.01	0.01	0.01	0.24
SUM	100.03	100.04	100.03	100.05	100.05	100.06	100.04	100.05	100.04	100.07	99.99	100.01	99.47	99.67	100.03	99.99
LOI	1.1	1.3	1.6	0.2	0.5	0.1	0.5	0.1	1.0	0.2	0.7	0.8	0.6	0.1	1.2	0.9
Trace elements, ppm																
Li	12.8	14.3	13.2	12.3	11.5	6.3	9.2	12.2	13.0	3.9	13.5	7.5	3.1	3.9	5.3	5.3
Be	0.83	0.83	0.82	0.71	0.89	0.82	1.38	0.84	0.57	0.79	1.02	0.96	0.92	0.91	0.36	0.77
Sc	14	13	17	21	6	6	8	5	27	3	16	18	1	0	39	43
V	64.9	69.2	87.9	119.3	8.3	5.9	8.1	14.0	204.0	9.3	129.9	178.5	2.3	7.4	233.9	421.6
Cr	16.6	15.6	15.2	6.0	0.5	0.5	0.7	1.0	7.0	0.5	65.3	66.2	0.2	0.7	298.0	35.7
Co	11.8	12.5	14.8	17.2	4.0	3.4	3.5	3.8	24.9	3.1	17.1	20.2	0.9	1.9	45.7	43.9
Ni	10.3	11.0	11.9	4.7	0.9	0.9	0.9	0.8	5.8	0.5	26.9	25.3	0.6	0.8	140.2	40.0
Cu	20	23	5	16	20	0	3	0	30	1	41	74	2	11	3	77
Zn	50	45	33	57	30	28	45	29	63	25	58	66	13	20	80	112
Ga	15.8	16.7	17.4	15.5	12.6	11.4	13.5	10.3	13.3	9.8	15.3	16.3	15.2	13.6	15.6	21.4
Rb	51.6	43.3	31.8	34.2	53.7	25.5	44.2	33.4	12.2	28.8	62.4	40.1	41.9	18.8	1.1	6.0
Sr	438	500	527	272	136	103	125	114	169	108	442	534	430	1047	256	247
Y	20.1	20.0	27.1	15.2	14.6	13.9	29.3	11.0	16.9	7.5	27.4	24.9	3.1	2.3	28.2	46.4
Zr	163	156	95	101	111	129	132	115	73	87	391	189	67	47	82	169
Nb	7.0	6.4	7.3	2.9	5.2	3.8	5.9	3.2	2.4	3.1	10.1	8.2	3.7	2.8	1.7	7.7
Mo	0.550	0.186	0.207	0.095	0.128	0.056	0.062	0.031	0.033	0.066	0.999	0.550	0.034	0.062	0.245	0.339
Sn	0.96	0.80	0.60	0.51	1.00	0.59	0.85	0.54	0.49	0.42	1.66	1.12	0.09	0.14	1.10	1.79
Cs	1.40	1.08	1.20	1.60	1.53	0.80	1.20	0.90	0.19	0.75	1.39	0.79	0.27	0.24	0.05	0.09
Ba	404	402	315	235	278	304	351	296	121	331	454	356	811	1798	31	102
La	20.1	19.9	22.9	8.2	15.5	10.6	14.1	9.1	5.9	10.1	32.9	26.5	7.2	5.6	3.7	11.1
Ce	43.0	39.1	50.7	16.7	27.8	20.0	29.6	16.7	13.0	18.1	68.8	56.0	14.1	13.8	11.0	28.8
Pr	5.4	5.0	6.5	2.1	2.9	2.2	3.5	1.8	1.7	1.8	8.3	7.0	1.5	1.8	1.8	4.4
Nd	20.9	19.6	26.1	8.5	9.9	8.2	14.3	6.7	7.5	6.6	32.1	28.6	4.7	7.0	9.5	21.1
Sm	4.33	3.93	5.62	2.08	1.96	1.78	3.51	1.44	1.93	1.32	6.21	5.53	0.69	1.14	3.11	6.00
Eu	0.96	0.98	1.25	0.66	0.48	0.49	0.70	0.55	0.60	0.58	1.45	1.42	0.25	0.50	1.12	2.09
Gd	3.69	3.45	5.01	2.31	1.91	1.85	3.94	1.43	2.28	1.13	5.58	5.08	0.45	0.69	4.30	7.62
Tb	0.56	0.53	0.76	0.38	0.33	0.31	0.68	0.24	0.40	0.18	0.83	0.75	0.07	0.08	0.72	1.25
Dy	3.42	3.17	4.61	2.44	2.23	2.11	4.56	1.68	2.71	1.18	4.87	4.38	0.40	0.44	4.73	7.98
Ho	0.69	0.65	0.93	0.54	0.49	0.48	1.03	0.38	0.61	0.26	0.99	0.89	0.09	0.08	1.01	1.67
Er	1.94	1.86	2.59	1.61	1.50	1.47	3.08	1.20	1.82	0.79	2.73	2.44	0.29	0.20	2.83	4.64
Tm	0.29	0.28	0.39	0.25	0.25	0.25	0.49	0.20	0.29	0.13	0.41	0.36	0.05	0.03	0.43	0.68
Yb	1.95	1.91	2.48	1.75	1.83	1.75	3.34	1.47	1.97	0.99	2.72	2.36	0.41	0.20	2.75	4.33
Lu	0.30	0.31	0.38	0.29	0.32	0.29	0.55	0.25	0.32	0.17	0.42	0.37	0.07	0.03	0.43	0.67
Hf	4.64	4.36	2.84	2.59	3.04	3.36	3.87	3.09	1.97	2.35	9.36	5.06	2.47	1.14	2.23	4.34
Ta	0.52	0.37	0.34	0.17	0.36	0.24	0.35	0.21	0.12	0.19	0.53	0.41	0.25	0.16	0.10	0.47
Pb	8.69	7.91	3.56	4.41	9.72	9.11	9.67	11.72	4.98	8.89	9.64	7.30	18.51	9.33	0.80	8.49
Th	9.4	7.2	3.6	2.0	5.6	2.6	4.9	2.7	1.0	2.8	9.0	3.7	2.1	0.9	0.2	0.8
U	3.71	2.32	1.17	0.73	0.89	0.72	1.64	1.14	0.37	0.86	2.88	1.23	0.55	0.30	0.09	1.03
Lan/Smn	2.9	3.2	2.5	2.5	4.9	3.7	2.5	3.9	1.9	4.8	3.3	3.0	6.5	3.0	0.7	1.1
Gdn/Ybn	1.5	1.5	1.6	1.1	0.8	0.9	1.0	0.8	0.9	0.9	1.7	1.7	0.9	2.8	1.3	1.4
Lin/Hon	4.4	5.1	3.3	5.3	5.5	3.1	2.1	7.5	5.0	3.4	3.2	2.0	8.2	12.0	1.2	0.8

TABLE A3
(continued)

Sample	503	226	231	233	235	297	399	400	426	427	428	429	432	449	450	506
Region	NWB	NWB	NWB	NWB	NWB	NWB	NWB	NWB	NWB	NWB	NWB	NWB	NWB	NWB	NWB	NWB
Location	RakS	Vals	Vals	Vals	Vals	Vin	Kors	Kors	Kopp	Kopp	Kopp	Kopp	Kopp	Sima	Sima	RakS
Type	MF	ME	ME	ME	ME	ME	ME	ME	ME	ME	ME	ME	ME	ME	ME	ME
SiO2	53.23	50.78	52.71	49.26	55.85	45.61	51.70	52.00	50.03	48.54	50.06	52.10	52.43	52.00	55.63	49.59
TiO2	0.63	2.01	1.43	2.12	0.75	2.31	0.90	1.07	0.72	1.10	0.79	0.86	1.14	0.91	0.97	0.61
Al2O3	15.71	17.16	18.82	15.33	18.88	16.12	18.34	21.02	20.18	19.40	19.96	19.32	19.55	15.66	17.75	15.09
FeO	10.54	10.30	8.50	11.40	6.67	14.94	8.78	7.02	9.08	10.43	9.34	8.40	8.55	9.56	7.61	10.32
MnO	0.18	0.15	0.12	0.16	0.13	0.20	0.14	0.11	0.15	0.15	0.15	0.14	0.14	0.19	0.11	0.20
MgO	6.54	5.22	4.58	6.82	3.14	6.73	5.36	3.32	6.43	6.53	5.66	5.35	3.81	6.73	3.70	9.63
CaO	10.26	9.39	8.65	10.79	7.85	9.40	8.91	9.30	10.37	10.96	10.29	9.35	8.73	12.08	7.28	9.44
Na2O	2.06	3.79	4.04	2.85	4.17	2.65	4.07	4.79	2.64	2.41	3.20	3.80	4.27	1.60	3.35	2.73
K2O	0.39	0.55	0.43	0.59	1.74	1.43	0.99	0.50	0.18	0.20	0.16	0.27	0.75	0.75	2.80	1.83
P2O5	0.07	0.35	0.20	0.33	0.44	0.31	0.38	0.40	0.13	0.11	0.23	0.26	0.33	0.21	0.34	0.19
CO2	0.22	0.07	0.11	0.11	0.15	0.15	0.07	0.11	0.07	0.04	0.04	0.04	0.15	0.18	0.37	0.33
S	0.18	0.07	0.08	0.11	0.01	0.02	0.01	0.01	0.01	0.01	0.01	0.01	0.03	0.02	0.10	0.04
SUM	100.01	99.84	99.67	99.87	99.78	99.87	99.65	99.65	99.99	99.88	99.89	99.90	99.88	99.89	100.01	100.00
LOI	0.9	0.7	1.1	0.9	1.6	1.9	0.9	0.8	0.1	0.1	0.3	0.5	0.5	1.0	0.8	1.0
Trace elements, ppm																
Li	7.5	7.8	9.3	7.2	15.7	35.8	11.3	4.6	1.7	2.3	3.0	6.6	8.4	11.1	20.7	32.1
Be	0.47	0.99	0.86	1.00	1.61	0.91	1.18	1.29	0.36	0.40	0.42	0.63	0.86	1.23	1.26	1.40
Sc	44	23	18	31	10	31	21	11	23	29	24	24	23	19	19	34
V	238.0	252.6	192.3	306.2	137.8	267.9	204.5	141.1	172.9	247.9	222.1	174.5	194.0	127.1	138.2	226.9
Cr	49.9	19.2	25.8	184.3	6.4	100.5	27.6	9.8	55.4	45.9	51.5	51.3	36.1	221.5	37.4	495.7
Co	36.7	38.0	33.3	42.5	16.6	54.9	28.4	17.8	31.4	40.5	30.4	27.9	21.9	14.4	17.7	40.4
Ni	19.8	21.8	31.5	54.7	7.0	99.5	18.3	8.6	45.7	45.7	31.6	32.0	19.2	170.1	14.4	144.0
Cu	65	35	40	49	25	153	2	11	23	133	48	41	73	5	58	47
Zn	70	104	82	101	88	131	114	77	72	78	78	76	86	80	66	115
Ga	15.1	24.1	22.5	22.2	20.8	24.1	23.2	26.3	17.9	18.0	19.1	19.4	20.5	20.6	19.4	16.0
Rb	6.1	6.3	6.9	6.2	41.5	43.3	18.1	7.6	2.2	3.0	1.1	2.3	14.2	24.5	96.0	56.1
Sr	133	511	543	426	1436	359	1203	1633	748	719	784	757	643	419	575	304
Y	18.3	24.7	18.1	25.4	24.5	37.3	19.3	18.3	8.4	10.2	9.1	16.6	28.6	26.3	25.8	11.0
Zr	25	150	155	175	160	177	76	187	14	24	10	24	157	150	170	57
Nb	2.1	34.3	14.6	29.6	14.5	12.6	4.2	7.7	1.2	2.7	0.7	4.6	9.6	13.4	15.4	3.0
Mo	0.064	0.954	0.354	1.138	1.151	0.985	0.071	0.054	0.096	0.159	0.069	0.121	0.209	0.435	7.888	0.401
Sn	0.46	1.49	0.99	1.83	1.38	1.85	0.98	1.09	0.23	0.35	0.27	0.33	1.05	1.90	2.32	1.06
Cs	0.18	0.20	0.33	0.12	2.16	1.39	0.64	0.35	0.20	0.10	0.07	0.07	0.39	1.09	2.63	2.19
Ba	72	194	154	189	528	315	449	227	98	96	98	181	272	176	445	318
La	5.3	25.1	16.6	22.7	57.2	15.9	29.8	23.2	6.5	7.0	7.2	14.9	23.1	32.0	33.1	21.3
Ce	12.4	55.1	35.0	48.7	127.1	37.8	66.3	57.9	13.3	14.6	15.1	30.9	53.3	65.3	71.8	42.3
Pr	1.7	6.8	4.5	6.1	15.4	5.4	8.6	8.3	1.7	1.9	2.0	4.0	7.2	7.8	9.2	5.1
Nd	7.5	26.8	18.1	25.0	58.5	24.1	36.7	36.5	7.4	8.3	8.7	17.0	30.7	29.5	35.3	19.8
Sm	2.11	5.76	4.16	5.82	9.73	6.31	7.53	7.50	1.63	1.91	1.96	3.60	6.67	5.70	6.77	3.62
Eu	0.70	1.91	1.43	1.86	2.43	2.05	2.07	2.07	0.92	0.90	0.98	1.33	1.65	1.40	1.53	0.95
Gd	2.61	5.42	3.95	5.71	7.11	6.63	5.25	5.40	1.62	1.91	1.93	3.34	5.84	4.83	5.33	2.63
Tb	0.44	0.82	0.61	0.86	0.93	1.07	0.69	0.70	0.24	0.29	0.28	0.48	0.85	0.74	0.77	0.36
Dy	2.87	4.64	3.44	4.96	4.79	6.59	3.70	3.54	1.47	1.76	1.66	2.89	5.05	4.43	4.50	1.96
Ho	0.64	0.90	0.67	0.96	0.87	1.37	0.68	0.63	0.30	0.36	0.33	0.59	1.02	0.88	0.88	0.38
Er	1.84	2.34	1.75	2.48	2.25	3.70	1.81	1.55	0.85	1.03	0.89	1.60	2.76	2.50	2.46	1.04
Tm	0.28	0.32	0.24	0.34	0.32	0.54	0.26	0.21	0.13	0.15	0.12	0.23	0.40	0.38	0.38	0.15
Yb	1.88	1.96	1.46	2.01	1.96	3.38	1.62	1.27	0.86	1.04	0.82	1.53	2.56	2.44	2.48	1.00
Lu	0.30	0.28	0.21	0.28	0.28	0.50	0.24	0.18	0.14	0.16	0.13	0.25	0.39	0.38	0.38	0.16
Hf	0.97	3.81	3.67	4.35	4.23	4.56	2.10	4.19	0.45	0.71	0.34	0.74	4.48	4.09	4.48	1.57
Ta	0.10	1.62	0.75	1.54	0.92	0.63	0.18	0.27	0.06	0.14	0.04	0.21	0.36	0.66	0.68	0.14
Pb	3.51	3.66	3.20	3.28	13.65	6.81	5.72	4.21	2.20	2.71	2.52	4.51	7.12	9.84	8.07	7.97
Th	0.7	1.5	1.0	1.8	14.6	1.3	4.6	0.3	0.4	0.5	0.2	0.3	2.2	4.6	9.4	6.2
U	0.25	0.47	0.37	0.68	3.72	0.61	1.50	0.30	0.15	0.20	0.08	0.13	1.25	1.07	3.46	1.94
Lan/Smn	1.6	2.7	2.5	2.4	3.7	1.6	2.5	1.9	2.5	2.3	2.3	2.6	2.2	3.5	3.0	3.7
Gdn/Ybn	1.1	2.2	2.2	2.3	2.9	1.6	2.6	3.4	1.5	1.5	1.9	1.8	1.8	1.6	1.7	2.1
Lin/Hon	2.7	2.0	3.2	1.8	4.2	6.1	3.9	1.7	1.3	1.5	2.1	2.7	1.9	3.0	5.5	19.7

TABLE A3

(continued)

Sample	515	516	517	519	521	531	442	227	430
Region	NWB	NWB	NWB	NWB	NWB	NWB	NWB	NWB	NWB
Location	Åfjo	Åfjo	Åfjo	RakN	RakN	Vals	Foll	Vals	Kopp
Type	ME	ME	ME	ME	ME	ME	AB	HBL	HBL
SiO2	49.89	47.46	45.70	48.31	53.49	52.97	49.28	39.16	47.60
TiO2	0.97	1.12	1.07	0.19	0.97	1.57	1.11	5.50	0.99
Al2O3	18.65	19.15	21.23	21.75	17.08	18.07	15.33	8.35	9.29
FeO	9.54	10.63	9.77	4.60	8.81	9.22	7.40	16.50	12.82
MnO	0.15	0.16	0.14	0.07	0.16	0.12	0.10	0.27	0.22
MgO	5.85	6.27	5.89	8.38	5.75	4.46	7.23	12.05	15.58
CaO	9.88	12.03	13.07	15.00	9.17	7.89	9.90	13.81	11.90
Na2O	3.96	2.64	2.51	1.27	3.51	4.25	3.55	0.91	1.05
K2O	0.72	0.25	0.25	0.18	0.67	1.17	2.78	0.41	0.34
P2O5	0.25	0.27	0.26	0.03	0.28	0.23	1.10	2.78	0.01
CO2	0.11	0.04	0.11	0.26	0.11	0.04	1.97	0.11	0.07
S	0.03	0.01	0.01	0.01	0.01	0.02	0.15	0.04	0.01
SUM	100.00	100.03	100.01	100.05	100.01	100.01	99.90	99.89	47.60
LOI	0.7	0.6	0.7	1.5	0.7	0.7	2.8	0.6	0.9
Trace elements, ppm									
Li	6.5	6.6	5.8	3.5	10.0	16.6	42.9	6.6	6.0
Be	0.65	0.56	0.49	0.19	0.75	0.78	2.62	0.57	0.28
Sc	26	38	32	24	26	15	11	53	79
V	199.7	280.9	238.0	52.2	173.9	155.9	112.2	703.1	416.9
Cr	42.4	88.6	84.9	717.7	100.0	20.2	209.6	7.2	807.2
Co	29.5	32.4	29.9	26.6	25.6	27.9	23.8	74.3	68.7
Ni	37.3	24.4	28.4	75.1	38.7	28.6	184.0	80.6	275.1
Cu	118	6	35	2	36	22	25	19	2
Zn	76	83	73	26	80	63	97	145	107
Ga	17.9	19.6	19.6	13.0	17.4	20.3	21.0	20.6	15.4
Rb	10.0	1.5	2.2	4.2	12.5	29.0	95.7	2.2	1.8
Sr	659	739	756	708	645	585	2883	100	118
Y	22.4	32.3	22.0	4.7	20.4	14.3	27.4	69.2	31.7
Zr	49	43	41	16	90	104	231	112	31
Nb	5.0	5.9	5.5	0.8	5.3	14.9	18.1	51.6	4.7
Mo	0.898	0.092	0.135	0.036	0.462	0.875	0.107	0.199	0.067
Sn	0.96	0.91	0.63	0.15	0.83	1.01	1.25	2.45	1.18
Cs	0.38	0.02	0.14	0.11	0.55	0.61	5.28	0.09	0.06
Ba	115	73	63	75	183	221	449	34	27
La	16.1	15.1	12.4	3.9	17.7	16.6	177.2	83.1	5.4
Ce	35.5	38.9	31.5	8.4	38.7	34.0	362.2	167.5	20.3
Pr	4.9	5.7	4.5	1.1	5.0	4.1	42.2	21.1	3.5
Nd	21.2	26.6	20.4	4.9	21.6	17.0	155.2	86.2	17.7
Sm	4.32	5.84	4.34	0.99	4.20	3.60	23.16	18.93	4.92
Eu	1.33	1.49	1.26	0.42	1.33	1.19	5.00	4.33	1.39
Gd	4.36	6.12	4.44	0.97	4.13	3.44	11.54	17.73	5.43
Tb	0.65	0.93	0.66	0.14	0.60	0.49	1.29	2.54	0.84
Dy	3.80	5.49	3.85	0.85	3.52	2.67	6.00	13.94	5.15
Ho	0.77	1.11	0.78	0.17	0.72	0.51	0.94	2.60	1.06
Er	2.13	3.01	2.14	0.43	1.93	1.32	2.10	6.39	2.93
Tm	0.32	0.43	0.31	0.06	0.29	0.18	0.27	0.82	0.44
Yb	2.10	2.75	1.98	0.38	1.91	1.19	1.57	4.61	2.85
Lu	0.33	0.42	0.30	0.06	0.30	0.18	0.22	0.61	0.45
Hf	1.62	1.75	1.62	0.48	2.52	2.94	5.33	3.61	1.54
Ta	0.20	0.23	0.22	0.05	0.28	0.89	0.71	2.09	0.19
Pb	7.04	2.33	3.11	2.42	10.47	9.44	49.47	0.76	0.94
Th	1.0	0.9	0.3	0.5	2.7	4.1	23.7	1.4	0.2
U	0.57	0.33	0.10	0.20	0.89	1.24	5.18	1.25	0.08
Lan/Smn	2.3	1.6	1.8	2.4	2.6	2.9	4.8	2.7	0.7
Gdn/Ybn	1.7	1.8	1.8	2.1	1.8	2.3	5.9	3.1	1.5
Lin/Hon	2.0	1.4	1.7	5.0	3.3	7.6	10.7	0.6	1.3

Region: L-R, Lensvik-Rissa areas; NWB, northwestern belts.

Named boxes in figure 1: Åfjo, Åfjord; Foll, Follafoss; Kopp, Kopparen; Kors, Korsvika; Lens, Lensvik; RakN, Råkvåg North; RakS, Råkvåg South; Revs, Revsneshagen; Rissa, Rissa; Sima, Simadalen; Vals, Valset-Rishaugen; Ver, Verran; Vin, Vingan.

Type: PG, "plagiogranite"; Adak, adakite; Ad'tic, adakitic; FE, felsic, $La_n/Sm_n>1.5$, LREE-enriched; Pec, peculiar; MF, mafic, $Gd_n/Yb_n<1.45$; ME, mafic, $Gd_n/Yb_n>1.45$, AB, alkali basalt; HBL, hornblendite.

REFERENCES

Aleinikoff, J. N., and Moench, R. H., 1987, U–Pb geochronology and Pb isotopic systematics of plutonic rocks in northern New Hampshire: Ensimatic vs. ensialic sources: Geological Society of America Abstracts with Programs, v. 19, n. 1, p. 1.

——— 1992, U–Pb zircon ages of the Ordovician Ammonoosuc Volcanics and related plutons near Littleton and Milan, New Hampshire: Geological Society of America Abstracts with Programs, v. 24, n. 3, p. 2.

Aleinikoff, J. N., Rankin, D. W., Moench, R. H., and Walsh, G. J., 2015, New SHRIMP U–Pb zircon ages for felsic Ammonoosuc Volcanics, northern NH–VT: Geological Society of America Abstracts with Programs, v. 47, n. 3, p. 41.

Alvarado, G. E., Soto, G. J., Schmincke, H.–U., Bolge, L. L., and Sumita, M., 2006, The 1968 andesitic lateral blast eruption at Arenal Volcano, Costa Rica: Journal of Volcanology and Geothermal Research, v. 157, n. 1–3, p. 9–33, http://dx.doi.org/10.1016/j.jvolgeores.2006.03.035

Andersen, T. B., 1998, Extensional tectonics in the Caledonides of southern Norway, an overview: Tectonophysics, v. 285, n. 3–4, p. 333–351, http://dx.doi.org/10.1016/S0040-1951(97)00277-1

Andréasson, P. G., Gee, D. G., Whitehouse, M. J., and Schöberg, H., 2003, Subduction-flip during Iapetus Ocean closure and Baltica–Laurentia collision, Scandinavian Caledonides: Terra Nova, v. 15, n. 6, p. 362–369, http://dx.doi.org/10.1046/j.1365-3121.2003.00486.x

Armstrong, H. A., and Owen, A. W., 2001, Terrane evolution of the paratectonic Caledonides of northern Britain: Journal of the Geological Society, London, v. 158, p. 475–486, http://dx.doi.org/10.1144/jgs.158.3.475

Arth, J. G., 1979, Some trace elements in trondhjemites–their implications to magma genesis and paleotectonic setting, *in* Barker, F., editor, Trondhjemites, Dacites and Related Rocks: Amsterdam, Elsevier, Developments in Petrology, v. 6, chapter 3, p. 123–132, http://dx.doi.org/10.1016/B978-0-444-41765-7.50008-3

Barbieri, M., Caggianelli, A., DiFlorio, M. R., and Lorenzoni, S., 1994, Plagiogranites and gabbroic rocks from the Mingora ophiolitic melange, Swat Valley, NW Frontier Province, Pakistan: Mineralogical Magazine, v. 58, p. 553–566, http://dx.doi.org/10.1180/minmag.1994.058.393.03

Barker, S. J., Wilson, C. J. N., Baker, J. A., Millet, M.–A., Rotella, M. D., Wright, I. C., and Wysoczanski, R. J., 2012, Geochemistry and petrogenesis of silicic magmas in the intra-oceanic kermadec arc: Journal of Petrology, v. 54, n. 2, p. 351–391, http://dx.doi.org/10.1093/petrology/egs071

Barnes, C. G., Prestvik, T., Barnes, M. A. W., Anthony, E. Y., and Allen, C. M., 2003, Geology of a magma transfer zone: The Hortavær Igneous Complex, north-central Norway: Norwegian Journal of Geology, v. 83, n. 3, p. 187–208, http://foreninger.uio.no/ngf/ngt/pdfs/NJG_83_187-208.pdf

Barnes, C. G., Dumond, G., Yoshinobu, A. S., and Prestvik, T., 2004, Assimilation and crystal accumulation in a mid-crustal magma chamber: the Sausfjellet pluton, north-central Norway: Lithos, v. 75, n. 3–4, p. 389–412, http://dx.doi.org/10.1016/j.lithos.2004.04.036

Barnes, C. G., Prestvik, T., Sundvoll, B., and Surratt, D., 2005, Pervasive assimilation of carbonate and silicate rocks in the Hortavær igneous complex, north-central Norway: Lithos, v. 80, n. 1–4, p. 179–199, http://dx.doi.org/10.1016/j.lithos.2003.11.002

Barnes, C. G., Frost, C. D., Yoshinobu, A. S., McArthur, K., Barnes, M. A., Allen, C. M., Nordgulen, Ø., and Prestvik, T., 2007, Timing of sedimentation, metamorphism, and plutonism in the Helgeland Nappe Complex, north-central Norwegian Caledonides: Geosphere, v. 3, n.6, p. 683–703, http://dx.doi.org/10.1130/GES00138.1

Barnes, C. G., Prestvik, T., Li, Y., McCulloch, L., Yoshinobu, A. S., and Frost, C. D., 2009, Growth and zoning of the Hortavær intrusive complex, a layered alkaline pluton in the Norwegian Caledonides: Geosphere, v. 5, n. 3, p. 286–301, http://dx.doi.org/10.1130/GES00210.1

Beard, J. S., 1998, Polygenetic tonalite–trondhjemite–granodiorite (TTG) magmatism in the Smartville Complex, Northern California with a note on LILE depletion in plagiogranites: Mineralogy and Petrology, v. 64, n. 1, p. 15–45, http://dx.doi.org/10.1007/BF01226562

Birkland, A., Nordgulen, Ø., Cuming, G. L., and Bjørlykke, A., 1993, Pb–Nd–Sr isotopic constraints on the origin of the Caledonian Bindal Batholith, central Norway: Lithos, v. 29, n. 3–4, p. 257–271, http://dx.doi.org/10.1016/0024-4937(93)90020-D

Bjerkgård, T., and Bjørlykke, A., 1994, The stratabound sulphide deposits in the Folldal area, Southern Trondheim Region, Norway: Norsk Geologisk Tidsskrift, v. 74, p. 213–237.

Boe, R., Sturt, B. A., and Ramsay, D. M. 1993, The conglomerates of the Sel Group, Otta–Våqå area, Central Norway: An example of a terrane-linking succession: Norges geologiske undersøkelse Bulletin, v. 425, p. 1– 23.

Bolge, L. L., Carr, M. J., Feigenson, M. D., and Alvarado, G. E., 2006, Geochemical stratigraphy and magmatic evolution at Arenal volcano, Costa Rica: Journal of Volcanology and Geothermal Research, v. 157, n. 1–3, p. 34–48, http://dx.doi.org/10.1016/j.jvolgeores.2006.03.036

Bolge, L. L., Carr, M. J., Milidakis, K. I., Lindsay, F. N., and Feigenson, M. D., 2009, Correlating geochemistry, tectonics, and volcanic volume along the Central American volcanic front: Geochemistry, Geophysics, Geosystems, v. 10, http://dx.doi.org/10.1029/2009GC002704

Bonev, N., and Stampfli, G., 2008, Gabbro, plagiogranite and associated dykes in the supra-subduction zone Evros Ophiolites, NE Greece: Geological Magazine, v. 146, n. 1, p. 72–91, http://dx.doi.org/10.1017/S0016756808005396

Boone, G. M., 1983, The Hurricane Mountain Formation Melange and unconformably overlying Lower to Middle Ordovician volcanics, Brassua Lake and Moosehead Lake Quadrangles, *in* Caldwell, D. W., and Hanson, L. S., editors, Guidebook, The Greenville–Millinocket Regions, North-Central Maine: New England Intercollegiate Geologic Conference, 75th annual meeting, p. 31–44.

Brophy, J. G., and Pu, X., 2012, Rare earth element–SiO2 systematics of mid-ocean ridge plagiogranites and

host gabbros from the Fournier oceanic fragment, New Brunswick, Canada: A field evaluation of some model predictions: Contributions to Mineralogy and Petrology, v. 164, n. 2, p. 191–204, http://dx.doi.org/10.1007/s00410-012-0732-x

Brueckner, H. K., and van Roermund, H. L. M., 2004, Dunk tectonics: A multiple subduction/eduction model for the evolution of the Scandinavian Caledonides: Tectonics, v. 23, n. 2, p. 1–20, http://dx.doi.org/10.1029/2003tc001502

Bruton, D. L., and Harper, D. A. T., 1981, Brachiopods and trilobites of the early Ordovician serpentine Otta Conglomerate, south central Norway: Norsk Geologisk Tidsskrift, v. 61, p. 153–181.

——— 1988, Arenig–Llandovery stratigraphy and faunas across the Scandinavian Caledonides: Geological Society, London, Special Publications, v. 38, p. 247–268, http://dx.doi.org/10.1144/GSL.SP.1988.038.01.15

Chew, D. M., and Strachan, R. A., 2013, The Laurentian Caledonides of Scotland and Ireland, *in* Corfu, F., Gasser, D., and Chew, D. M., editors, New Perspectives on the Caledonides of Scandinavia and Related Areas: Geological Society, London, Special Publications, v. 390, p. 45–91, http://dx.doi.org/10.1144/SP390.16

Coish, R., Kim, J., Twelker, E., Zolkos, S., and Walsh, G., 2015, Geochemistry and origin of metamorphosed mafic rocks from the Lower Paleozoic Moretown and Cram Hill Formations of north-central Vermont: Delamination magmatism in the western New England Appalachians: American Journal of Science, v. 315, n. 9, p. 809–845, http://dx.doi.org/10.2475/09.2015.02

Coleman, R. G., and Donato, M. M., 1979, Oceanic plagiogranite revisited, *in* Barker, F., editor, Trondhjemites, Dacites, and Related Rocks: Amsterdam, Elsevier Scientific Publishing, Developments in Petrology, v. 6, chapter 5, p. 149–168, http://dx.doi.org/10.1016/B978-0-444-41765-7.50010-1

Defant, M. J., and Drummond, M. S., 1990, Derivation of some modern arc magmas by melting of young subducted lithosphere: Nature, v. 347, p. 662–665, http://dx.doi.org/10.1038/347662a0

Dilek, Y., and Thy, P., 2006, Age and petrogenesis of plagiogranite intrusions in the Ankara mélange, central Turkey: Island Arc, v. 15, n. 1, p. 44–57, http://dx.doi.org/10.1111/j.1440-1738.2006.00522.x

Dorais, M. J., Workman, J., and Aggarwal, J., 2008, The petrogenesis of the Highlandcroft and Oliverian plutonic suites, New Hampshire: Implications for the structure of the Bronson Hill Terrane: American Journal of Science, v. 308, n. 1, p. 73–99, http://dx.doi.org/10.2475/01.2008.03

Drake, A. A., Jr., Sinha, A. K., Laird, J., and Guy, R. E., 1989. The Taconic orogen, *in* Hatcher, R. D., Jr., Thomas, W. A., and Viele, G. W., editors, The Appalachian–Ouachita Orogen in the United States: Geological Society of America, The Geology of North America, v. F-2, p. 101–177, http://dx.doi.org/10.1130/dnag-gna-f2.101

Drinkwater, J. L., Brew, D. A., and Ford, A. B., 1995, Geology, petrography, and geochemistry of granitic rocks from the Coast Mountains Complex near Juneau, southeastern Alaska: United States Geological Survey, Open File Report 95–638, 119 p.

Dunning, G. R., and Grenne, T., 2000, U–Pb age dating and paleotectonic significance of trondhjemite from the type locality in the central Norwegian Caledonides: Norges geologiske undersøkelse Bulletin, v. 437, p. 57–65.

Dunning, G. R., and Pedersen, R. B., 1988, U–Pb ages of ophiolites and arc-related plutons of the Norwegian Caledonides: Implications for the development of Iapetus: Contributions to Mineralogy and Petrology, v. 98, n. 1, p. 13–23, http://dx.doi.org/10.1007/BF00371904

Dypvik, H., and Brunfelt, A. O., 1976, Rare-earth elements in Lower Palaeozoic epicontinental and eugeosynclinal sediments from the Oslo and Trondheim regions: Sedimentology, v. 23, n. 3, p. 363–378, http://dx.doi.org/10.1111/j.1365-3091.1976.tb00055.x

Ewart, A., 1982, The mineralogy and petrology of Tertiary–Recent orogenic volcanic rocks: With special reference to the andesitic–basaltic compositional range, *in* Thorp, R. S., editor, Andesites: Orogenic Andesites and Related Rocks: New York, John Wiley and Sons, p. 25–95.

Ewart, A., Bryan, W. B., Chappell, B. W., and Rudnick, R. L., 1994, Regional geochemistry of the Lau–Tonga arc and backarc systems, *in* Hawkins, J., Parson, L., and Allan, J., editors, Proceedings of the Ocean Drilling Program: Scientific Results, v. 135, p. 385–425, http://dx.doi.org/10.2973/odp.proc.sr.135.141.1994

Eyuboglu, Y., Santosh, M., and Chung, S.–L., 2011, Crystal fractionation of adakitic magmas in the crust–mantle transition zone: Petrology, geochemistry and U–Pb zircon chronology of the Seme adakites, eastern Pontides, NE Turkey: Lithos, v. 121, n. 1–4, p. 151–166, http://dx.doi.org/10.1016/j.lithos.2010.10.012

Floyd, P. A., Yaliniz, M. K., and Goncuoglu, M. C., 1998, Geochemistry and petrogenesis of intrusive and extrusive ophiolitic plagiogranites, Central Anatolian Crystalline Complex, Turkey: Lithos, v. 42, n. 3–4, p. 225–241, http://dx.doi.org/10.1016/S0024-4937(97)00044-3

Fossen, H., and Dunlap, W. J., 2006, Age constraints on the late Caledonian (Scandian) deformation in the Major Bergen Arc, SW Norway: Norwegian Journal of Geology, v. 86, p. 59–70.

France, L., Koepke, J., Ildefonse, B., Cichy, S. B., and Deschamps, F., 2010, Hydrous partial melting in the sheeted dike complex at fast spreading ridges: Experimental and natural observations: Contributions to Mineralogy and Petrology, v. 160, n. 5, p. 683–704, http://dx.doi.org/10.1007/s00410-010-0502-6

Freund, S., Beier, C., Krumm, S., and Haase, K. M., 2013, Oxygen isotope evidence for the formation of andesitic–dacitic magmas from the fast-spreading Pacific–Antarctic Rise by assimilation–fractional crystallization: Chemical Geology, v. 347, p. 271–283, http://dx.doi.org/10.1016/j.chemgeo.2013.04.013

Freund, S., Haase, K. M., Keith, M., Beier, C., and Garbe-Schönberg, D., 2014, Constraints on the formation of geochemically variable plagiogranite intrusions in the Troodos Ophiolite, Cyprus: Contributions to Mineralogy and Petrology, v. 167, p. 1–22, http://dx.doi.org/10.1007/s00410-014-0978-6

Furnes, H., Brekke, H., Nordås, J., and Hertogen, J., 1986, Lower Palaeozoic convergent plate margin

volcanism on Bømlo, southwest Norwegian Caledonides: Geochemistry and petrogenesis: Geological Magazine, v. 123, n. 2, p, 123–142, http://dx.doi.org/10.1017/S0016756800029782
Furnes, H., Dilek, Y., and Pedersen, R. B., 2012, Structure, geochemistry, and tectonic evolution of trench–distal backarc oceanic crust in the western Norwegian Caledonides, Solund–Stavfjord ophiolite (Norway): Geological Society of America Bulletin, v. 124, n. 7–8, p. 1027–1047, http://dx.doi.org/10.1130/B30561.1
Fyffe, L. R., Johnson, S. C., and van Staal, C. R., 2011, A review of Proterozoic to Early Paleozoic lithotectonic terranes in New Brunswick, Canada, and their tectonic evolution during Penobscot, Taconic, Salinic, and Acadian orogenesis: Atlantic Geology, v. 47, p. 211–248, http://dx.doi.org/10.4138/atlgeol.2011.010
Gale, G. H., 1974, Geokjemiske undersøkelser av kaledonske vulkanitter og intrusiver i Midt- og Syd-Norge: Dell II–Analytiske data: Norges geologiske undersøkelse, Report 1228B, 45 p.
Gale, G. H., and Roberts, D., 1974, Trace element geochemistry of Norwegian Lower Paleozoic basic volcanics and its tectonic implications: Earth and Planetary Science Letters, v. 22, n. 4, p. 380–390, http://dx.doi.org/10.1016/0012-821X(74)90148-4
Gao, Y., Hou, Z., Kamber, B. S., Wei, R., Meng, X., and Zaho, R., 2007, Adakite-like porphyries from the southern Tibetan continental collision zones: Evidence for slab melt metasomatism: Contributions to Mineralogy and Petrology, v. 153, n. 1, p. 105–120, http://dx.doi.org/10.1007/s00410-006-0137-9
Gaschnig, R. M., Vervoort, J. D., Lewis, R. S., and Tikoff, B., 2011, Isotopic evolution of the Idaho Batholith and Challis Intrusive Province, northern US Cordillera: Journal of Petrology, v. 52, n. 12, p. 2397–2429, http://dx.doi.org/10.1093/petrology/egr050
Gautneb, H., and Roberts, D., 1989, Geology and petrochemistry of the Smøla–Hitra Batholith, Central Norway: Norges geologiske undersøkelse Bulletin, v. 416, p. 1–24.
Gee, D. G., 1981, The Dictyonema-bearing phyllites at Nordaunevoll, eastern Trøndelag, Norway: Norsk Geologisk Tidsskrift, v. 61, p. 93–95.
——— 2005, Scandinavian Caledonides (with Greenland), *in* Selley, R. C., Cocks, L. R. M., and Plimer, I. R., editors, Encyclopedia of Geology: Amsterdam, Elsevier, p. 64–74, http://dx.doi.org/10.1016/B0-12-369396-9/00420-2
Gee, D. G., Fossen, H., Henriksen, N., and Higgins, A. K., 2008, From the Early Paleozoic Platforms of Baltica and Laurentia to the Caledonide Orogen of Scandinavia and Greenland: Episodes, v. 31, n. 1, p. 44–51.
Gerlach, D. C., Leeman, W. P., and Lallemant, H. G. A., 1981, Petrology and geochemistry of plagiogranite in the Canyon Mountain Ophiolite, Oregon: Contributions to Mineralogy and Petrology, v. 77, n. 1, p. 82–92, http://dx.doi.org/10.1007/BF01161505
Grenne, T., 1987, Marginal basin type metavolcanites of the Hersjø Formation, eastern Trondheim District, Central Norwegian Caledonides: Norges geologiske undersøkelse Bulletin, v. 412, p. 29–42.
——— 1989a, Magmatic evolution of the Løkken SSZ Ophiolite, Norwegian Caledonides: Relationships between anomalous lavas and high-level intrusions: Geological Journal, v. 24, n. 4, p. 251–274, http://dx.doi.org/10.1002/gj.3350240403
——— 1989b, The feeder zone to the Løkken ophiolite-hosted massive sulfide deposit and related mineralizations in the central Norwegian Caledonides: Economic Geology, v. 84, n. 8, p. 2173–2195, http://dx.doi.org/10.2113/gsecongeo.84.8.2173
Grenne, T., and Lagerblad, B., 1985, The Fundsjø Group, central Norway–a Lower Paleozoic island arc sequence: Geochemistry and regional implications, *in* Gee, D. G., and Sturt, B. A., editors, The Caledonide Orogen–Scandinavia and Related Areas, Part 2: Chichester, England, John Wiley and Sons, p. 745–760.
Grenne, T., and Roberts, D., 1980, Geochemistry and volcanic setting of the Ordovician Forbordfjell and Jonsvatn greenstones, Trondheim region, central Norwegian Caledonides: Contributions to Mineralogy and Petrology, v. 74, n. 4, p. 375–386, http://dx.doi.org/10.1007/BF00518118
——— 1998, The Hølonda porphyrites, Norwegian Caledonides; Geochemistry and tectonic setting of Early-Mid-Ordovician shoshonitic volcanism: Journal of the Geological Society, London, v. 155, n. 1, p. 131–142, http://dx.doi.org/10.1144/gsjgs.155.1.0131
Grimes, C. B., Ushikubo, T., Kozdon, R., and Valley, J. W., 2013, Perspectives on the origin of plagiogranite in ophiolites from oxygen isotopes in zircon: Lithos, v. 179, p. 48–66, http://dx.doi.org/10.1016/j.lithos.2013.07.026
Gromet, L. P., and Roberts, D., 2010, Early Ordovician ages of zircons from felsic rocks and a conglomerate clast, Frosta peninsula, central Norwegian Caledonides: Norges geologiske undersøkelse Bulletin, v. 450, p. 60–64.
Hacker, B. R., and Gans, P. B., 2005, Continental collisions and the creation of ultrahigh-pressure terranes: Petrology and thermochronology of nappes in the central Scandinavian Caledonides: Geological Society of America Bulletin, v. 117, n. 1–2, p. 117–134, http://dx.doi.org/10.1130/B25549.1
Hansen, J., Skjerlie, K. P., Pedersen, R. B., and De La Rosa, J., 2002, Crustal melting in the lower parts of island arcs: An example from the Bremanger Granitoid Complex, west Norwegian Caledonides: Contributions to Mineralogy and Petrology, v. 143, n. 3, p. 316–335, http://dx.doi.org/10.1007/s00410-001-0342-5
Harper, D. A. T., Niocaill, C. M., and Williams, S. H., 1996, The palaeogeography of early Ordovician Iapetus terranes: An integration of faunal and palaeomagnetic constraints: Palaeogeography, Palaeoclimatology, Palaeoecology, v. 121, n. 3–4, p. 297–312, http://dx.doi.org/10.1016/0031-0182(95)00079-8
Harper, D. A. T., Bruton, D. L., and Rasmussen, C. M. Ø., 2008, The Otta brachiopod and trilobite fauna: Palaeogeography of Early Palaeozoic terranes and biotas across Baltoscandia: Fossils and Strata, v. 54, p. 31–40.
Heim, M., Grenne, T., and Prestvik, T., 1987, The Resfjell ophiolite fragment, southwest Trondheim region, central Norwegian Caledonides: Norges geologiske undersøkelse Bulletin, v. 409, p. 49–71.

Hidalgo, S., Monzier, M., Martin, H., Chazot, G., Eissen, J.–P., and Cotton, J., 2007, Adakitic magmas in the Ecuadorian volcanic front: Petrogenesis of the Iliniza Volcanic Complex (Ecuador): Journal of Volcanology and Geothermal Research, v. 159, n. 4, p. 366–392, http://dx.doi.org/10.1016/j.jvolgeores.2006.07.007

Hidalgo, P. J., Vogel, T. A., Rooney, T. O., Currier, R. M., and Layer, P. W., 2011, Origin of silicic volcanism in the Panamanian arc: Evidence for a two-stage fractionation process at El Valle volcano: Contributions to Mineralogy and Petrology, v. 162, n. 6, p. 1115–1138, http://dx.doi.org/10.1007/s00410-011-0643-2

Hollocher, K., Bull, J., and Robinson, P., 2002, Geochemistry of the metamorphosed Ordovician Taconian magmatic arc, Bronson Hill anticlinorium, western New England: Physics and Chemistry of the Earth, v. 27, n. 1–3, p. 5–45, http://dx.doi.org/10.1016/S1474-7065(01)00002-X

Hollocher, K., Robinson, P., Walsh, E., and Terry, M. P., 2007, The Neoproterozoic Ottfjället dike swarm of the Middle Allochthon, traced geochemically into the Scandian hinterland, Western Gneiss Region, Norway: American Journal of Science, v. 307, n. 6, p. 901–953, http://dx.doi.org/10.2475/06.2007.02

Hollocher, K., Robinson, P., Walsh, E., and Roberts, D., 2012, Geochemistry of amphibolite-facies volcanics and gabbros of the Støren Nappe in extensions west and southwest of Trondheim, Western Gneiss Region, Norway: A key to correlations and paleotectonic settings: American Journal of Science, v. 312, n. 4, p. 357–416, http://dx.doi.org/10.2475/04.2012.01

Ickert, R. B., Thorkelson, D. J., Marshall, D. D., and Ullrich, T. D., 2007, Eocene adakitic volcanism in southern British Columbia: Remelting of arc basalt above a slab window: Tectonophysics, v. 464, n. 1–4, p. 164–185, http://dx.doi.org/10.1016/j.tecto.2007.10.007

Jiang, Y.–H., Liao, S.–Y., Yang, W.–Z., and Shen, W.–Z., 2008, An island arc origin of plagiogranites at Oytag, western Kunlun orogen, northwest China: SHRIMP zircon U–Pb chronology, elemental and Sr–Nd–Hf isotopic geochemistry and Paleozoic tectonic implications: Lithos, v. 106, n. 3–4, p. 323–335, http://dx.doi.org/10.1016/j.lithos.2008.08.004

Jöns, N., Bach, W., and Schroeder, T., 2009, Formation and alteration of plagiogranites in an ultramafic-hosted detachment fault at the Mid-Atlantic Ridge (ODP Leg 209): Contributions to Mineralogy and Petrology, v. 157, p. 625–639, http://dx.doi.org/10.1007/s00410-008-0357-2

Karabinos, P., Samson, S. D., Hepburn, J. C., Stoll, H. M., and Aleinikoff, J. N., 1996, The Taconian Orogeny in New England: Collision between Laurentia and the Shelburne Falls Arc: Geological Society of America Abstracts with Programs: v. 24, n. 3, p. 70.

Karabinos, P., Samson, S. D., Hepburn, J. C., and Stoll, H. M., 1998, Taconian orogeny in the New England Appalachians: Collision between Laurentia and the Shelburne Falls arc: Geology, v. 26, n. 3, p. 215–218, http://dx.doi.org/10.1130/0091-7613(1998)026<0215:TOITNE>2.3.CO;2

Kaur, G., and Mehta, P. K., 2005, The Gothara plagiogranite: Evidence for oceanic magmatism in a non-ophiolitic association, North Khetri Copper Belt, Rajasthan, India?: Journal of Asian Earth Sciences, v. 25, n. 5, p. 805–819, http://dx.doi.org/10.1016/j.jseaes.2004.08.003

Kiliç, A. D., 2009, Petrographical and geochemical properties of plagiogranites and gabbros in Guleman ophiolite: Mineral Research and Exploration Bulletin, v. 139, p. 33–49.

Kopke, J., Feig, S. T., Snow, J., and Freise, M., 2004, Petrogenesis of oceanic plagiogranites by partial melting of gabbros: An experimental study: Contributions to Mineralogy and Petrology, v. 146, n. 4, p. 414–432, http://dx.doi.org/10.1007/s00410-003-0511-9

Kopke, J., Berndt, J., Feig, S. T., and Holtz, F., 2007, The formation of SiO_2–rich melts within the deep oceanic crust by hydrous partial melting of gabbros: Contributions to Mineralogy and Petrology, v. 153, n. 1, p. 67–84, http://dx.doi.org/10.1007/s00410-006-0135-y

Kusky, T. M., Chow, J. S., and Bowring, S. A., 1996, Age and origin of the Boil Mountain ophiolite and Chain Lakes massif, Maine: Implications for the Penobscottian orogeny: Canadian Journal of Earth Sciences, v. 34, p. 646–654, http://dx.doi.org/10.1139/e17-051

Le Bas, M. J., 2000, IUGS reclassification of the high-Mg and picritic volcanic rocks: Journal of Petrology, v. 41, n. 10, p. 1467–1470, http://dx.doi.org/10.1093/petrology/41.10.1467

Le Bas, M. J., LeMaitre, R. W., Streckeisen, A., and Zanettin, B., 1986, A chemical classification of volcanic rocks based on the total alkali–silica diagram: Journal of Petrology, v. 27, n. 3, p. 745–750, http://dx.doi.org/10.1093/petrology/27.3.745

Lippard, S. J., and Roberts, D., 2010, Geochemistry and palaeogeographical setting of greenstone units on Frosta peninsula, Nord-Trøndelag, Central Norwegian Caledonides: Norges geologiske undersøkelse Bulletin, v. 450, p. 48–59.

Loeschke, J., 1976a, Major element variations in Ordovician pillow lavas of the Støren Group, Trondheim region, Norway: Norsk Geologisk Tidsskrift, v. 56, Special Supplement 2, p. 141–159.

——— 1976b, Petrochemistry of eugeosynclinal magmatic rocks of the area around Trondheim (Central Norwegian Caledonides): Jahrbuch für Mineralogie Abhandlungen, v. 128, p. 41–72.

Loeschke, J., and Schock, H. H., 1980, Rare earth element contents of Norwegian greenstones and their geotectonic implications: Norsk Geologisk Tidsskrift, v. 60, p. 29–37.

Lundmark, A. M., and Corfu, F., 2007, Age and origin of the Årdal dike complex, SW Norway: False isochrons, incomplete mixing, and the origin of Caledonian granites in basement nappes: Tectonics, v. 26, n. 2, TC2007, http://dx.doi.org/10.1029/2005TC001844

Lyons, J. B., Aleinikoff, J. N., and Zartman, R. E., 1986, Uranium–thorium–lead ages of the Highlandcroft plutonic suite, northern New England: American Journal of Science, v. 286, n. 6, p. 489–509, http://dx.doi.org/10.2475/ajs.286.6.489

Lytle, M. L., Kelly, K. A., Hauri, E. H., Gill, J. B., Papia, D., and Arculus, R. J., 2012, Tracing mantle sources and Samoan influence in the northwestern Lau back-arc basin: Geochemistry, Geophysics, Geosystems, v. 13, n. 10, http://dx.doi.org/10.1029/2012GC004233

Macdonald, F. A., Ryan–Davis, J., Coish, R. A., Crowley, J. L., and Karabinos, P., 2014, A newly identified

Gondwanan terrane in the northern Appalachian Mountains: Implications for the Taconic orogeny and closure of the Iapetus Ocean: Geology, v. 42, n. 2, p. 539–542, http://dx.doi.org/10.1130/G35659.1
McBirney, A. R., 1998, The Skaergaard Layered Series. Part V. Included Trace Elements: Journal of Petrology, v. 39, n. 2, p. 255–276, http://dx.doi.org/10.1093/petroj/39.2.255
McDonough, W. F., and Sun, S., 1995, The composition of the Earth: Chemical Geology, v. 120, n. 2–3, p. 223–253, http://dx.doi.org/10.1016/0009-2541(94)00140-4
Meyer, G. B., Grenne, T., and Pedersen, R. B., 2003, Age and tectonic setting of the Nesåa Batholith: Implications for Ordovician arc development in the Caledonides of Central Norway: Geological Magazine, v. 140, n. 5, p. 573–594, http://dx.doi.org/10.1017/S0016756803008069
Melezhik, V. A., Gorokhov, I. M., Fallick, A. E., Roberts, D., Kusnetzov, A. B., Zwaan, B. K., and Pokrovsky, B. G., 2002, Isotopic stratigraphy suggests Neoproterozoic ages and Laurentian ancestry for high-grade marbles from the North-Central Norwegian Caledonides: Geological Magazine, v. 139, n. 4, p. 375–393, http://dx.doi.org/10.1017/S0016756802006726
Melezhik,V. A., Zwaan, B. K, Motuza, G., Roberts, D., Solli, A., Fallick, A. E., Gorokhov, I. M., and Kusnetzov, A. B., 2003, New insights into the geology of high-grade Caledonian marbles based on isotope chemostratigraphy: Norwegian Journal of Geology, v. 83, p. 209–242.
Mendum, J. R., 2012, Late Caledonian (Scandian) and proto-Variscan (Acadian) orogenic events in Scotland: Journal of the Open University Geological Society, v. 33, n. 1, p. 37–51.
Milovanović, D., Srećković-Batoćanin, D., Savić, M., and Popovic, D., 2012, Petrology of plagiogranite from Sjenica, Dinaridic Ophiolite Belt (southwestern Serbia): Geologica Carpathica, v. 63, n. 2, p. 97–106, http://dx.doi.org/10.2478/v10096-012-0008-4
Moench, R. H., 1993, Highlights of metamorphic stratigraphy and tectonics in western Maine to northeastern Vermont, *in* Cheney, J. T., and Hepburn, J. C., editors, Field Trip Guidebook for the Northeastern United States, v. 2: Boston, Geological Society of America, annual meeting, p. DD1–DD32.
Moench, R. H., and Aleinikoff, J. N., 2003, Stratigraphy, geochronology, and accretionary terrane settings of two Bronson Hill arc sequences, northern New England: Physics and Chemistry of the Earth, v. 28, n. 1–3, p. 113–160, http://dx.doi.org/10.1016/S1474-7065(03)00012-3
Moench, R. H., Boone, G. M., Bothner, W. A., Boudette, E. L., Hatch, N. L., Jr., Hussey, A. M., II, and Marvinney, R. G., 1995, Geologic map of the Sherbrooke–Lewiston area, Maine, New Hampshire, and Vermont, United States, and Quebec, Canada: United States Geological Survey, Miscellaneous Investigations Series, Map I-1898-D, 1:250,000, 2 sheets, with pamphlet.
Monjaret, M. C., Bellon, H., and Maillet, P., 1991, Magmatism of the troughs behind the New Hebrides island arc (RV Jean Charcot SEAPSO 2 cruise): K–Ar geochronology and petrology: Journal of Volcanology and Geothermal Research, v. 46, n. 3–4, p. 265–280, http://dx.doi.org/10.1016/0377-0273(91)90088-H
Mørk, M. B. E., Sundvoll, B., and Stabel, A., 1997, Sm–Nd dating of gabbro- and garnet-bearing contact metamorphic/anatectic rocks from Krutfjellet, Nordland, and some geochemical aspects of the intrusive: Norsk Geologisk Tidsskrift, v. 77, p. 39–50.
Murphy, J. B., and Dostal, J., 2007, Continental mafic magmatism of different ages in the same terrane: Constraints on the evolution of an enriched mantle source: Geology, v. 35, n. 4, p. 335–338, http://dx.doi.org/10.1130/G23072A.1
Nakada, S., Maillet, P., Monjaret, M. C., Fujinawa, A., and Urabe, T., 1994, High-Na dacite from the Jean Charcot Trough (Vanuatu), southwest Pacific: Marine Geology, v. 116, n. 1–2, p. 197–213, http://dx.doi.org/10.1016/0025-3227(94)90176-7
Neuman, R. B., 1964, Fossils in Ordovician tuffs, northeastern Maine: United States Geological Survey Bulletin, v. 1181–E, 38 p.
Neuman, R. B., and Harper, D. A. T., 1992, Paleogeographic significance of Arenig–Llanvirn Toquima Table Head and Celtic brachipod assemblages, *in* Webby, B. D., and Laurie, J. R., editors, Global perspectives on Ordovician Geology: Rotterdam, Netherlands, Balkema Press, p. 241–254.
Nilsen, O., Sundvoll, B., Roberts, D., and Corfu, F., 2003, U–Pb geochronology and geochemistry of trondhjemites and a norite pluton from the SW Trondheim Region, Central Norwegian Caledonides: Norges geologiske undersøkelse Bulletin, v. 441, p. 5–16.
Nilsen, O., Corfu, F., and Roberts, D., 2007, Silurian gabbro–diorite–trondhjemite plutons in the Trondheim Nappe Complex, Caledonides, Norway: Petrology and U–Pb geochronology: Norwegian Journal of Geology, v. 87, p. 329–342.
Nilsson, L.–P., and Roberts, D., 2014, A trail of ophiolitic debris and its detritus along the Trøndelag–Jämtland border: Correlations and palaeogeographical implications: Norges geologiske undersøkelse Bulletin, v. 453, p. 29–41.
Nissen, A. L., Roberts, D., and Gromet, L. P., 2006, U–Pb zircon ages of a tonalite and a granodiorite dyke from the southeastern part of the Bindal Batholith, central Norwegian Caledonides: Norges geologiske undersøkelse Bulletin, v. 446, p. 5–9.
Nordgulen, Ø., and Schoenborg, B., 1990, The Caledonian Heilhornet Pluton, north-central Norway: Geological setting, radiometric age and implications for the Scandinavian Caledonides: Journal of the Geological Society, London, v. 147, n. 3, p. 439–450, http://dx.doi.org/10.1144/gsjgs.147.3.0439
Nordgulen, Ø., Bickford, M. E., Nissen, A. L., and Wortman, G. L., 1993, U–Pb zircon ages from the Bindal Batholith, and the tectonic history of the Helgeland Nappe Complex, Scandinavian Caledonides: Journal of the Geological Society, London, v. 150, n. 4, p. 771–783, http://dx.doi.org/10.1144/gsjgs.150.4.0771
Nordgulen, Ø., Braathen, A., Corfu, F., Osmundsen, P.–T., and Husmo, T., 2002, Polyphase kinematics and geochronology of the Kollstraumen detachment: Norwegian Journal of Geology, v. 82, p. 299–316.
Norman, M. D., Leeman, W. P., and Mertzman, S. A., 1992, Granites and rhyolites from the northwestern U.S.A.: Temporal variation in magmatic processes and relations to tectonic setting: Transactions of the

Royal Society of Edinburgh, Earth and Environmental Sciences, v. 83, p. 71–81, http://dx.doi.org/10.1017/S0263593300007768
Osmundsen, P. T., Eide, E. A., Haabesland, N. E., Roberts, D., Andersen, T. B., Kendrick, M., Bingen, B., Braathen, A., and Redfield, T. F., 2006, Kinematics of the Høybakken detachment zone and the Møre–Trøndelag Fault Complex, central Norway: Journal of the Geological Society, London, v. 163, n. 2, p. 303–318, http://dx.doi.org/10.1144/0016-764904-129
Pannemans, B., and Roberts, D., 2000, Geochemistry and petrogenesis of trondhjemites and granodiorite from Gauldalen, central Norwegian Caledonides: Norges geologiske undersøkelse Bulletin, v. 437, p. 43–56.
Paterson, S. R., Žák, J., and Janoušek, V., 2008, Growth of complex sheeted zones during recycling of older magmatic units into younger: Sawmill Canyon area, Tuolumne batholith, Sierra Nevada, California: Journal of Volcanology and Geothermal Research, v. 177, n. 2, p. 457–484, http://dx.doi.org/10.1016/j.jvolgeores.2008.06.024
Pearce, J. A., and Parkinson, I. J., 1993, Trace element models for mantle melting: Application to volcanic arc petrogenesis, *in* Prichard, H. M., Alabaster, T., Harris, N. B. W., and Neary, C. R., editors, Magmatic Processes and Plate Tectonics: Geological Society, London, Special Publications, v. 76, p. 373–403, http://dx.doi.org/10.1144/gsl.sp.1993.076.01.19
Pearce, J. A., and Stern, R. J., 2006, Origin of back-arc basin magmas: Trace element and isotope perspectives, *in* Christie, D. M., Fisher, C. R., Lee, S. –M., and Givens, S., editors, Back-Arc Spreading Systems–Geological, Biological, Chemical, and Physical Interactions: American Geophysical Union, Geophysical Monograph Series, v. 166, p. 63–86, http://dx.doi.org/10.1029/166GM06
Pearce, J. A., Harris, N. B. W., and Tindle, A. G., 1984, Trace element discrimination diagrams for the tectonic interpretation of granitic rocks: Journal of Petrology, v. 25, n. 4, p. 956–983, http://dx.doi.org/10.1093/petrology/25.4.956
Pearce, J. A., Ernewein, M., Bloomer, S. H., Parson, L. M., Murton, B. J., and Johnson, L. E., 1994, Geochemistry of Lau Basin volcanic rocks: influence of ridge segmentation and arc proximity: Geological Society, London, Special Publications, v. 81, p. 53–75, http://dx.doi.org/10.1144/GSL.SP.1994.081.01.04I
Pedersen, P. Å., ms, 1981, Resedimenterte konglomerater og turbiditter på overgangen mellom undre/øve Hovingruppe (Llandeilo–Caradoc) i Åsen området, Nord-Trøndelag: University of Bergen, Norway, M. S. thesis, 127 p.
Pedersen, R. B., and Dunning, G. R., 1997, Evolution of arc crust and relations between contrasting sources: U–Pb (age), Nd and Sr isotope systematics of the ophiolitic terrain of SW Norway: Contributions to Mineralogy and Petrology, v. 128, n. 1, p. 1–15, http://dx.doi.org/10.1007/s004100050289
Pedersen, R. B., and Hertogen, J., 1990, Magmatic evolution of the Karmøy Ophiolite Complex, SW Norway: Relationships between MORB–IAT–boninitic–calc-alkaline and alkaline magmatism: Contributions to Mineralogy and Petrology, v. 104, n. 3, p. 277–293, http://dx.doi.org/10.1007/BF00321485
Pedersen, R. B., Furnes, H., and Dunning, G. R., 1991, A U/Pb age for the Sulitjelma Gabbro, North Norway: Further evidence for the development of a Caledonian marginal basin in Ashgill–Llandovery time: Geological Magazine, v. 128, n. 2, p. 141–153, http://dx.doi.org/10.1017/S0016756800018331
Pedersen, R. B., Bruton, D. L., and Furnes, H., 1992, Ordovician faunas, island arcs and ophiolites in the Scandinavian Caledonides: Terra Nova, v. 4, n. 2, p. 217–222, http://dx.doi.org/10.1111/j.1365-3121.1992.tb00475.x
Pedersen, R. B., Nordgulen, Ø., Barnes, C. G., Prestvik, T., and Barnes, M. A., 1999, U–Pb dates from dioritic and granitic rocks in Velfjord, north-central Norway: Norsk Geologisk Förenings, winter meeting abstracts, Geonytt, v. 16, p. 81.
Perfit, M. R., and Fornari, D. J., 1983, Geochemical studies of abyssal lavas recovered by DSRV *Alvin* from eastern Galapagos Rift, Inca Transform, and Ecuador Rift 2. Phase chemistry and crystallization history: Journal of Geophysical Research-Solid Earth, v. 88, n. B12, p. 10530–10550, http://dx.doi.org/10.1029/JB088iB12p10530
Plank, T., and Langmuir, C. H., 1988, An evaluation of the global variations in the major element chemistry of arc basalts: Earth and Planetary Science Letters, v. 90, n. 4, p. 349–370, http://dx.doi.org/10.1016/0012-821X(88)90135-5
Ramsay, D. M., and Sturt, B. A., 1998, Excursion guide: The Otta nappe and its integration into the Trondheim Nappe in the south-central Scandinavian Caledonides: Norges Geologiske undersokelse, Report 98.103, 44 p.
Rankin, D. W., Tucker, R. D., and Amelin, Y., 2012, Reevaluation of the Piermont–Frontenac allochthon in the Upper Connecticut Valley: Restoration of a coherent Boundary Mountains–Bronson Hill stratigraphic sequence: Geological Society of America Bulletin, v. 125, n. 5–6, p. 998–1024, http://dx.doi.org/10.1130/B30590.1
Rao, D. R., Rai, H., and Kumar, J. S., 2004, Origin of oceanic plagiogranite in the Nidar ophiolitic sequence of eastern Ladakh, India: Current Science, v. 87, n. 7, p. 999–1005.
Ratajeski, K., Glazner, A. F., and Miller, B. V., 2001, Geology and geochemistry of mafic to felsic plutonic rocks in the Cretaceous intrusive suite of Yosemite Valley, California: Geological Society of America Bulletin, v. 113, n. 11, p. 1486–1502, http://dx.doi.org/10.1130/0016-7606(2001)113<1486:GAGOMT>2.0.CO;2
Ratcliffe, N., Hames, W. E., and Stanley, R. S., 1999, Taconian orogeny in the New England Appalachians: Collision between Laurentia and the Shelburne Falls Arc; Comment: Geology, v. 27, n. 4, p. 381, http://dx.doi.org/10.1130/0091-7613(1999)027<0381:toitne>2.3.co;2
Reagan, M. K., Hanan, B. B., Heizler, M. T., Hartman, B. S., and Hickey–Vargas, R., 2008, Petrogenesis of volcanic rocks from Saipan and Rota, Mariana Islands, and implications for the evolution of nascent island arcs: Journal of Petrology, v. 49, n. 3. p. 441–464, http://dx.doi.org/10.1093/petrology/egm087

Reagan, M. K., Ishizuka, O., Stern, R. J., Kelley, K. A., Ohara, Y., Blichert-Toft, J., Bloomer, S. H., Cash, J., Fryer, P., Hanan, B. B., Hickey-Vargas, R., Ishii, T., Kimura, J.-I., Peate, D. W., Rowe, M. C., and Woods, M., 2010, Fore-arc basalts and subduction initiation in the Izu–Bonin–Mariana system: Geochemistry, Geophysics, Geosystems, v. 11, n. 3, p. 1–17, http://dx.doi.org/10.1029/2009GC002871

Richards, J. P., Ullrich, T., and Kerrich, R., 2006, The Late Miocene–Quaternary Antofalla volcanic complex, southern Puna, NW Argentina: Protracted history, diverse petrology, and economic potential: Journal of Volcanology and Geothermal Research, v. 152, n. 3–4, p. 197–239, http://dx.doi.org/10.1016/j.jvolgeores.2005.10.006

Roberts, D., 1980, Petrochemistry and palaeogeographic setting of the Ordovician volcanic rocks of Smøla, central Norway: Norges geologiske undersøkelse Bulletin, v. 359, p. 43–60.

——— 1982a, Rare earth element patterns from the Ordovician volcanites of Smøla, Nordmøre, west-central Norway: Norsk Geologisk Tidsskrift, v. 62, p. 207–209.

——— 1982b, Disparate geochemical patterns from the Snåsavatn greenstone, Nord Trøndelag, central Norway: Norges geologiske undersøkelse Bulletin, v. 373, p. 63–73.

——— 1982c, En foreløpig rapport om geokjemien av Frostagrønnsteinene: Norges geologiske undersøkelse Report (unnumbered), 4 p.

——— 1987, Geochemistry and Rb–Sr dating of the Muruvik rhyolite tuff, Trondheimsfjord, central Norway: Norges geologiske undersøkelse Bulletin, v. 412, p. 43–53.

Roberts, D., 2003, The Scandinavian Caledonides: Event chronology, palaeogeographic settings and likely modern analogues: Tectonophysics, v. 365, n. 1–4, p. 283–299, http://dx.doi.org/10.1016/S0040-1951(03)00026-X

Roberts, D., and Sundvoll, B., 2000, Geochemistry and Rb–Sr isochron age of trondhjemite dykes from the Gula Complex, near Snøan, Central Norway: Norges geologiske undersøkelse Bulletin, v. 437, p. 67–74.

Roberts, D., and Tucker, R. D., 1991, U–Pb zircon age of the Meklevatnet granodiorite, Gjersvik Nappe, Central Norwegian Caledonides: Norges geologiske undersøkelse Bulletin, v. 421, p. 33–38.

——— 1998, Late Cambrian U–Pb zircon age of a meta-trondhjemite from Ytterøya, Trondheimsfjorden, Central Norwegian Caledonides: Norsk Geologisk Tidsskrift, v. 78, p. 253–258.

Roberts, D., Grenne, T., and Ryan, P. D., 1984, Ordovician marginal basin development in the central Norwegian Caledonides, *in* Kokelaar, B. P., and Howells, M. F., editors, Marginal Basin Geology-Volcanic and Associated Sedimentary and Tectonic Processes in Modern and Ancient arginal Basins: Geological Society, London, Special Publications, v. 16, p. 233–244, http://dx.doi.org/10.1144/gsl.sp.1984.016.01.18

Roberts, D., Sturt, B. A., and Furnes, H., 1985, Volcanite assemblages and environments in the Scandinavian Caledonides and the sequential development history of the mountain belt, *in* Gee, D. G., and Sturt, B. A., editors, The Caledonide Orogen–Scandinavia and related areas, Part 1: Chichester, England, John Wiley and Sons, p. 919–930.

Roberts, D., Walker, N., Slagstad, T., Solli, A., and Krill, A. G., 2002, U–Pb zircon ages from the Bymarka ophiolite, near Trondheim, central Norwegian Caledonides, and regional implications: Norsk Geologisk Tidsskrift, v. 82, p. 19–30.

Roberts, D., Nordgulen, Ø., and Melezhik, V., 2007, The Uppermost Allochthon in the Scandinavian Caledonides: From a Laurentian ancestry through Taconian orogeny to Scandian crustal growth on Baltica, *in* Hatcher, R. D., Jr., Carlson, M. P., McBride, J. H., and Martinez Catalan, J. R., editors, 4-D Framework of Continental Crust: Geological Society of America Memoirs, v. 200, p. 357–377, http://dx.doi.org/10.1130/2007.1200(18)

Robinson, P., Tucker, R. D., Bradley, D., Berry, H. N., IV, and Osberg, P. H., 1998, Paleozoic orogens in New England: GFF, v. 120, n. 2, p. 119–148, http://dx.doi.org/10.1080/11035899801202119

Robinson, P., Solli, A., Hollocher, K., Osmundsen, P. T., Roberts, D., and Tucker, R. D., 2008, Day 5: Scandian geology of the outer Trondheimsfjord region, *in* Robinson, P., Roberts, D., and Gee, D. G., editors, A Tectonostratigraphic Transect Across the Central Scandinavian Caledonides, Oslo, Norway, 33rd International Geological Congress, Field Trip Guidebook: Norges geologiske undersøkelse Report 2008.064, Part II, preliminary, p. 5-1–5-37.

Robinson, P., Roberts, D., Gee, D. G., and Solli, A., 2014, A major synmetamorphic Early Devonian thrust and extensional fault system in the Mid Norway Caledonides: Relevance to exhumation of HP and UHP rocks, *in* Corfu, F., Gasser, D., and Chew, D. M., editors: New Perspectives on the Caledonides of Scandinavia and Related Areas: Geological Society, London, Special Publications, v. 390, p. 241–270, http://dx.doi.org/10.1144/sp390.24

Rollinson, H., 2009, New models for the genesis of plagiogranites in the Oman ophiolite: Lithos, v. 112, n. 3–4, p. 603–614, http://dx.doi.org/10.1016/j.lithos.2009.06.006

Shaw, A. M., Hauri, E. H., Behn, M. D., Hilton, D. R., MacPherson, C. G., and Sinton, J. M., 2012, Long-term preservation of slab signatures in the mantle inferred from hydrogen isotopes: Nature Geoscience, v. 5, p. 224–228, http://dx.doi.org/10.1038/ngeo1406

Shervais, J. W., 2008, Tonalites, trondhjemites, and diorites of the Elder Creek ophiolite, California: Low-pressure slab melting and reaction with the mantle wedge, *in* Wright, J. E., and Shervais, J. W., editors, Ophiolites, Arcs, and Batholiths: A Tribute to Cliff Hopson: Geological Society of America Special Papers, v. 438, p. 113–132, http://dx.doi.org/10.1130/2008.2438(03)

Shuto, K., Sato, M., Kawabata, H., Osanai, Y., Nakano, N., and Yashima, R., 2013, Petrogenesis of Middle Miocene primitive basalt, andesite and garnet-bearing adakitic rhyodacite from the Ryozen Formation: Implications for the tectono-magmatic evolution of the NE Japan Arc: Journal of Petrology, v. 54, n. 12, p. 2413–2454, http://dx.doi.org/10.1093/petrology/egt052

Sigmond, E. M. O., Gustavson, M., and Roberts, D., 1984, Berggrunnskart over Norge: Norges geologiske undersøkelse, scale 1:1,000,000, 1 sheet.

Singer, B. S., Smith, K. E., Jicha, B. R., Beard, B. L., Johnson, C. M., and Rogers, N. W., 2011, Tracking

open-system differentiation during growth of Santa Maria volcano, Guatemala: Journal of Petrology, v. 52, n. 12, p. 2335–2363, http://dx.doi.org/10.1093/petrology/egr047
Sinton, J. M., Ford, L. L., Chappell, B. W., and McColloch, M. T., 2003, Magma genesis and mantle heterogeneity in the Manus back-arc basin, Papua New Guinea: Journal of Petrology, v. 44, n. 1, p. 159–195, http://dx.doi.org/10.1093/petrology/44.1.159
Skjerlie, K. P., 1992, Petrogenesis and significance of late Caledonian granitoid magmatism in western Norway: Contributions to Mineralogy and Petrology, v. 110, n. 4, p. 473–487, http://dx.doi.org/10.1007/BF00344082
Slagstad, T., 2001, The Bymarka ophiolite–field trip guide: Norsk Geologisk Forening, 13 p.
——— 2003, Geochemistry of trondhjemites and mafic rocks in the Bymarka ophiolite fragment, Trondheim, Norway: Petrogenesis and tectonic implications: Norsk Geologisk Tidsskrift, v. 83, p. 167–185.
Slagstad, T., Davidsen, B., and Daly, J. S., 2011, Age and composition of crystalline basement rocks on the Norwegian continental margin: Offshore extension and continuity of the Caledonian–Appalachian orogenic belt: Journal of the Geological Society, London, v. 168, n. 5, p. 1167–1185, http://dx.doi.org/10.1144/0016-76492010-136
Slagstad, T., Pin, C., Roberts, D., Kirkland, C. L., Grenne, T., Dunning, G., Sauer, S., and Andersen, T., 2013, Tectonomagmatic evolution of the Early Ordovician suprasubduction-zone ophiolites of the Trondheim Region, Mid–Norwegian Caledonides, *in* Corfu, F., Gasser, D., and Chew, D. M., editors, New Perspectives on the Caledonides of Scandinavia and Related Areas: Geological Society, London, Special Publications, v. 390, p. 541–561, http://dx.doi.org/10.1144/SP390.11
Solli, A., and Nordgulen, Ø., 2008, Bedrock map of Norway and the Caledonides in Sweden and Finland: Geological Survey of Norway, scale 1:2,000,000, 1 sheet.
Stanley, R. S., and Ratcliffe, N. M., 1985, Tectonic synthesis of the Taconian orogeny in western New England: Geological Society of America Bulletin, v. 96, n. 10, p. 1227–1250, http://dx.doi.org/10.1130/0016-7606(1985)96<1227:TSOTTO>2.0.CO;2
Stephens, M. B., and Gee, D. G., 1985, A tectonic model for the evolution of the eugeoclinal terranes in the central Scandinavian Caledonides, *in* Gee, D. G., and Sturt, B. A., editors, The Caledonide Orogen–Scandinavia and Related Areas, Part 2: Chichester, England, John Wiley and Sons, p. 953–978.
——— 1989, Terranes and polyphase accretionary history in the Scandinavian Caledonides history, *in* Dallmeyer, R. D., editor, Terranes in the circum-Atlantic Paleozoic orogens: Geological Society of America Special Papers, v. 230, p. 17–30, http://dx.doi.org/10.1130/SPE230-p17
Stephens, M. B., Kullerud, K., and Claesson, S., 1993, Early Caledonian tectonothermal evolution in outboard terranes, central Scandinavian Caledonides: New constraints from U–Pb zircon dates: Journal of the Geological Society, London, v. 150, n. 1, p. 51–56, http://dx.doi.org/10.1144/gsjgs.150.1.0051
Straub, S. M., Goldstein, S. L., Class, C., Schmidt, A., and Govez-Tuena, A., 2010, Slab and mantle controls on the Sr–Nd–Pb–Hf isotope evolution of the post 42 Ma Izu–Bonin volcanic arc: Journal of Petrology, v. 51, n. 5, p. 993–1026, http://dx.doi.org/10.1093/petrology/egq009
Sturt, B. A., Ramsay, D. M., and Bjerkgård, T., 1997, Revisions of the tectonostratigraphy of the Otta–Røros tract: Norges geologiske undersøkelse Bulletin, v. 433, p. 8–9.
Sun, S., and McDonough, W. F., 1989, Chemical and isotopic systematics of oceanic basalts: Implications for mantle composition and processing, *in* Saunders, A. D., and Norry, M. J., editors, Magmatism in the Ocean Basins: Geological Society, London, Special Publications, v. 42, p. 313–345, http://dx.doi.org/10.1144/gsl.sp.1989.042.01.19
Thomas, J. B., and Sinha, A. K., 1999, Field, geochemical, and isotopic evidence for magma mixing and assimilation and fractional crystallization processes in the Quottoon Igneous Complex, northwestern British Columbia and southeastern Alaska: Canadian Journal of Earth Sciences, v. 36, n. 5, p. 819–831, http://dx.doi.org/10.1139/e99-001
Tietzsch-Tyler, D., and Roberts, D., 1990, Steinkjer, Berggrunnskart: Norges geologiske undersøkelse, map 1723–3, scale 1:50 000.
Torsvik, T. H., and Cocks, L. R. M., 2013, New global palaeogeographical reconstructions for the Early Palaeozoic and their generation, *in* Harper, D. A. T., and Servais, T., editors, Early Palaeozoic Biogeography and Palaeogeography: Geological Society, London, Memoir 38, p. 5–24, http://dx.doi.org/10.1144/m38.2
Tucker, R. D., and Robinson, P., 1990, Age and setting of the Bronson Hill magmatic arc: A re-evaluation based on U–Pb zircon ages in southern New England: Geological Society of America Bulletin, v. 102, n. 10, p. 1404–1419, http://dx.doi.org/10.1130/0016-7606(1990)102<1404:AASOTB>2.3.CO;2
Tucker, R. D., Robinson, P., Solli, A., Gee, D. G., Thorsnes, T., Krogh, T. E., Nordgulen, Ø., and Bickford, M. E., 2004, Thrusting and extension in the Scandian hinterland, Norway: New U–Pb ages and tectonostratigraphic evidence: American Journal of Science, v. 304, n. 6, p. 477–532, http://dx.doi.org/10.2475/ajs.304.6.477
Turner, S., Caulfield, J., Rushmer, T., Turner, M., Cronin, S., Smith, I., and Handley, H., 2012, Magma evolution in the primitive, intra-oceanic Tonga Arc: Rapid petrogenesis of dacites at Fonualei Volcano: Journal of Petrology, v. 53, n. 6, p. 1231–1253, http://dx.doi.org/10.1093/petrology/egs005
Valley, P. M., Walsh, G. J., and McAleer, R. J., 2015, New U–Pb zircon ages from the Bronson Hill arc, west-central New Hampshire: Geological Society of America Abstracts with Programs, v. 47, n. 3, p. 41.
van Staal, C. R., and Barr, S. M., 2013, Lithospheric architecture and tectonic evolution of the Canadian Appalachians and associated Atlantic margin, *in* Percival, J. A., Cook, F. A., and Clowes, R. M., editors, Tectonic Styles in Canada: The Lithoprobe Perspective: Geological Association of Canada Special Paper 49, p. 41–95.
van Staal, C. R., Whalen, J. B., McNicoll, V. J., Pehrsson, S., Lissenberg, C. J., Zagorevski, A., van Breemen, O., and Jenner, G. A., 2007, The Notre Dame arc and the Taconic orogeny in Newfoundland, *in* Hatcher, R. D., Jr., Carlson, M. P., McBride, J. H., and Martínez Catalán, J. R., editors, 4-D Framework of

Continental Crust: Geological Society of America Memoir 200, p. 511–552, http://dx.doi.org/10.1130/2007.1200(26)
Vedeler, S., ms, 2013, Structural and Petrological Study of the Klemetsaunet plagiogranite, Trondheim, Norway: Trondheim, Norway, Norwegian University of Science and Technology, Department of Geology and Mineral Resources Engineering, M. S. thesis, 53 p.
Vermeesch, P., 2012, On the visualisation of detrital age distributions: Chemical Geology, v. 312–313, p. 190–194, http://dx.doi.org/10.1016/j.chemgeo.2012.04.021
Vetti, V. V., and Fossen, H., 2012, Origin of contrasting Devonian supradetachment basin types in the Scandinavian Caledonides: Geology, v. 40, n. 6, p. 571–574, http://dx.doi.org/10.1130/G32512.1
Vogt, T., 1945, The geology of part of the Hølonda–Horg district, a type area in the Trondheim Region: Norsk Geologisk Tidsskrift, v. 25, p. 449–528.
Waldron, J. W. F., Schofield, D. I., Murphy, J. B., and Thomas, C. W., 2014, How was the Iapetus Ocean infected with subduction?: Geology, v. 42, n. 12, p. 1095–1098, http://dx.doi.org/10.1130/G36194.1
Wanless, V. D., Perfit, M. R., Ridley, W. I., and Klein, E., 2010, Dacite petrogenesis on mid-ocean ridges: Evidence for oceanic crustal melting and assimilation: Journal of Petrology, v. 51, n. 12, p. 2377–2410, http://dx.doi.org/10.1093/petrology/egq056
Whalen, J. B., Jenner, G. A., Longstaffe, F. J., Gariépy, C., and Fryer, B. J., 1997, Implications of granitoid geochemical and isotopic (Nd, O, Pb) data from the Cambrian–Ordovician Notre Dame arc for the evolution of the Central Mobile Belt, Newfoundland Appalachians, *in* Sinha, A. K., Whalen, J. B., and Hogan, J. P., editors, The Nature of Magmatism in the Appalachian Orogen: Geological Society of America Memoir 191, p. 367–396, http://dx.doi.org/10.1130/0-8137-1191-6.367
Whattam, S. A., Malpas, J., Ali, J. R., Lo, C.–H., and Smith, I. E. M., 2005, Formation and emplacement of the Northland Ophiolite, northern New Zealand: SW Pacific tectonic implications: Journal of the Geological Society, London, v. 162, n. 2, p. 225–241, http://dx.doi.org/10.1144/0016-764903-167
Wilson, J. R., Hansen, B. T., and Pedersen, S., 1983, Zircon U–Pb evidence for the age of the Fongen–Hillingen complex, Trondheim region, Norway: GFF, v. 105, n. 1, p. 68–70.
Wintsch, R. P., Yi, K., and Han, D., 2015, Evidence from U-Pb shrimp ages of detrital zircons for evolving provenances for peri-Gondwanan forearc metasediments, western Connecticut: Geological Society of America Abstracts with Programs, v. 47, n. 3, p. 42.
Wood, D. A., 1980, The application of a Th–Hf–Ta diagram to problems of tectonomagmatic classification and to establishing the nature of crustal contamination of basaltic lavas on the British Tertiary Volcanic Province: Earth and Planetary Science Letters, v. 50, n. 1, p. 11–30, http://dx.doi.org/10.1016/0012-821X(80)90116-8
Yaliniz, M. K., 2008, A geochemical attempt to distinguish forearc and back arc ophiolites from the "supra-subduction" central Anatolian ophiolites (Turkey) by comparison with modern oceanic analogues: Ofioliti, v. 33, n. 2, p. 119–129.
Yaliniz, M. K., Floyd, P. A., and Göncüoğlu, M. C., 2000, Petrology and geotectonic significance of plagiogranite from the Sarikaraman Ophiolite (central Anatolia, Turkey): Ofioliti, v. 25, n. 1, p. 31–37.
Yoshinobu, A. S., Barnes, C. G., Nordgulen, Ø., Prestvik, T., Fanning, M., and Pedersen, R. B., 2002, Ordovician magmatism, deformation, and exhumation in the Caledonides of central Norway: An orphan of the Taconic orogeny?: Geology, v. 30, n. 10, p. 883–886. http://dx.doi.org/10.1130/0091-7613(2002)030<0883:OMDAEI>2.0.CO;2
Zagorevski, A., and van Staal, C. R., 2011, The record of Ordovician arc–arc and arc–continent collisions in the Canadian Appalachians during the closure of Iapetus, *in* Brown, D., and Ryan, P. D., editors, Arc–Continent Collision, Frontiers in Earth Sciences: Heidelberg, Springer–Verlag, p. 341–371.
Zartman, R. E., and Leo, G. W., 1985. New radiometric ages on gneisses of the Oliverian domes in New Hampshire and Massachusetts: American Journal of Science, v. 285, n. 3, p. 267–280, http://dx.doi.org/10.2475/ajs.285.3.267